Universität Zürich[UZH]

Department of Geography

The forest dieback during the 1970s and 1980s in Central Europe - A retrospective analysis using tree-ring width and stable isotopes

GEO 511 Master's Thesis

Author: Seraina Brandes, 18-727-552

Supervised by: Prof. Dr. Paolo Cherubini (paolo.cherubini@wsl.ch), Dr. Stefan Klesse (stefan.klesse@wsl.ch), Dr. Matthias Saurer (matthias.saurer@wsl.ch)

Faculty representative: Prof. Dr. Markus Egli

31.01.2025

University of Zurich[UZH]

Department of Geography

The forest dieback during the 1970s and 1980s in Central Europe - A retrospective analysis using tree-ring width and stable carbon isotopes

Jizera Mountains (source: Wikimedia Commons/Lovecz)

Author:
Seraina Brandes (18-727-552)

Supervised by:
Prof. Dr. Paolo Cherubini, WSL
Dr. Matthias Saurer, WSL
Dr. Stefan Klesse, WSL

Faculty Representative:
Prof. Dr. Markus Egli, University of Zurich

31.1.2025

Content

Acknowledgements

First, I want to express my heartfelt thanks to Prof. Dr. Paolo Cherubini, my main supervisor from the Research Unit Forest Dynamics of the Dendrosciences Group at WSL, for his guidance, encouragement, and invaluable feedback throughout this project. His support and expertise were central for completing this thesis.

I am also very grateful to Dr. Stefan Klesse and Dr. Matthias Saurer, also from the Research Unit Forest Dynamics at WSL, for their helpful advice, constructive suggestions, and consistent support. Their guidance in applying meaningful statistical methods and interpreting results was invaluable and greatly contributed to the success of this work.

Special thanks go to Prof. Dr. Hans-Peter Kahle from the University of Freiburg and Dr. Miloš Rydval from the Czech University of Life Sciences Prague for their support during fieldwork and result evaluation, their valuable feedback, and for always being open for discussing questions, ideas and challenges.

This research would not have been possible without the support of the Swiss Federal Institute for Forest, Snow and Landscape Research WSL, which provided funding, a workplace, and access to its tree-ring laboratories and other essential resources.

I would like to thank Anne Verstege, Daniel Nievergelt, and Loïc Schneider from WSL's technical staff for their help with fieldwork preparation, lab work, and IT tasks. A big thanks also goes to Dr. Krešimir Begovič, Dr. Liangjun Zhu and Danyang Yuan for their help during fieldwork.

I also wish to thank Prof. Dr. Markus Egli, the faculty representative from the Department of Geography at the University of Zurich, for his support and guidance during this process.

I am also grateful to the University of Zurich and Free University of Berlin, where I completed my studies. And I truly appreciate my colleagues and fellow students for their collaboration, discussions, and constant moral support throughout this journey.

I would also like to thank the local foresters for their support in locating suitable study sites and allowing me to collect dendrochronological samples, which was crucial for this thesis.

Lastly, I want to thank my family and friends, especially my sister Dr. Andrea Brandes and my friend Cornelia Kästli, for proofreading my thesis. I am also deeply grateful to my understanding partner and my caring mother for their encouragement, patience, and trust in me. Their support kept me motivated during challenging times.

Finally, to everyone who helped me in any way during this work, thank you.

Abstract

This study investigated the causes of forest dieback during the 1970s and 1980s in Central Europe, focusing on Norway spruce and European beech in three regions with differing pollution histories: the Swiss Central Plateau (SCP), the Black Forest (BF), and the Black Triangle (BT). Dendroecological analyses of tree-ring widths and stable carbon isotope ($\delta^{13}C$) data were used to assess tree responses to stress. The study analyzed sulfur oxides (SO_x), nitrogen oxides (NO_γ), and ammonia (NH_x) deposition, alongside extreme drought events and climate variability. It is suggested that drought, along with bark beetle outbreaks, was the main cause of tree stress, tree mortality and forest dieback at the SCP and BF sites. The severe 1976 drought strongly reduced spruce growth, while the deeper-rooted beech showed greater resilience but also experienced stress during extreme drought events. At the BT site, high sulfur deposition combined with nitrogen deposition led to severe soil acidification, nutrient imbalances, and physiological damage, making pollution the main cause for stress on trees. Extreme frost events and cold summers exacerbated stress at BT, particularly for spruce, which is more sensitive to pollution and suffered prolonged growth stagnation. In contrast, beech, although more affected by frost and thus initially showing a faster decrease in growth, recovered more quickly. Droughts also put additional stress on the trees at BT but were not a major factor in the growth declines of the 1970s and 1980s. Nitrogen deposition initially stimulated growth at the SCP and BF sites but later heightened drought sensitivity, contributing to increased drought stress in recent years alongside the rising frequency of severe droughts. In recent years, drought has become a growing problem even at BT, where pollution previously overshadowed its effects. This study highlighted the interaction of climatic extremes, air pollution, site-specific factors, and species-specific traits in impacting forest health. Long-lasting legacy effects from pollution remain important at BT, while increasing frequency of severe droughts endangers forest resilience across Central Europe. Understanding these dynamics is central for sustainable forest management and adapting to future environmental challenges.

List of figures

List of tables

1. Introduction

1.1 Forest dieback in Central Europe

During the last century several episodes of forest decline occurred in Central Europe. One of the most publicly discussed occurred in the 1970s and 1980s. It was characterized by widespread symptoms of tree damage and tree mortality across Central Europe. The phenomenon was impacting species like Norway spruce (*Picea abies*), European beech (*Fagus sylvatica*), and silver fir (*Abies alba*). Prior to the 1970s some isolated observations of declining tree health, mainly yellowing of foliage and needle browning, were reported in areas close to industrial centers. At this time, forest decline was mostly observed near heavily polluted zones and was not yet recognized as a widespread issue or even a broader crisis. The scale of damage had not yet become a major public or scientific concern (Kolář et al. 2017). At the end of the 1970s a sharp decline of silver fir stands was observed in some parts of Germany, a phenomenon termed *Tannensterben* or "fir dieback" (Schütt 1977). It was also observed in large areas of Central Europe, including Switzerland, with an alarming dieback in the 'Black Triangle', a heavily industrialized region at the Czech-German-Polish border. This area was severely affected by local industrial pollution during the 1970s and 1980s, as well as in previous decades, due to coal mining and brown coal combustion in power plant stations (Kolář et al., 2017; Rydval and Wilson, 2012; Schweingruber et al., 1983).

Later, during the 1980s, a more diffuse and widespread decline in both coniferous and broadleaved forests was observed across Central Europe. This broader phenomenon, termed *Waldsterben* or "forest dieback" impacted also key tree species like Norway spruce and European beech. Affected trees showed a variety of distinct symptoms including needle and leaf discoloration or loss, necrosis, crown thinning, dead or declining branches, reduced radial growth, altered sprout formation, fine root decay and resin bleeding. Also, symptoms already known from water-stress or nutrient deficiencies have been observed. Due to the diversity of these symptoms, it was assumed to be an unprecedented disease often leading to the death of affected trees which then results in forest dieback. Unlike earlier, localized damage near polluted industrial centers, this large-scale forest decline was characterized by complex and heterogeneous symptoms that scientists struggled to explain, leading to growing concern that Central Europe faced an ecological crisis (Schütt and Cowling 1985; Cherubini et al. 2021).

As the area of affected forests rapidly expanded, mass media coverage heightened public concern over the widespread forest damage in Central Europe. *Waldsterben* became a widely recognized term, as media showed the severity of the dieback through powerful imagery and headlines, triggering public shock and panic reactions. The discourse was about an environmental crisis with serious implications for forest health and public well-being. The issue became an important political topic, highlighting the cultural and ecological importance of forests, particularly in Germany where forests are considered a symbol of national identity. Thus, it was elevated from an environmental problem to a crisis of national

heritage. *Waldsterben* became a symbol of the growing fear of the destructive potential of human activities on the environment, creating strong emotional responses from the public (Fig. 1 and 2). Environmentalist movements emerged supported by poor or nonexistent science (Von Detten et al. 2012; Cherubini et al. 2021).

Fig. 1: Poster from the group Aktion Waldsterben of Freiburg, Germany in the 1980s: power stations sulphurize, politicians waffle and the forest dies (source: Mitwelt Stiftung Oberrhein)

Fig. 2: Demonstration against Waldsterben in front of the federal parliament building in Bern, Switzerland 1984 (source: ETH Library)

The limited scientific understanding of *Waldsterben* in its early stages can be attributed to the assumed unprecedented scale and complexity of its symptoms. This made it challenging to study the phenomenon as there was no established framework or method for investigating it. Early signs of forest decline were limited to localized and small-scale occurrences, often attributed to specific environmental conditions. As a result, the issue did not gain notable scientific attention until it was assumed to be a widespread and large-scale phenomenon (Roberts 1983; Schütt and Cowling 1985). However, as research advanced, extensive dendroecological and dendroclimatological studies were conducted, more and more of these provided valuable insights into the forest decline associated with *Waldsterben* (Kandler and Innes 1995). Air pollution was identified as a key factor driving forest dieback in Central Europe, particularly in the heavily industrialized Black Triangle region. More recently studies highlighted that climate stressors also exacerbate the impact on already weakened forests (Bosela et al., 2019; Cienciala et al., 2018; Kolář et al., 2017; Rydval and Wilson, 2012; Vacek et al., 2020).

In less polluted areas, various growth patterns and underlying reasons were identified during the 1970s and 1980s. In contrast to the observation of strongly declining fir, spruce and beech growth, maintained stable or even slightly increased at some sites during that period (Dulamsuren et al. 2017; Bosela et al. 2018). Although contradicting observations were made, reduced growth trends for all three species have been noted at several sites in less polluted areas across Central Europe which were in many cases

suggested to be attributed to drought (Dulamsuren et al. 2017; Kolář et al. 2017; Krejza et al. 2021; Spiecker and Kahle 2023). Despite the general observation of negative effects of drought on growth of all three species, differing statements were made about their drought sensitivity (Dulamsuren et al. 2017; Bosela et al. 2018; Leuschner and Meier 2018). Thus, many findings are contradictory, as the complexity of factors influencing tree growth leads to various explanations. Since tree growth represents the combined effects of numerous interacting factors across space and time throughout a tree's lifespan, forest decline emerges as a similarly complex phenomenon with multiple, interconnected causes. As a result, the general underlying causes of forest dieback during the 1970s and 1980s could not always be identified with certainty (Schweingruber 1996; Bosela et al. 2018; Cienciala et al. 2018; Bosela et al. 2019; Cherubini et al. 2021).

1.2 Air pollution and acid rain

The rapid industrialization of Central Europe, particularly after World War II, led to a dramatic increase in air pollution, primarily due to emissions of sulfur dioxide (SO_2), nitrogen oxides (NO_x), and particulate matter from coal-fired industries, factories, and transportation. Additionally, agricultural intensification contributed to an increase in reduced nitrogen compounds (NH_x). Variations in sources, such as agriculture, industry, households, and traffic, combined with differing atmospheric deposition rates, have resulted in distinct spatial and temporal patterns of N deposition between reduced and oxidized compounds. NO_x deposition is more prevalent in urban and industrial areas, while NH_x deposition is predominantly found in agricultural and rural regions (Kopáček and Veselý 2005). N deposition can have both positive and negative effects on ecosystems. While it may enhance plant growth through fertilization, high N inputs can also cause toxicity to above-ground plant parts, leading to growth reductions, leaf injury, and changes in plant physiology (Braun et al. 2017; Tresch et al. 2023). Industrial centers like the Ruhr region in Germany, Upper Silesia in Poland, and Bohemia in the Czech Republic, became hotspots of air pollution. Forests near these point-polluted areas, particularly in the Black Triangle, showed classic symptoms of SO_2 toxicity, such as needle browning, crown thinning, and defoliation (Keller 1984; Landolt and Keller 1985; Rydval and Wilson 2012; Kolář et al. 2017). By the 1970s, studies soon identified acid rain, formed when SO_2 and NO_x combined with atmospheric moisture, as a significant driver of forest ecosystem degradation. Acid rain caused the acidification of forest soils, leading to the leaching of essential nutrients such as calcium and magnesium, as well as the mobilization of harmful metals such as aluminum. This combination weakened tree roots and limited their uptake of water and essential nutrients. The direct as well as the long-term effects of acid rain resulted in widespread growth declines, reduced resilience, and increased tree mortality (Bosela et al., 2018; Kolář et al., 2015; Rydval and Wilson, 2012).

The concept of critical loads emerged as an important tool for understanding and managing the impacts of air pollution on ecosystems. A critical load is defined as the threshold of deposition of a specific pollutant below which, according to current knowledge, no significant harmful effects occur on sensitive

elements of the environment (Nilsson and Grennfelt 1988; Grennfelt et al. 2020). In forest ecosystems, this threshold is particularly important in determining the deposition limits for sulfur (S) and nitrogen (N) compounds that ecosystems can tolerate without irreversible damage. When critical loads are exceeded, soil acidification, eutrophication, and vegetation stress occur, which, together with climatic stress, contribute to increased tree mortality. The distinction between acidification and eutrophication is central for understanding the impacts of S and N deposition. Acidification primarily results from SO_2 and NO_x, while NH_x also contributes indirectly through soil processes such as nitrification. These compounds lower soil pH, deplete base cations, and increase the mobility of toxic metals, exerting stress on trees. In contrast, eutrophication is when ecosystems receive too many nutrients due to high N inputs, which can lead to nutrient imbalances, alter microbial communities in soils or cause fast-growing plants to take over, leading to shifts in plant communities respectively reduction of biodiversity. Furthermore, accumulated nitrates can leach into groundwater or run off into nearby water bodies, contributing to aquatic eutrophication. Both processes are suggested to have played a central role in the historical forest decline observed in Central Europe (Nilsson and Grennfelt 1988; De Vries et al. 2015; Bobbink et al. 2022; Siegwolf et al. 2022).

Although these effects were most severe in the Black Triangle, acid rain and pollution were generally recognized as a primary driver behind forest dieback in Central Europe and the Black Triangle became symbolic of forest decline. The pressure from environmental movements and the public discussion about *Waldsterben* forced governments to the adoption of measures to reduce pollution emissions and to invest public fund in forest health research and monitoring programs (Cherubini et al. 2021). Since the 1980s, significant efforts to reduce air pollution were implemented across Europe. The concept of critical loads has been instrumental in setting emission reduction targets under international agreements (De Vries et al. 2015). The 1979 Convention on Long-Range Transboundary Air Pollution (CLRTAP) and its subsequent protocols in the 1980s and 1990s set strict limits on S and N emissions and required countries to adopt cleaner technologies and emission controls in power plants and factories. These regulations led to a sharp decline in SO_2 and NO_x emissions, resulting in reduced acid rain and improved air quality across Central Europe, particularly in the most affected regions. With reduced air pollution and acid deposition, most forests in affected areas began to show signs of recovery. However, the recovery has been uneven due to the long-lasting effects of soil acidification, which continue to impact nutrient availability and forest resilience (Bosela et al., 2018; Cherubini et al., 2021; Kolář et al., 2015; Rydval and Wilson, 2012).

1.3 Climate change and droughts

In addition to the impacts of pollution, climatic stress such as droughts intensified the forest decline in Central Europe. A drought is a period of abnormally low precipitation that leads to a shortage of water, impacting soil moisture, groundwater, rivers, and lakes (Hänsel et al. 2022). It disturbs the water balance in ecosystems and imposes water stress on trees, also compounding the effects of pollution-weakened

roots and acidified soils (Vacek et al. 2020; Hájek et al. 2021). Since the 1976 drought, the 2003 and 2018/2019 droughts are recognized as some of the most severe over the past 2100 years, drastically reducing tree growth and inducing widespread tree mortality (Schuldt et al. 2020; Büntgen et al. 2021; Spiecker and Kahle 2023). However, summer droughts in Europe are not exclusively a phenomenon of the 21st century. Severe drought events were already recorded during the 1940s and 1950 and in earlier centuries. In the second half of the twentieth century, a general declining trend toward drier conditions connected to climate change can be observed, combined with an increasing trend of temperatures fluctuations in precipitation (Schuldt et al. 2020; Hänsel et al. 2022).

Drought can be classified into three main types, each defined by its specific impacts. Meteorological drought, to which this study refers, occurs when a region experiences significantly less precipitation than usual over a specific period. It is the most fundamental form of drought, serving as the basis for other types. When this lack of rainfall reduces soil moisture to the point that crops and vegetation can no longer grow effectively, it leads to agricultural drought. If the water shortage persists, it can impact larger water systems, such as rivers, lakes, and groundwater reserves, resulting in hydrological drought. The impacts of a drought event can last much longer than the precipitation deficits itself. The increase of global surface temperature with an associated rise in vapor pressure deficit intensifies the severity of drought events, particularly during the hottest periods of the year. Recent droughts have frequently been accompanied by extremely high temperatures or heatwaves. Such events, often described as "global-change-type droughts" or "hotter droughts", are notable for their more severe impacts compared to droughts occurring under more typical climatic conditions (Schuldt et al. 2020; Hänsel et al. 2022).

Severe droughts have lasting impacts on forest health by affecting carbon (C) and water balance, impairing plant functioning and reducing tree growth on the one hand but also by increasing susceptibility to pests and pathogens on the other hand. Despite varying drought-sensitivity of different tree species, drought affects both coniferous and broadleaved trees. It causes symptoms such as crown thinning, needle and leaf discoloration or loss, and, in extreme cases, tree mortality. However, not all tree species suffered to the same extent during past drought events (Zang et al. 2014; Bosela et al. 2018; Pretzsch et al. 2020; Schuldt et al. 2020; Bottero et al. 2021). Studies showed that the reaction of trees to drought can differ within the same site and even more so at different sites. While some trees suffered strongly from the extended water shortages and elevated temperatures, others maintained their health and showed just little to no signs of stress (Klesse et al. 2022; Neycken et al. 2024). The timing, intensity, and duration of a drought are critical factors in determining the extent of the stress experienced by trees (McDowell et al. 2008; Wu et al. 2022). Depending on when seasonal droughts occur during the growth cycle of a tree, it can have different physiological and ecological consequences. Fir, spruce, and beech are all highly sensitive to drought, but they respond differently because their functional traits, like rooting depth, water-use efficiency, and wood anatomy, determine how vulnerable they are to specific aspects of drought stress (McDowell et al. 2008; Hartl-Meier et al. 2015b; Rukh et al. 2023). Beside temporal

there is also regional variability of drought impact. Forests in temperate regions experience greater vulnerability to drought, particularly in continental areas with lower precipitation and higher evaporation rates (Lindner et al. 2010). Trees at high elevation where growth is temperature-limited could even benefit from drought as the growing season is extended or optimized due to the higher temperatures (Dulamsuren et al. 2017; Bottero et al. 2021).

Dendroecological studies using tree-ring width (TRW) and stable carbon isotope ^{13}C analysis confirm cumulative negative impacts of climatic extremes and pollution on tree growth, also intensifying forest dieback during the 1970s and 1980s (Bosela et al., 2019; Hájek et al., 2021; Putalová et al., 2019; Rydval and Wilson, 2012; Šimůnek et al., 2019; Vacek et al., 2020, 2019). Furthermore, the observation that trees weakened by one drought are more susceptible to subsequent stress has become a growing concern, particularly as climate change projections suggest that droughts will become more frequent and intense in the future. The relationship between drought and forest decline has become a focus of research on forest resilience under climate change (Allen et al. 2010; Boden et al. 2014; Bottero et al. 2021; Spiecker and Kahle 2023). The *Waldsterben* crisis of the late 20th century not only highlighted the fragility of forest ecosystems but also catalyzed the development of advanced methods to monitor and understand the complex dynamics of how forests respond to their environment. Among these, dendroecological research has played a key role in understanding interactions between pollutants, climate stress, and forest health, providing a fundamental basis for more detailed analyses of forest responses to environmental challenges (Cherubini et al., 2021).

1.4 Dendrosciences

Building on this foundation, dendrosciences have developed as an interdisciplinary field that focuses on tree rings to understand past environmental conditions, ecological processes, and forest dynamics. At the core of this field is dendrochronology, the study of annual tree-ring growth, which provides a precise timeline for analyzing environmental changes by crossdating and interpreting tree-ring patterns. This makes the reconstruction of past events and environmental conditions possible and thus provides insights in forest dynamics. Within dendrochronology, dendroecology studies the relationships between tree-ring characteristics and ecological as well as environmental factors. It examines how factors such as light, soil conditions, stand dynamics, climate, and pollution influence tree growth. By analyzing ring widths and stable isotope compositions, dendroecology provides insights into both natural variability and anthropogenic influences, which both contribute to better understand forest health and the causes of forest dieback. As a subfield of dendroecology, dendroclimatology focuses on how climate influences tree growth over time and provides valuable information on past climate variability and trends. This knowledge is crucial for understanding how changing climate interacts with other stressors, such as pollution. All in all, dendrosciences offer a powerful framework for studying the complex interactions between trees, their environment, and long-term ecological processes, particularly useful in the context of analyzing forest dieback (Frank et al., 2022; Fritts, 1976; Schweingruber, 1988).

1.4.1 Tree growth and tree rings

Tree growth is a complex process influenced by genetic factors, environmental conditions, and internal physiological functions. Trees grow in both height and radial dimensions. Height growth occurs through apical meristems at the tips of shoots and roots, while radial growth is driven by the vascular cambium, a thin layer of dividing cells located between the bark and the wood. The cambium produces new xylem cells (wood) on the inside and phloem cells (bark) on the outside. Over time, the accumulation of xylem cells forms the trunk, branches, and roots of the tree and enables water and nutrient transport while it also provides structural support. Annual growth rings are formed because of seasonal variations in cambial activity. Tree growth takes place during the months of the growing season. In spring and early summer, when conditions are favorable, the cambium produces earlywood, which is characterized by large, thin-walled cells which are optimized for efficient water transport. As growth slows down in summer and fall, latewood is produced. It consists of smaller, thicker-walled cells that provide mechanical strength. This cyclical growth creates clear annual rings (Fig. 3) in temperate climates, such as those in Central Europe. These tree rings serve as chronological records of environmental conditions, and they are widely used in dendroecological and dendroclimatological studies (Speer 2009; Frank et al. 2022). Broadleaved trees and coniferous trees show different growth patterns and wood structures. Broadleaved species like beech produce wood with vessels for water transport and often have complex anatomical features. In contrast, coniferous trees such as spruce have tracheids for both water conduction and mechanical support, resulting in a wood structure that is simpler and more uniform. These structural differences influence how each tree type responds to environmental conditions and how their growth rings reflect those influences (Rathgeber et al., 2022; Schwein-gruber, 1988; Speer, 2009).

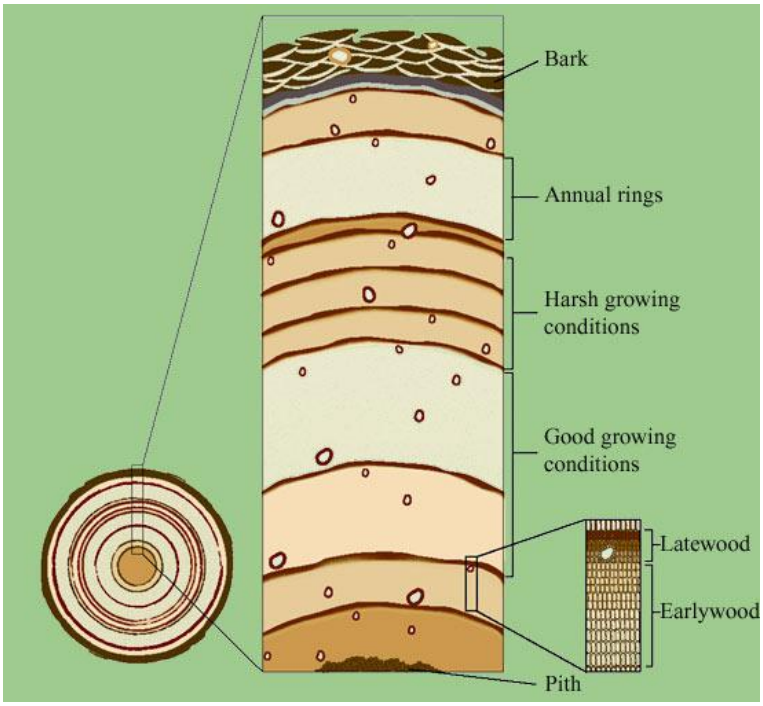

Fig. 3: Tree-ring growth (source: Earth Science Australia)

A range of internal and external factors influence tree growth. Internal factors include a tree's genetic composition which determines its growth potential, while physiological processes such as photosynthesis, respiration, and nutrient storage regulate growth. External factors, including climate, particularly temperature, precipitation, and sunlight, but also site characteristics, such as slope position as well as soil properties like nutrient availability and moisture content are important external factors. Biotic

factors, such as competition, herbivory, and fungal or insect attacks could also affect growth, as well as anthropogenic influences, including forest management, pollution, soil degradation, and fertilization (Schweingruber 1988; Schweingruber 1996; Hughes et al. 2011; Frank et al. 2022). Stressors, such as drought or high atmospheric pollution, often lead to reduced growth resulting in narrower rings. These stress factors can disrupt photosynthesis and other metabolic processes and thus directly impact tree growth (Dhir 2016; Putalová et al. 2019). However, because growth is influenced by many factors, it is often challenging to observe uniform reactions or to disentangle their individual causes. By integrating tree-ring analysis with complementary methods such as stable isotope analyses, it is possible to gain more detailed insights into how trees and forests respond to multiple stressors over time (Cherubini et al., 2021).

1.4.2 Tree-ring stable isotope ^{13}C

Among these methods, the study of stable carbon isotopes ($\delta^{13}C$) in tree rings stands out as a particularly valuable tool for examining how trees react to environmental stressors, such as drought and air pollution. $\delta^{13}C$ serves as a physiological indicator, capturing the relationship between the uptake of C through photosynthesis and its loss via the stomata. Combined with TRW $\delta^{13}C$ provides insights into how stressors impact both internal physiological processes and the overall vitality of trees (Cherubini et al. 2021; Cernusak et al. 2022; Siegwolf et al. 2022). Stable isotopes are forms of the same element with different numbers of neutrons, resulting in varying atomic masses. Carbon-12 (^{12}C) is lighter and more abundant, and carbon-13 (^{13}C) is heavier. For photosynthesis, plants preferentially absorb the lighter ^{12}C isotope due to its faster diffusivity and favorable enzymatic reactions during C fixation. This process, known as isotopic fractionation, is influenced by environmental factors, thus the resulting ratio of ^{13}C to ^{12}C in plant material reflects physiological and environmental conditions. This ratio is expressed as $\delta^{13}C$, which is the relative deviation of the isotope ratio in the sample compared to an international reference standard. This standardization allows precise comparison of $\delta^{13}C$ values across different samples and sites by linking isotopic composition to physiological and environmental processes (Andreu-Hayles et al. 2022; Brooks et al. 2022; Cernusak et al. 2022; Werner and Cormier 2022) When C is assimilated, it is transported as carbohydrates to the cambium, where it becomes part of the cellulose in tree rings. This process locks the $\delta^{13}C$ signature of the surrounding environmental conditions at the time of growth into the wood of a tree. Analyzing this wood then allows for reconstruction of these conditions (Kagawa et al. 2022).

TRW can vary widely due to the numerous factors influencing it, making it a less reliable measure of stress. In contrast, $\delta^{13}C$ provides a more accurate reflection of physiological responses to environmental stressors. Conditions as they occur during a drought event have a strong influence on $\delta^{13}C$ values. Reduced water availability causes stomatal closure which limits CO_2 uptake and lowers the internal CO_2 concentration (c_i) relative to atmospheric levels (c_a). Because trees discriminate against the heavier isotopes ^{13}C under normal conditions, plant $\delta^{13}C$ values are more negative than atmospheric $\delta^{13}C$. Under stress conditions, such as water shortage, the discrimination declines which results in less negative

respectively higher $\delta^{13}C$ values in tree rings. Additional extreme climatic events, such as prolonged heatwaves, amplify these effects. High temperatures exacerbate water-stress, reduce photosynthetic efficiency, and increase $\delta^{13}C$ enrichment in tree rings. These mechanisms provide a clear physiological signal of stress in the wood from the respective year. In contrast, tree rings are not always narrow during stress periods because trees may use stored C reserves or prioritize growth in certain tissues. This makes $\delta^{13}C$ a particularly robust indicator of stress, even when growth rates don't show clear changes (Andreu-Hayles et al. 2022; Cernusak et al. 2022). Furthermore, air pollutants also strongly influence $\delta^{13}C$ by disrupting photosynthesis and stomatal function. SO_2 damages leaf tissues, reduces chlorophyll content and impairs C assimilation. NO_x and NH_x compounds stress trees by altering nutrient availability, stomatal behavior, and photosynthetic efficiency. These disruptions also reduce the discrimination against ^{13}C, resulting in higher $\delta^{13}C$ values, which serve as reliable indicators of pollution-related stress (Siegwolf et al. 2022). Chronic stress conditions, such as prolonged drought and persistent pollution, can exceed physiological thresholds and cause large-scale tree mortality and contribute to forest dieback. $\delta^{13}C$ offers a method to detect tipping points and understand the shift from stress to mortality, providing critical insights into forest decline under changing environmental conditions (Cherubini et al. 2021).

1.5 Aim of this study, research questions and hypotheses

Even though many studies have been conducted, the causes of forest decline during the 1970s and 1980s remain controversial. Interestingly, symptoms such as foliage reductions and discoloration, observed during the forest dieback in the late 1970s, have also been noted following later droughts, particularly during the 2000s and in recent years. Notably, 1976 was a year of severe summer drought in Central Europe (Sousa-Silva et al. 2018; Cherubini et al. 2021; Hänsel et al. 2022). Combined with drought sensitivity of fir, spruce, and beech trees, this raises the question of whether drought events, rather than air pollution, were the primary drivers of the observed forest dieback in diffusely polluted regions during the 1970s and 1980s. Although air pollution was said to be the main reason for past episodes of forest dieback in Central Europe, not all tree species suffered equally or recovered since the improvement of air quality in the 1990s. This is often difficult to comprehend for the roused public and governments that have invested considerable resources in relevant research, monitoring programs and adopted measures (Skelly and Innes 1994; Kandler and Innes 1995; Cherubini et al. 2021). Thus, the aim of this Master's thesis is to investigate the causes of forest dieback episodes during the 1970s and 1980s, focusing on Norway spruce and European beech in three regions with varying historical pollution loads. Both species were impacted by forest dieback and are among the most important tree species in Central Europe, due to their wide distribution and central role in timber production (Leuschner 2020).

To address this, TRW and $\delta^{13}C$ are analyzed as more reliable indicators for tree vitality and forest health compared to crown foliage transparency, which has been criticized for its subjectivity and lack of specificity (Cherubini et al., 2021). The hypothesis of this thesis is that droughts were the primary drivers of forest dieback episodes in areas with low or diffuse air pollution levels in Central Europe during the

1970s and 1980s. Additionally, it is assumed that in areas with heavy air pollution during this period, forest dieback was predominantly caused by air pollutants, with drought acting as an amplifying factor. In recent decades, however, even in heavily polluted areas, forest decline is hypothesized to have been primarily drought-induced. For both spruce and beech at all three study sites, I expect a decline in tree-ring growth and an increase in $\delta^{13}C$ values during drought years. In the heavily polluted area, I anticipate reduced tree-ring growth and elevated $\delta^{13}C$ values for both species during the peak pollution period. In contrast, in the lightly or moderately polluted areas, I expect minimal or no significant changes during the same period, except during the drought year of 1976. For the moderately polluted area, I anticipate at least slight changes due to its slightly higher pollution levels compared to the low polluted area.

Different approaches and indices are used to evaluate the intensity, frequency, and duration of drought conditions, leading to varying suggestions for the most severe drought years in Central Europe since the 1970s. These definitions and rankings are typically based on meteorological data and reflect a climatic perspective. In this study, I will analyze tree responses to past droughts to investigate differences among these events. By doing so, I aim to quantify drought impacts and propose a corresponding ranking from the perspective of tree responses. The results will also be contextualized using species indicator values, which suggests that spruce is more drought-sensitive than beech (Leuschner and Meier 2018). Therefore, I would expect narrower tree rings and higher $\delta^{13}C$ increases for spruce than for beech during drought years. Additionally, since beech is known to be more tolerant of pollution than spruce (Křeček and Hořická 2006; Kuneš et al. 2024), I anticipate narrower tree rings and higher $\delta^{13}C$ increase in spruce tree rings during periods of extremely high pollution.

2. Material and methods

2.1 Study sites

The study sites were chosen to represent varying levels of historical air pollution. The three selected areas are the Swiss Central Plateau (SCPA+B) with low and diffuse pollution, the Black Forest (BF) with moderate and diffuse pollution, and the Black Triangle (BT) with heavy pollution mainly from point pollution sources (Fig. 4 and 5). At each site spruce and beech are growing in mixed beech forests which enables direct comparisons of their responses to environmental stress. Silver fir is known for its sensitivity to pollution. Therefore it would have been an ideal species for this study, but due to historical forest management practices it is rare in the Black Triangle. This fact required to focus on spruce and beech (Rydval and Wilson 2012). Despite efforts to select sites with comparable ecological conditions, differences in elevation, soil properties, and climate could not be completely eliminated.

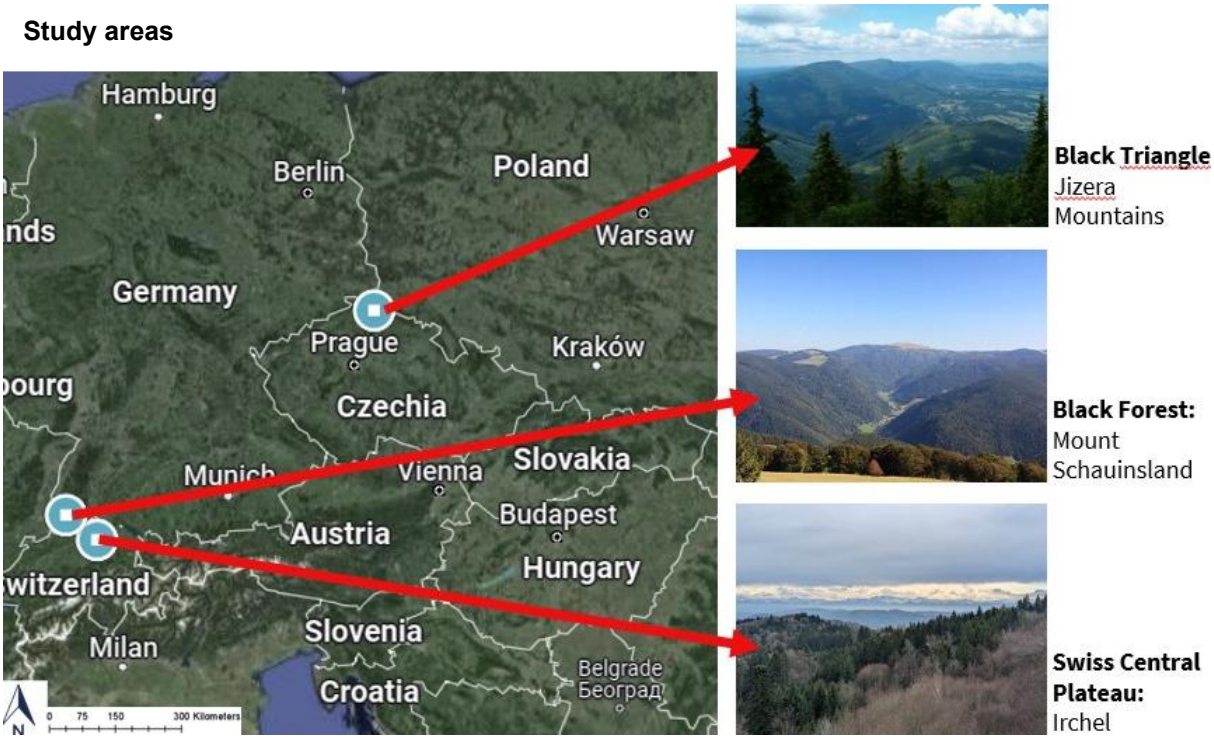

Fig. 4: Study areas (source: Google Maps, own photos)

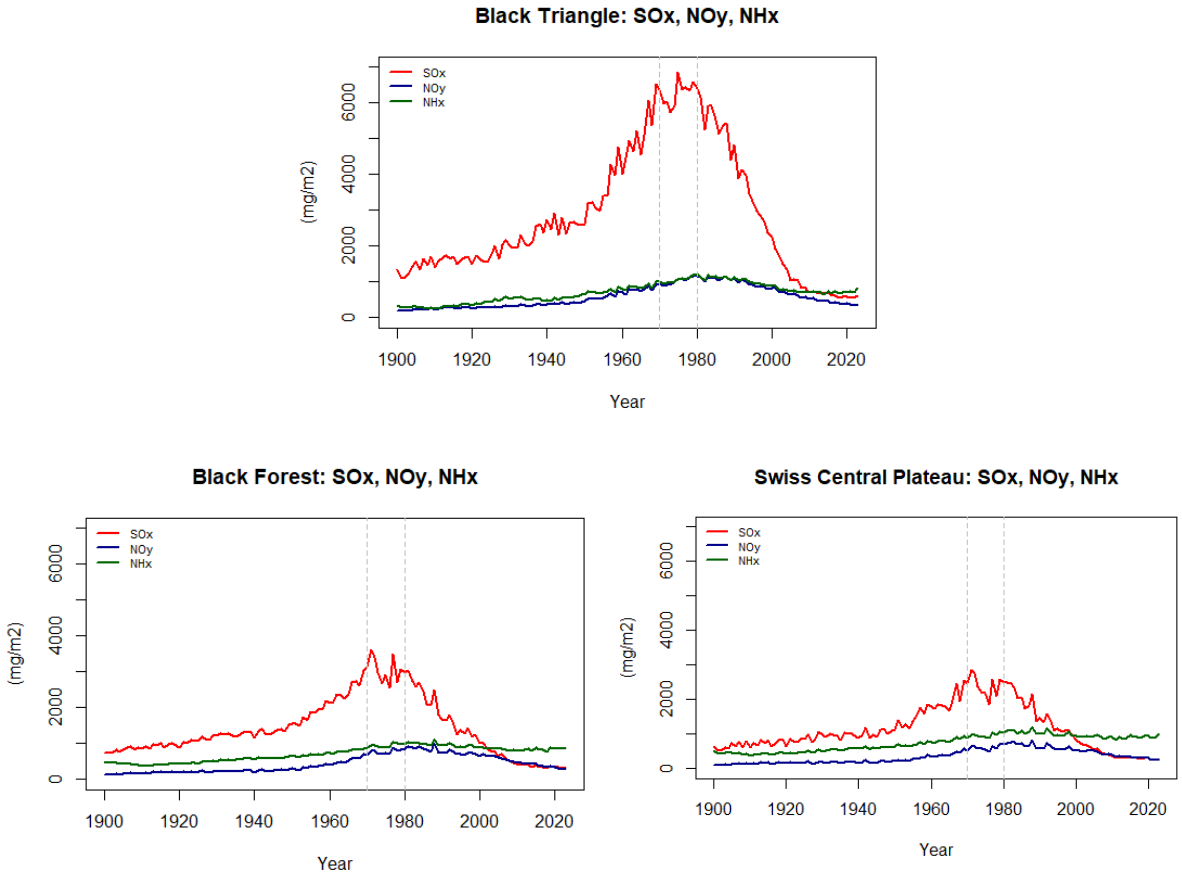

Fig. 5: Pollution at the study sites with marked peak pollution (grey) (based on data from Engardt et al., 2017)

2.1.1 Swiss Central Plateau

The first study site, named SCPA+B, is in the Irchel region, part of the Swiss Central Plateau, in the canton of Zürich, Switzerland. It lies in the countryside about 15 km northeast of Zurich, respectively 5 km northwest of Winterthur at 8°35'55" E and 47°32'46" N. This area is characterized by rolling hills, temperate forests, and agricultural landscapes. The Irchel is a prominent small hill range with a length of about 6 km and a width of about 2 km which directly borders the Rhine on the northwestern side. On 600–700 m.a.s.l there is a plateau with an elevation called Buechemer-Irchel at 694 m (swisstopo, 2024).

The Irchel region has a temperate climate with four distinct seasons and moderate annual temperature fluctuations (Fig. 6). Warm summers, with average temperatures above 15°C peaking in July and August together with cold winters around 0°C define the region with an annual mean temperature of 8.0°C. The annual precipitation averages 1032 mm and is distributed relatively evenly throughout the year, often as snow in winter. Precipitation patterns are influenced by the region's plateau location and remain consistent, with the highest rainfall occurring in late spring to early summer. According to Köppen-Geiger classification this region is placed in the Temperate Oceanic Climate (Cfb) category (ClimateDT, 2024; Köppen, 1918).

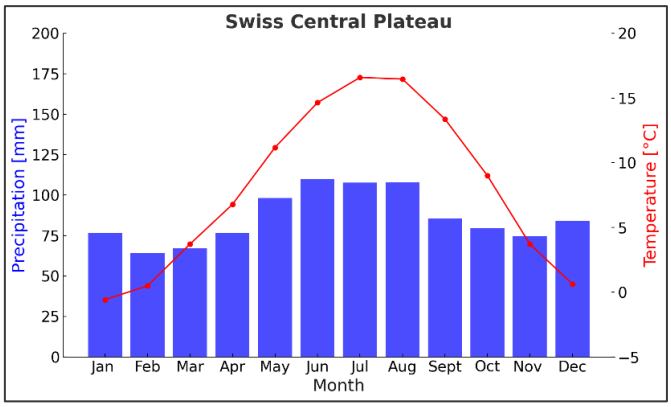

Fig. 6: Climate diagram SCPA+B (based on data from Marchi et al., 2024)

In this area, two sampling locations (Fig. 7 and 8) were selected at an elevation of approximately 660 m.a.s.l. on the plateau. The vegetation map of the area, combined with knowledge from local foresters, did not identify any slopes comparable to the two other study areas in terms of soil and plant communities. Therefore, the plateau was chosen as it matched these criteria. Efforts were made in advance to find a suitable study area in various other parts of the Swiss Central Plateau, but without success, as in most cases, one of the tree species was either absent or far too young at the required elevation. During fieldwork on Irchel, it became apparent that the spruces at the first sampling site were too young for this study, which required to include another sampling site. SCPA, the first site, contains younger trees and has been managed by forestry in recent years, while SCPB is located approximately 700 m to the north, in an area with older trees that has not experienced forestry interventions in recent decades. Irchel, which is Celtic for oak, was originally covered with oak forests, but these were removed in the

past due to human activity. According to the local forester, the area was reforested with spruce in many places after World War II. The forests in the Irchel region are part of the temperate broadleaf and mixed forest biome. The vegetation at the sampling locations is dominated by species such as European beech, Norway spruce and silver fir, with a mix of deciduous and coniferous trees.

The soil at the sampling locations is predominantly acidic brown earth and parabrown earth (luvisol), partially very weakly pseudogleyed, with a high clay content and fine soil texture, classified as clayey loam. They are moderately fertile, slightly water-logging and thus provide good water retention, resulting in a balanced water regime that benefits forest ecosystems due to reduced risk of drought stress. The geological composition is influenced by calcareous molasse deposits, and the area was not glaciated during the last ice age. These soils are derived from gravel deposits of the Mindel glaciation period and are characterized by normal permeability, moderate aeration, with plant-available rooting depth ranging from moderately deep to deep (Geoportal Kanton Zürich, 2024).

At the Irchel, historical pollution was low and diffuse with a slight increase of SO_x since the 1960s peaking around the 1970s followed by its gradual decline thereafter. NH_x and NO_γ deposition also increased, but to a lesser extent and reached their peak a bit later, during the 1980s. NO_γ then declined while NH_x only decreased minimally and remained at an almost unchanged level (Engardt et al. 2017). These trends reflect industrial growth, agricultural intensification, and subsequent pollution controls. While the Irchel region did not experience the severe industrial pollution pressures of areas like the Black Triangle, research in the 1980s attributed forest damage in this area to emissions (Wandeler 1982). Today, the forest faces N deposition from agriculture and climate variability. Rising temperatures and shifting precipitation patterns have increased droughts, stressing the ecosystem. The local forester identifies storms, droughts and bark beetle outbreaks as main causes for tree stress at this site.

Fig. 7: Managed site with younger trees on the Irchel plateau, SCPA (own photo)

Fig. 8: Unmanaged site with older trees on the Irchel plateau, SCPB (own photo)

2.1.2 Black Forest

The second study site, named BF, is located at the western slope of the Schauinsland mountain in Southern Black Forest, in Baden-Württemberg, Germany. It lies around 6 km south of Freiburg im Breisgau in its city district Günterstal at 7°52'21.7"E and 47°55'36.0"N. The BF is a large, dense forested mountain range in southwestern Germany, bordered by the Rhine Valley to the west and south. It covers an area of approximately 6000 km² and stretches for about 160 km from the south to the north with a width of 35–50 km. Some of the peaks are rising above 1000 m.a.s.l, such as Feldberg (1493 m) or Schauinsland (1284 m) . Geologically, the southern Black Forest is primarily composed of granite and gneiss. Glaciation during the Würm Ice Age shaped the region which resulted in geomorphological forms, such as U-shaped valleys, cirques, and moraines with periglacial solifluction deposits composing the underlying geology (Google Maps, 2024; LGRB, 2024).

The study site lies at an elevation around 750 m.a.s.l in the montane zone, where cooler temperatures and higher precipitation are prevailing compared to lowland areas. Its position is at right angles to the prevailing westerly winds that bring precipitation. It is characterized by moderate temperatures peaking in July and August, consistent precipitation, and distinct seasonal variations (Fig. 9). It experiences four clear seasons, with an annual average temperature of 7.2°C. Summers are warm with average temperatures above 15°C, while winters are cold and below 0°C, often snowy. The average yearly precipitation in the region is around 1668 mm (ClimateDT, 2024). According to Köppen-Geiger classification, BF is located within the temperate oceanic climate zone (Cfb) (Köppen 1918).

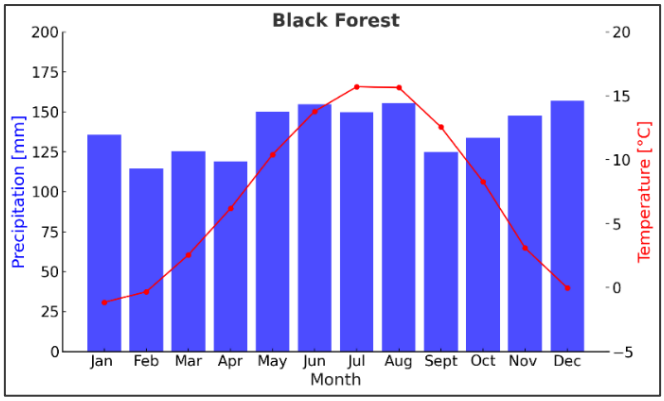

Fig. 9: Climate diagram BF (based on data from Marchi et al., 2024)

The BF derives its name from its dense, dark forests, though the dominance of conifers that can be seen today was less pronounced in the early Middle Ages when the name originated. Human activity has influenced the forest's composition over time. Extensive deforestation occurred by the mid-19th century due to high demand for fuel and timber, combined with grazing which often prevented natural regeneration. The introduction of regulated forestry in the 19th century resulted in widespread afforestation which led to the forests which are typical for the region today. At the study site, the forest is a mixed stand dominated by European beech, silver fir, and Norway spruce (LGRB, 2024).

The BF sampling location (Fig. 10) is situated at a winter slope and thus receives less direct sunlight during the winter months, tending to retain snow longer. The soil at the site developed from gneiss and is classified as brown earth, a common soil type in temperate forests with low acid buffer capacity and moderate fertility. Management practices at the site include recommendations for lime application to address potential pH imbalances and calcium deficiencies in the soil (Chair of Forest Growth and Dendroecology UFR, 2024; Hruška et al., 2023; LGRB, 2024). The slope reduces soil depth, affecting water runoff and microclimatic conditions (Leuschner 2020). The substrate is loamy-gravelly, which ensures good drainage and aeration, resulting in a balanced water regime which is neither excessively dry nor waterlogged (Brady and Weil, 2017; Chair of Forest Growth and Dendroecology UFR, 2024).

Fig. 10: Site at hillslope of the Schauinsland mountain, BF (photo: Hans-Peter Kahle)

At the BF site, historical pollution was low to moderate and diffuse, as no coal mining or power plants are located in the immediate vicinity. Despite this, SO_x slightly increased since the 1960s peaking around the 1970s followed by its gradual decline thereafter. Also, NH_x and NO_γ deposition increased, but to a lesser extent and reached their peak a bit later, during the 1980s. NO_γ then declined while NH_x only decreased minimally and remained at an almost unchanged level (Engardt et al. 2017). The decline in air pollution is attributed to air improvement measures introduced since the 1980s. NH_x emissions have decreased less as they mainly originate from livestock farming and agricultural fertilization which still continues (LUBW 2010).

In the late 1970s, a regional decline in forest growth and dieback of silver fir and Norway spruce was observed in the BF. Research proposed various hypotheses to explain the dieback, with air pollution and acid rain often cited as primary causes. While BF did not experience the severe pollution levels seen in areas near point sources, the diffuse nature of pollution still posed challenges to the region's forest ecosystems. However, various controversies also arose in relation to these reasons and questions about the lack of precedence (Kahle and Spiecker 1996). Recent research has shown that probably droughts causing reduced water availability have been closely associated with increased tree mortality and decreased growth. Successive hot and dry summers intensified these effects, causing prolonged drought impacts that persisted for several years. Additionally, droughts not only weakened trees directly but also promoted bark beetle outbreaks, which further increased mortality rates (Spiecker and Kahle 2023).

2.1.3 Black Triangle

The third sampling location, named BT, lies in the Jizera Mountains (Jizerské hory) which are in northern Bohemia, Czech Republic near the Polish border and are part of the Western Sudetes at 15°08'04.4"E and 50°51'26.4"N. This mountainous area, spanning approximately 565 km², is characterized by a plateau between 700 and 900 m.a.s.l with peaks rising above 1000 m.a.s.l, such as Smrk (1124 m) and Jizera (1123 m) (Google Maps, 2024). The Jizera Mountains have a temperate climate with distinct four seasons (Fig. 11). Winters are cold with average temperatures below 0°C, and summers are mild above 10°C, with an annual mean temperature of 4.9°C, representing a predominantly cool climate. Precipitation is evenly distributed throughout the year, averaging 1373 mm annually (ClimateDT 2024). According to the Köppen-Geiger climate classification system, the BT region falls under the humid continental Dfb class. This classification is typical for regions in higher elevations, including parts of Central and Eastern Europe or mountainous areas (Köppen 1918). The climate is very humid because the Jizera Mountains are the first transcontinental barrier of the humid oceanic flow from the North Sea. Westerly winds bring moist oceanic air, resulting in frequent precipitation and substantial snowfall. In general, the precipitation sums in the Jizera Mts are typically 50% higher than in the surrounding lowlands (Lábusová et al. 2019; Kuneš et al. 2024). Recent climate trends, including rising temperatures and changing precipitation patterns, have increased the frequency and intensity of droughts. Historical droughts of the last decades have caused significant reductions in soil moisture and exacerbated stress on forests. Anticyclonic weather patterns, such as the Azores High during summer, are key drivers of these droughts, blocking moist air inflow and leading to prolonged dry periods (Brázdil et al. 2009).

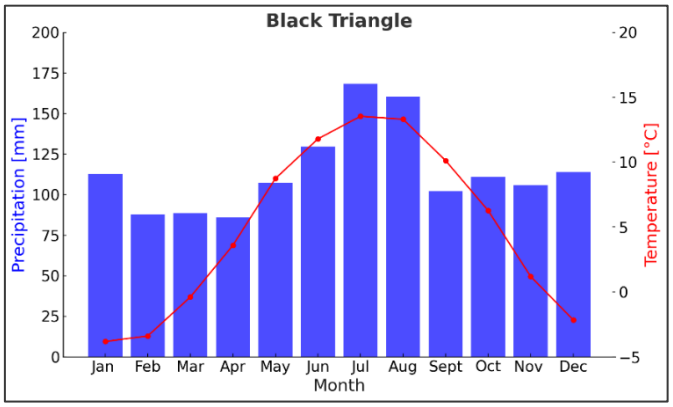

Fig. 11:Climate diagram BT (based on data from Marchi et al., 2024)

The BT site lies within the already mentioned Black Triangle, historically known for its extreme air pollution during the 20th century and its severely impacted environment and frequent winter smog episodes. In the 1970s and 1980s, the Jizera Mountains, like other mountain ranges in the region, experienced widespread forest decline due to heavy air pollution stress followed by outbreaks of insect pests. The most severe damage occurred in wind-exposed areas at elevations above 750 m. The most heavily affected stands have been removed through salvage logging (Akselsson et al. 2004; Kuneš et al. 2024). The main sources of pollution affecting the Jizera Mountains were power plant complexes located in

Turów, Hirschfelde, Hagenwerder, and Boxberg in Poland and Germany, due to the dominant air currents in the region. SO_2 emissions in the area increased more than tenfold between the 1950s and 1980s. The Turów Coal Mine (Fig 12 and 13), located near Bogatynia, Poland, directly borders the Jizera Mountains and has been a major contributor to the region's environmental degradation. It is active since 1904 and significantly expanded during the mid-20th century, Turów remains one of the largest open-pit lignite (brown coal) mines in Europe. The mine fuels the Turów Power Plant (Fig. 14), a coal-fired facility operational since 1962, which was a major emitter of SO_2, NO_x, and particulate matter during the 20th century. The emissions of the power plant peaked in the 1970s and 1980s which heavily contributed to soil acidification and forest dieback across the Jizera Mountains. Combined with harsh meteorological conditions and nutrient-poor soils, these emissions created severe stress for the local forests, particularly for Norway spruce. Although modernization efforts during the 1990s, including the installation of flue-gas desulfurization systems, drastically reduced SO_2 emissions, the mine and plant's legacy effects continue to influence the region. Soil acidification, magnesium depletion, and other nutrient imbalances persist, exacerbating the vulnerability of forests to climatic stress (Lomský et al. 2012; Rydval and Wilson 2012). Additionally, the ongoing expansion of the Turów Mine poses new challenges. The extension of mining activities closer to the Czech border has raised concerns about groundwater depletion, which could further reduce water availability in the Jizera Mountains and intensify the impacts of drought (Brázdil et al. 2009). The Turów Power Plant is situated about 16 km northwest of the sampling location, which allows an examination of the regional impacts of point-source pollution on forest ecosystems. The BT site was heavily exposed to S and N deposition during the 1960–1990s period. SO_x deposition peaked in the 1970s and then gradually declined. NO_γ and NH_x deposition peaked later, in the 1980s, and both decreased afterward, with NO_γ declining slightly more than NH_x (Hůnová et al. 2014; Engardt et al. 2017).

Fig. 12: Turów coal mine and power plant (own photo)

Fig. 13: Turów coal mine (photo: Wikimedia Commons/Anna Uciechowska)

Fig. 14: Turów power plant (photo: Wikimedia Commons/Werni1)

Fig. 15: Jizera Mountains in the early 1990s. Most of the upper plateau was covered by the clear-cut tracts and died forests (photo: Kuneš et al., 2024)

Fig. 16: Study site at the Jizera Mountains, BT (own photo)

The Jizera Mountains were originally covered by diverse mixed forests, predominantly composed of Norway spruce, European beech, and silver fir. During the period of forest dieback, Norway spruce was particularly affected (Fig. 15). Huge areas were clear-cut as a result, and reforestation efforts prioritized fast-growing spruce monocultures. However, these monocultures are highly susceptible to drought, pests, and other ecological pressures (Lomský et al. 2012). Current restoration initiatives aim to increase species diversity, with a particular focus on reintroducing European beech which is known for its superior resilience to both drought and pollution (Křeček and Hořická 2006; Kuneš et al. 2024). The BT sampling location (Fig. 16) is situated at a western slope at the border to the Jizerskohorské Bučiny, an UNESCO World Heritage Site and one of Central Europe's oldest and most extensive natural beech forests. These forests are characterized by their exceptional biodiversity. The natural vegetation in the study area includes mainly mountain acidic beech-dominated forests and small areas of high-elevation spruce forests. The area also reflects the challenges associated with soil acidification, historical air pollution, and climatic extremes (Lomský et al. 2012; Rydval and Wilson 2012; Lábusová et al. 2019). The soils of the sampling location are predominantly acidic brown earths and Podzols, derived from granitic

and granodioritic parent materials. These soils are naturally nutrient-poor and have low buffering capacity, making them highly sensitive to both drought and pollution. Despite all the complications, most of the clear-cut tracts in the Jizera Mountains were replanted successively between 1990 and 2010 and soil and water chemistry improved (Lomský et al. 2012; Kuneš et al. 2024).

2.2 Environmental data

2.2.1 Climate data

Because there were no climate stations near the sampling sites, climate data covering 1901 to 2023 came from the ClimateDT portal. This is a global tool that provides high-resolution monthly temperature and precipitation data, making it especially useful for regions with complex landscapes. It combines data from multiple sources, including the CHELSA 1981–2010 climatology, CRU-TS historical climate data, and future climate projections from CMIP5 and CMIP6 models. The system uses a method called dynamic downscaling, which adjusts climate data for local conditions. This includes bilinear interpolation and corrections for temperature changes with elevation, known as lapse rates. Unlike the standard lapse rate (6.5°C per 1000 meters), ClimateDT accounts for the actual temperature changes in a specific area. These adjustments ensure more accurate temperature and precipitation estimates, especially in areas with significant elevation differences. A major benefit of ClimateDT is its ability to connect historical and future climate data. For historical data (1901 to the present), the system applies anomalies based on the 1981–2010 baseline to CRU-TS datasets. For future scenarios, consistent baselines are used to reduce biases. This makes ClimateDT a reliable alternative when direct climate measurements are not available (Marchi et al. 2024).

In this study, mean monthly temperature and total monthly precipitation data were used as primary climate variables. Monthly average temperatures for each year were calculated using the minimum and maximum temperatures provided for each month by ClimateDT. To do this, monthly minimum and maximum values were summed and then averaged by dividing the sum by two. These data then were used to calculate the Standardized Precipitation-Evapotranspiration Index (SPEI), a drought index that combines precipitation and potential evapotranspiration (PET) to assess moisture balance anomalies. SPEI is well suited for evaluating short- and long-term droughts. Its calculation followed the methodology outlined by Vicente-Serrano et al. (2010), using the R package "SPEI". The process involved several key steps to analyze drought conditions. First, PET was calculated using monthly temperature data and the site latitude, applying the Thornthwaite method. This ensured that temperature-driven evapotranspiration was accurately represented for each site. Next, the water balance was determined by subtracting PET from monthly precipitation, providing a measure of water surplus or deficit for each time step. The water balance data was then analyzed over various time scales, ranging from 1 to 12 months, to compute SPEI. This step captured cumulative drought or wet conditions over short to long periods, and any infinite or anomalous values from computation errors were replaced with plausible minimum values to maintain data quality. Significant drought years were identified by filtering SPEI values at a five-month

scale for those less than or equal to -1.5, which indicates severe drought conditions (Mckee et al. 1993). For all three sites, data from 1970 to 2023 were used to extract drought years based on this threshold, which revealed key periods of climate extremes during the study period.

This methodology was applied uniformly across all three study sites to ensure consistent calculations and facilitate comparison. By using temperature and precipitation data to calculate PET and water balance, SPEI provided a robust measure of drought intensity and duration for each sampling location. SPEI was selected instead of other drought indices, such as the Standardized Precipitation Index (SPI) or Palmer Drought Severity Index (PDSI), because it incorporates both precipitation and temperature data. This allows SPEI to account for evapotranspiration dynamics, making it more sensitive to the effects of climate change and variations in moisture balance. Its flexibility across multiple time scales also makes it suitable for analyzing both short-term and long-term drought impacts on ecosystems (Vicente-Serrano et al. 2010).

2.2.2 Pollution data

Due to the lack of uniformly collected or generally consistent air pollution data going back far enough in time, modelled data were obtained from the European Monitoring and Evaluation Programme (EMEP). This is an internationally coordinated program that monitors and models air quality and deposition across Europe. The EMEP network exists since the 1970s and provides high-quality, regionally representative data on major air pollutants, including SO_x, NO_γ, and NH_x. It plays an important role in understanding transboundary air pollution and supports policy development under the UNECE Convention on Long-range Transboundary Air Pollution (CLRTAP). This framework was instrumental in driving air pollution legislation in the 1990s, leading to significant reductions in emissions of air pollutants across Europe. The EMEP database includes gridded atmospheric deposition data based on chemical transport models and observations from a network of measurement stations (Engardt et al. 2017).

For this study, SO_x, NO_γ, and NH_x deposition were used instead of airborne compounds to better understand the total deposition affecting ecosystems. They represent not only direct gaseous inputs but also contributions from particulate and aqueous phases, which are important to understand nutrient cycling and soil acidification. Additionally, the deposition of these compounds is often separated into wet deposition and dry deposition, however for this study total deposition rates including both were used. The data were provided on a rotated latitude-longitude grid of approximately 50x50 km² (0.44° x 0.44°) as used by the RCA3 climate model and associated chemical transport models (CTMs). Each grid cell contains information on specific deposition values of the represented area (Engardt et al. 2017). To get the data for the sampling locations, first the grid cell was defined by means of closest proximity to the specified grid points of the EMEP data set. If the coordinate of the sampling location was between two grid points, then the average of the corresponding pollution values was calculated and used for further analyses. Then modelled pollution data based on model emep_rv4p4 were extracted for the years 1900 to 2023.

To ensure the reliability of the modeled air pollution data, correlations were conducted with measurements from local air quality monitoring stations near the study area, which began operation in the late 1980s or mid-1990s. These local station datasets included yearly pollutant concentrations, which were compared to the EMEP data. Pearson's correlation was used for the comparison to assess the consistency between the two datasets and to identify any potential biases. This step ensured that the air quality data used in the analysis accurately represented local conditions and minimized discrepancies that could affect further analysis. Local SO_2 and NO_x data for SCPA+B from the Lägern station was provided by the National Air Pollution Monitoring Network (NABEL), while NH_x deposition data for the nearby Level II monitoring plot Lägern was obtained from the Swiss Federal Institute for Forest, Snow and Landscape Research (WSL). For BF, SO_2 and NO_x data from the Schwarzwald-Süd station was sourced from the Landesanstalt für Umwelt Baden-Württemberg (LUBW), and NH_x deposition data from the nearby Level II monitoring plot Conventwald was obtained from the Forest Research Institute Baden-Württemberg (FVA). For BT, SO_2 and NO_x data from the Frydlant-Udoli station was supplied by the Czech Hydrometeorological Institute (CHMI), though no local NH_x deposition data was available.

Critical load values for S and N in this study were provided by the Swiss Federal Office for the Environment (FOEN), the German Environment Agency (UBA), and the Czech Geological Survey (CGS). These values were calculated based on the methodologies outlined by CLRTAP (Hettelingh et al. 2017; Geupel et al. 2022; UBA 2024). Using data calculated with the same methods ensured consistency and comparability of the critical loads. They are derived from site-specific assessments that include soil properties, vegetation types, and climatic conditions. The maximum critical load for S (CLmaxS) defines the highest S deposition that an ecosystem can tolerate without harmful acidification effects. It ensures that the soil's ability to neutralize acids (ANC) is strong enough to counteract incoming acid inputs, thereby avoiding long-term harmful impacts on the ecosystem's health and functionality. CLmaxS depends on factors like soil buffering capacity, the availability of base cations, and weathering rates. This makes it a key measure for assessing how well forest soils can withstand S deposition, particularly in regions with soils that are highly sensitive to acidification (Augustin et al. 2005; UBA 2024).

Maximum critical loads for N (CLmaxN) are calculated with the Simple Mass Balance (SMB) model, which compares N inputs (deposition) to outputs such as plant uptake and leaching. This ensures that N leaching stays within safe limits to protect ecosystem health. The model also considers processes like N retention in the soil and its ability to store N without harming water quality or disrupting ecosystem balance. In some ecosystems, such as forests, the combined effects of S and N deposition must be considered. Conditional critical loads address how these pollutants interact, ensuring that the deposition of one does not worsen the impact of the other. The critical load function (CLF) integrates both S and N to establish safe deposition limits that maintain ecosystem health. This approach is particularly important in regions where both pollutants significantly contribute to acidification and nutrient disturbances (FOEN 2016; UBA 2024).

In practice, critical loads are mapped across ecosystems which are classified according to the classification of the European Nature Information System (EUNIS). Harmonized land-cover databases and spatial deposition models are used for the calculations. Then they are validated and compiled into a European database under the framework of CLRTAP. The Coordination Centre for Effects (CCE) Status Reports regularly deliver detailed data on critical loads, maps showing where these loads are exceeded, and updates on methodologies. These reports form the scientific basis for evaluating pollutant impacts, guiding emission reduction strategies, and protecting sensitive ecosystems (Thomas Daphne et al. 2021; Bobbink et al. 2022; UBA 2024). Because critical load assessments require detailed site-specific data, this study used the critical load values calculated from the above-mentioned institutions and provided by the CCE Status Reports rather than calculating these values for each study site (Hettelingh et al. 2017; Geupel et al. 2022). The deposition values were then compared with the critical loads. Values available in eq/ha/year were multiplied by 32 g(S)/mol and divided by 2 (valence of S) or multiplied by 14 g(N)/mol and divided by 1 (valence of N) and then adjusted by dividing by 10 to convert to mg/m²/year. For nitrogen, NO_γ and NH_x are summed to obtain the total N deposition.

2.3 Sampling

For this study, increment cores were collected from the two tree species Norway spruce and European beech. The sampling took place at four sites. At each site, five trees of each species were selected, resulting in a total of ten trees per site. From each selected tree, two cores were extracted at breast height (approximately 1.3 m) using an increment borer (Haglöf, Sweden) with a 0.5 cm diameter (Fig. 17 and 18). The cores were taken from the two opposite sides of the stem at an angle between 120° and 180°, ensuring that a representative portion of the tree's growth was sampled. On slopes, they were taken parallel to the slope to avoid compression or tension wood which trees can produce because of mechanical stress due to gravitational forces.

The field sampling was conducted during different months. At BF, the sampling was carried out in December 2023, at SCPA+B in February 2024, and BT in May 2024. Each tree was carefully chosen to meet specific criteria: mature trees of (co-)dominant crown class showing no visible signs of illness or injuries. Additionally, the trees were located similarly within the micro-topography, ensuring minimal ecological variability. They were not situated near forest clearings or traffic roads to avoid the influence of external disturbances. Except for the slightly younger spruces from SCPA, the trees selected for sampling had a minimum age of approximately 100 years.

Fig. 17: Coring tree with borer (own photo)

Fig. 18: Borer with core (own photo)

2.4 Sample preparation for tree-ring width analysis

After collecting, the increment cores were stored in paper tubes and labeled properly, maintaining clear identification of the species and sampling location before being transported to the laboratory. During the preparation process, each core was carefully cleaned to remove any dirt or contaminants, then air-dried and weighed down to avoid warping. Unlike the usual practice of mounting cores on core holders, these cores were processed directly to avoid potential contamination from glue or other materials that might interfere with the results. This approach ensured the integrity of the data and preserved the natural state of the samples for accurate isotope analysis.

2.4.1 Microtome

Following the initial preparation, the cores underwent further preparation using a core-microtome. This is a specialized tool designed for cutting entire increment cores with precision. It creates plane surfaces while preserving the open cell lumina, which makes the wood cells clearly visible. The core-microtome consists of two main components: a core holder and a rigid sledge guidance with a pivot holder for microtome knives (Fig 19). The core holder stabilizes the core during the cutting process, while the adjustable positioning table allows precise control over the depth of the cut. The microtome knife was positioned to ensure smooth, incremental cuts. Some moisture was applied to the core's surface before cutting, which prevented damage to the cell walls because the cores had been dried. The cutting procedure was performed in stages, typically in increments of 10–20 mm, to maintain an even surface and prevent cell damage (Gärtner and Nievergelt 2010).

After the cores were cut using the microtome, they were further processed by sanding. While the core-microtome produced smooth and precise surfaces, sanding provided additional refinement as it enhanced the contrast between the annual rings. This step ensured that the year boundaries were clearer and more distinct, which was important for accurate ring-width measurements, the related dating, as well as isotopic analysis. Sanding was conducted with extremely fine sandpaper to avoid roughening the surface or damaging the wood structure. This final step in preparation made it easier to detect and measure the ring boundaries afterwards, which ensured that the data obtained from the cores were of the highest quality for subsequent dendroecological analyses.

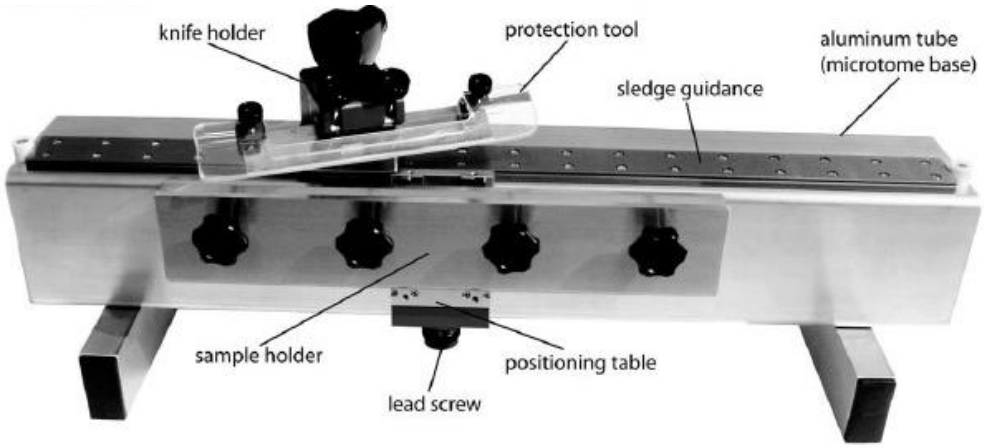

Fig. 19: Core-microtome (source: Gärtner and Nievergelt, 2010)

2.4.2 Digitalizing

After the cores were prepared using the core-microtome and sanding, high-quality digital images were created for further analysis using Skippy, a high-resolution image-capturing system developed at WSL (Fig. 20). For this the cores were separately placed on a computer-controlled platform that moved in predefined steps of 5 mm. At each step, a 61 MP camera (Sony Alpha 7R IV) with a Sony FE 90 mm f/2.8 Macro lens captured a high-resolution image. The autofocus of the camera resulted in clear, sharp photos with a resolution of 6500 dpi, which allowed precise visualization of individual cells and ring boundaries. To ensure accurate scaling, a calibration marker with millimeter measurements was placed next to the core during the imaging process. Once all photos from a core were captured, they were stitched into a single panoramic image for each core using PTGui (New House Internet Services BV). Blurry areas or photos were excluded during this process to ensure the final panorama was clear and sharp. The finished panorama was saved as a high-resolution TIF file to retain fine details for future applications. The digitization process captured even the faintest or narrowest rings that would have been difficult to discern with the naked eye. This sharpness ensured highly accurate data for the following dendrochronological and isotopic analyses. Additionally, these images served as a permanent digital archive of the core surfaces, allowing for future reanalysis and safeguarding (Gärtner et al., 2024).

Fig. 20: High-resolution image-capturing system Skippy (source: Gärtner et al., 2024)

2.5 Tree-ring width analyses

TRW analyses were conducted following the sampling preparation. This process includes measuring the TRW, crossdating the tree-ring series to ensure chronological accuracy, and examining relationships between tree growth, climate variations, and pollution levels.

2.5.1 Tree-ring width measurement

The TRW measurements were conducted using CooRecorder software (Cybis Elektronik & Data AB). This software is designed to accurately measure TRW from high-resolution images (Maxwell and Larsson 2021). The images used in this analysis are the stitched panoramas obtained in the previous step using Skippy. These images are loaded into CooRecorder for the measurement process. First, calibrating the photo was necessary by using the millimeter scale that was included in the photograph. This calibration step ensured that the image resolution was correctly interpreted by the software. When the image was calibrated, measurement points were placed along the boundaries of the tree rings, starting from the outermost ring and working inward. These points defined the width of each ring. The software can automatically detect ring boundaries, but it also allows manual adjustments if the boundaries are not clear or if there are anomalies in the sample, such as gaps or damage. This worked better for the spruce cores (Fig. 21) than for beech (Fig. 22), as the ring boundaries were more clearly recognizable due to the higher contrast. Thus, for beech the points had to be set all manually. After the measurements were complete, the data was saved in .pos files which contain coordinate data from TRW measurements and thus provides numerical data about TRW. The measured data from CooRecorder were organized in Cdendro (Cybis Elektronik & Data AB), where a collection of the samples from each species per site was created. These collections were saved as .fh files, which store TRW data for each sample. This type of file contains ring-width values arranged as a time series, along with metadata such as sample ID, species, and location. These files were used for further dendrochronological processing and analysis.

Fig. 21: Spruce core (own photo)

Fig. 22: Beech core (own photo)

2.5.2 Crossdating

After measuring the TRW, the next step was crossdating. This is the process of making sure that the tree-ring data from different samples or trees match the same years, which helped to create an accurate timeline of tree growth. The concept of crossdating, first developed by A.E. Douglass in the early 20th century, is fundamental to dendrochronology. It allows to establish exact calendar years for tree-ring formation, using patterns of ring growth that reflect environmental factors like climate. It is grounded in the principle of synchrony: trees in the same region show similar responses to environmental conditions. Years with extreme events, such as severe droughts, late frosts, unusually cold summers, or other climatic anomalies, leave clear and distinctive signals in the tree rings, making those years particularly useful for alignment. Crossdating also helps to identify irregularities such as missing rings (years when radial growth did not occur) or false rings (unusual growth interruptions that look like annual rings). By resolving these issues, crossdating ensures that the tree-ring sequences are precisely dated and aligned (Fritts and Swetnam 1989; Speer 2009).

For the procedure, first, the two cores (A & B) from the same tree were compared to ensure consistency in tree-ring counting and dating accuracy. Once the dating matched between the two cores, their ring-width measurements were averaged to represent the tree's growth pattern. In the next step, each core from another tree was crossdated with this initial average to check for matching patterns and ensure proper alignment. If a ring seemed to be missing in one sample while comparing the cores, the sample was brought back into CooRecorder. If a mistake was found in the measurement, then it was corrected or a missing ring was added manually. After successful crossdating, the two cores from the second tree were averaged with the initial average from the first tree. This iterative process was repeated for all sampled trees of the same species at one study site, resulting in a combined, crossdated timeline representing the species at the site. Finally, the average derived from the combined timeline was compared to a reference chronology of the same species growing at the same or a nearby site, as documented in

previous studies. These reference chronologies were kindly provided by Dr. Hans-Peter Kahle (University of Freiburg), Dr. Miloš Rydval (Czech University of Life Sciences Prague), and Daniel Nievergelt (WSL). This comparison allowed for an additional validation of the dating accuracy. The process was done using TSAP-WIN software (Rinntech Inc), which is made for crossdating tree-ring data. The software allowed to visually compare the tree-ring patterns from different samples and to make sure they align correctly. The software automatically calculates the distance between the measurement points and can save it in various file formats, including .rwd files. These .rwd files store TRW data and associated metadata, making them central for managing and processing measurements in dendrochronological studies. Crossdating is essential for creating reliable tree-ring chronologies, which form the foundation for further analyses. Without accurate crossdating, errors in ring alignment could lead to misleading conclusions, undermining the entire analysis.

2.5.3 Detrending of tree-ring width data

Detrending is a central step in dendroclimatology to separate climate signals from TRWdata. It removes long-term growth trends caused by tree age, size, or competition, and thus reduces "biological noise" and ensures that the data mainly reflect external factors like climate (Speer, 2009). Spline functions, especially cubic splines, are commonly used for this. They are flexible and can handle different growth patterns, preserving short-term variability which are essential for environmental reconstructions (Frank et al., 2022). The spline's length matters: shorter splines (e.g., 10 years) highlight fine-scale changes, while longer ones (e.g., 100 years) show broader trends. A 30-year spline often represents a good balance by keeping decadal and annual variations while removing long-term trends (Hughes et al., 2011). Standardization further processes the data by converting raw TRW into a Tree-Ring Width Index (RWI). This normalizes growth measurements by adjusting for the expected growth trend, ensuring that the resulting values reflect environmental influences rather than tree growth dynamics (Fritts & Swetnam, 1989). The RWI allows comparisons across different sites, species, and time periods, improving climate reconstructions and environmental analyses (Speer 2009).

The workflow for detrending was implemented in R using the dplR package, which is commonly used for dendrochronological analyses, and included the following steps:

1. **Data import and visualization**:
   TRW data were imported using the read.rwl() function for each site and species. First the raw data was visualized using ts.plot() to assess growth trends and identify any anomalies or patterns in the data.

2. **Building of undetrended chronologies**:
   Undetrended TRW chronologies were created by averaging the ring widths for each year, using the chron() function. The biweight robust mean was applied to minimize the impact of outliers. They were plotted as time series and served as a reference for subsequent detrending.

3. **Cubic spline detrending**:

   To remove long-term growth trends, splines with lengths of 10, 30, and 100 years were applied to the data using the detrend() function. The different splines were chosen to examine how short-term environmental variability can be retained while smoothing longer trends. With the detrended data, final RWI chronologies were built with the chron() function.

4. **Comparison of spline lengths and final selection**:

   The detrended chronologies for 10-, 30-, and 100-year splines for each species and site were plotted together with the undetrended chronology to evaluate their performance in order to select the most suitable spline for the following analyses. The 100-year spline, which is the least flexible, failed to capture short-term variations as it was too stiff. Thus, prolonged over- or underestimations of growth trends resulted. This limitation was particularly visible in the BT spruce data, where growth reductions during the 1970s and 1980s could not be smoothed effectively (Fig. 23). Similarly, abrupt changes in the BT beech data could not be addressed by the 100-year spline. In contrast, the 10-year spline closely followed year-to-year variations, smoothed management-related effects but the representation of long-term trends was reduced. The 30-year spline balanced long-term growth trends and short-term variability and stayed consistent across datasets. While differences from the 10-year spline were generally minor, the 30-year spline was selected for its ability to reflect broader growth patterns while retaining sensitivity to short-term changes and thus ensured that important environmental signals were accurately captured.

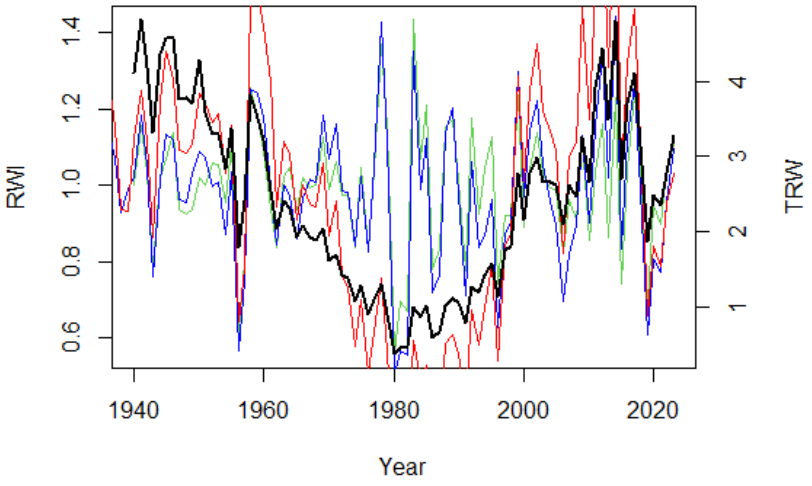

Fig. 23: BT spruce: undetrended chronology (black) with detrended chronologies for 10-year (green), 30-year (blue), and 100-year (red) splines

5. **Climate correlation analysis**:

   After building the final chronologies, year-to-year climate correlations, which are explained in more detail in a following section, were performed using the 10-, 30-, and 100-year detrended chronologies to examine possible differences. Although the overall patterns were consistent across all spline lengths, the correlation strength varied. The 30-year spline showed intermediate correlation strength and consistent patterns, which confirmed again the 30-year spline as the appropriate method choice for further analyses.

This approach ensured that the resulting chronologies were robust and suitable for analyzing the impacts of climate on tree growth in subsequent steps. RWI chronologies for beech and spruce were plotted together by site and species, with events such as years of highest pollution, recovery of air quality, and severe droughts previously identified using SPEI marked on the plots. These visualizations enabled qualitative assessments to identify potential relationships between these environmental stressors and observed growth reactions.

2.5.4 Statistical assessment of tree-ring chronology quality

Assessing the quality of TRW chronologies is a fundamental step in dendrochronology. This process ensures that the environmental signals captured in the dataset are robust and reliable for further analysis. Descriptive statistics such as the Expressed Population Signal (EPS), the average correlation between series (Rbar), and the Signal-to-Noise Ratio (SNR) are central tools in this evaluation. These metrics provide insights into the coherence and representativeness of the chronologies and thus facilitate the interpretation of environmental influences on tree growth (Cook et al. 1990; Speer 2009). Replication and statistical evaluation are important to ensure that chronologies accurately represent the environmental factors influencing tree growth. Metrics like Rbar, EPS, and SNR quantify the extent to which individual series share common environmental signals. EPS value ≥ 0.85 is considered a strong signal, indicating that a chronology reliably represents the broader population signal, while Rbar values above 0.5 highlight strong inter-sample coherence (Speer, 2009). High SNR values indicate a very strong common signal among tree-ring series and thus confirm the dominance of environmental signals over random noise, which makes a chronology suitable for ecological and climatic interpretations (Cook et al. 1990). In addition to these metrics, complementary descriptive statistics such as age range, mean age, and mean TRW were included to provide a more comprehensive understanding of tree growth dynamics. Also, mean TRW for 1970–1999 and 2000–2023 was calculated to assess changes in growth rates.

The quality of the TRW chronologies from this study was assessed using undetrended data in R. To create tree-level series, the treeMean() function was applied to aggregate core-level data for each tree. This ensured that each tree was equally represented in the analysis and minimized overlap from using multiple cores from the same tree. Tree-level means were calculated for all datasets. This aggregation ensured a robust representation of individual trees in the overall analysis. The aggregated tree-level means were converted into time series using the ts() function and visualized using ts.plot(). This step

provided a first overview of the growth patterns of the individual trees, helping to identify trends and potential anomalies in the data. Time series plots were created for all datasets to examine differences in growth patterns across sites and species. Descriptive statistics were computed using the rwi.stats() function. This provided values for Rbar, EPS, and SNR which validated the datasets for subsequent dendroecological analysis. Complementary metrics such as age range, mean age, and mean TRW were also derived from this function. Moving windows of 20 years with 10-year overlap were applied to assess how signal coherence and reliability changed over time. These analyses provided insights into periods of stronger or weaker signal consistency, which could reflect environmental influences or sampling variability.

2.5.5 Cumulative radial growth analysis

To investigate long-term growth trends and assess site-level dynamics, cumulative radial growth (CRG) was calculated for each tree and averaged across sites. The cumulative sums from the raw data were computed in R using the cumsum() function, which repeated adding the growth value of each year to the total of all previous years. As the pith is not always included or available in the sampled cores, the first year of the dataset does not necessarily correspond to the first year of growth of the tree. This method incorporated annual growth into a long-term trend, revealing patterns and changes over time. The CRG data were then converted into time series for visualizing growth trajectories of individual trees, site-level averages, and species-specific trends. Vertical lines were added to the plots to mark years associated with severe drought events and peak pollution. Like this, growth patterns in relation to environmental stressors could be visually interpreted.

Analyzing CRG provides valuable insights into the stand conditions affecting tree growth, reflecting ecological factors like competition, resource availability, and disturbance history. Differences in CRG curve levels can reveal site productivity or competition intensity, with higher levels indicating better growing conditions or reduced competition and lower levels suggesting greater competition, nutrient limitations, or stress. The shape of the curves indicates growth dynamics over time. Steeper curves suggest periods of accelerated growth due to favorable conditions, reduced competition, or suppression release, while flatter curves may point to stagnation caused by increased competition, poor climate conditions, pollution, or age-related constraints (Schwarz et al. 2020).

2.5.6 Climate and tree-ring width

The relationships between RWI and drought were further analyzed using Superposed Epoch Analysis (SEA) with standard errors. SEA is a statistical technique designed to identify the relationship between events, such as drought years, and time series data like RWI. It evaluates the average response of the time series during pre-defined time windows before, during, and after the drought events. Averaging across multiple drought events in SEA increases the SNR, making it easier to identify meaningful patterns against background variability. A double-bootstrap SEA approach was used in this study to address

uncertainties in event response relationships. This method repeatedly selected event years and calculated bootstrapped confidence intervals to address potential biases in selecting key years and account for the temporal structure of the data. It ensured accurate significance testing and captured the variability in growth responses to drought events (Rao et al., 2019).

For the analysis the R-script provided by Rao et al. (2019) was used. The input data consisted of RWI chronologies for beech and spruce, with selected drought years identified based on previously calculated SPEI values. However, only drought events with available data for at least three years before and after the event were included in the analysis. The SEA analysis was conducted using the sea_dbl() function. The SEA was performed separately for each species and region. Pre-event and post-event windows were defined as three years before and three years after each drought event, allowing for the examination of short-term growth responses and recovery patterns. Parameters such as the number of bootstrap samples (nboot = 1000), double-bootstrapping enablement (dbl = TRUE), and event-specific bootstrapped repetitions (nboot_event = 500) were applied to ensure robust significance testing. The calculations quantified the mean growth response and provided 99% confidence intervals for each year relative to the drought events. For each region and species, SEA provided average growth responses for each year relative to the drought events. These results were visualized with time series plots illustrating changes in RWI around drought years. The plots also included ribbons representing confidence intervals, which highlighted the reliability of the observed responses. The results provided insights into the sensitivity and resilience of tree growth to drought, and thus revealing species- and region-specific patterns of drought influence on tree growth.

For further data exploration, the relationship between RWI and climatic factors was investigated. High-frequency climate correlation analysis was conducted to explore the short-term relationships between climate variability and tree growth. This analytical approach specifically examines the influence of seasonal or monthly climate factors on RWI. The goal of this analysis was to pinpoint critical periods when these climate variables exert the strongest influence on tree growth. Identifying these relationships provided insights into the dynamic responses of beech and spruce to varying environmental conditions. The correlation analysis was conducted using the R-script “dplR and beyond_basic climate growth analysis” containing some useful functions developed by Dr. Stefan Klesse from WSL.

For this analysis, climate datasets for temperature, precipitation, and the previously calculated SPEI were used alongside RWI chronologies for beech and spruce. The time period starting in 1956 was chosen to ensure that all sites were represented by chronologies derived from data from five trees to ensure consistency and reliability across the dataset. To explore seasonal influences on tree growth, the monthly climate data were aggregated into larger seasonal windows using the function runningclimate_new(). This function enabled the creation of time series for varying seasonal lengths, ranging from individual months to twelve-month periods. Aggregation methods varied depending on the variable, with mean values calculated for temperature and sums for precipitation. To ensure the analysis captured high-

frequency variability, detrending was also applied to the climate data. The function spline.det() removed long-term trends by applying spline smoothing with a defined smoothing parameter, consistent with the 30-year spline used in tree-ring detrending. This step eliminated gradual changes over time while the interannual variability, which is central for identifying seasonal climate-growth relationships, was retained. The outputs included smoothed series, residuals, and ratios of the detrended data, all important for reliable correlation analysis. The central element of the analysis was the Climateplot_new() function, which was developed to compute correlations between RWI and aggregated climate datasets. This function analyzed RWI chronologies together with climate data as time-series, focusing on short-term climate impacts on tree growth. By using detrended data, it highlighted high-frequency variability and isolated the effects of climate on growth patterns. Using the Pearson correlation method, it measured the strength and direction of relationships between climate variables and tree growth, producing a matrix of correlation values. The rows of the matrix corresponded to seasonal lengths and the columns represented the end months of each aggregation period.

2.5.7 Air pollution and tree-ring width

Next, the relationship between air pollution and RWI was examined to understand its impact on tree growth over time. Scatterplots were used as the primary method to visualize the relationships between RWI and air pollutants for different species and regions. Separate scatterplots were generated for SO_x, NO_γ, and NH_x, each including regression lines to highlight trends in the data. These plots provided an initial visual assessment of how air pollution levels influenced tree growth during the analysis period. To further quantify these relationships, linear regression models were applied. These models analyzed how changes in air pollutant concentrations influenced RWI. They provided important statistical metrics for analysis and interpretation. The regression slope coefficient (β_1) was calculated to indicate the direction of the relationship, with positive values suggesting an increase in RWI with higher pollutant levels and negative values indicating a decrease. The coefficient of determination (R^2) was used to measure the proportion of variance in RWI that could be explained by changes in pollutant levels, highlighting the explanatory power of the regression model. Additionally, p-values were calculated to assess the statistical significance of these relationships, with smaller p-values (<0.05) suggesting a meaningful association between pollution levels and tree growth respectively with values above this threshold indicating that the observed relationships are likely due to random variation and are not statistically significant. By integrating regression models into the analysis, the study aimed to reveal differences in the sensitivity of beech and spruce to various pollutants and to identify regional variations in growth responses.

2.6 Carbon isotope analysis

After the TRW analysis, $\delta^{13}C$ analysis was carried out on BF and BT samples to further explore the physiological responses of trees to environmental factors. The study focused on $\delta^{13}C$ in tree rings as a marker for understanding the interaction between climatic and anthropogenic influences. This analysis built on previous findings from TRW, providing complementary insights (Andreu-Hayles et al. 2022).

2.6.1 Sample preparation for $\delta^{13}C$ analysis

To ensure accurate and reliable $\delta^{13}C$ measurements, precise sample preparation was critical. This involved the extraction of cellulose from tree-ring samples using a standardized protocol developed at WSL to ensure consistency and reliability. These following preparation steps ensured that the cellulose samples were of high purity and suitable for $\delta^{13}C$ analysis:

1. **Cutting and pooling:**

   Each annual ring from the year 1970 on was carefully separated under a microscope using a scalpel to ensure precision (Fig. 24). The material from the two cores of the same tree was then pooled prior to cellulose extraction. Pooling reduced the influence of individual core anomalies and thus reduced potential biases due to intra-tree variability. This improved the reliability and representativeness of the signal and enhanced comparability between samples from different species. Because some cores lacked sufficient material for $\delta^{13}C$ analysis in certain years, the tree rings were grouped into 5-year blocks from 1978–1997. This method was applied across all species and sites to ensure better comparability. Then, Teflon bags were prepared by cutting them in half and resealing the lower part to form smaller pockets. The wood samples were weighed into the Teflon bags (Fig. 25) and the weights were recorded on the extraction datasheets. The bags were then sealed with a heat sealer and labeled with binary codes for identification (Fig. 26).

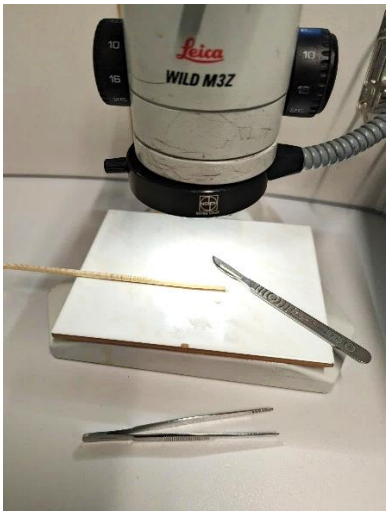

Fig. 24: Cutting the cores (own photo)

Fig. 25: Weighing into Teflon bags (own photo)

Fig. 26: Teflon bags with binary codes (own photo)

2. **Cellulose extraction:**

   The next step was cellulose extraction (Fig. 27), which involved chemically removing non-cellulosic components such as hemicellulose and lignin. This step ensured that only chemically stable material was analyzed which reduced the variability and improved the comparability across species and samples. Precision during ring separation and cellulose extraction ensured consistent and comparable results across samples (Helle et al. 2022).

Step 1: sodium hydroxide (NaOH) wash: A 5% NaOH solution (50 g NaOH per 1 L deionized water) was prepared. Up to 50 Teflon bags were placed in a 250 mL Erlenmeyer flask and covered with 500 mL of NaOH solution. The flask was heated in a water bath at 60°C for 2 hours. After 2 hours, the solution was poured out, and the bags were rinsed with boiling deionized water. This process was repeated to ensure thorough removal of non-cellulosic components.

Step 2: sodium chlorite ($NaClO_2$) treatment: A 7% $NaClO_2$ solution (87.5 g $NaClO_2$ per 1 L deionized water) was prepared, with the pH adjusted to 4–5 using 2–4 mL of glacial acetic acid. The Teflon bags were placed in the solution and heated at 60°C in a water bath. The solution was replaced every 10 hours, with a total extraction time of 30 hours to ensure complete delignification. Following this step, the samples were rinsed three times with boiling deionized water to remove any residual chemicals.

3. **Drying, homogenization, freeze-drying and folding**

After the washing steps, the Teflon bags were pre-dried to reduce moisture and placed in a drying oven at 60°C for ca. 6 hours. Once dried, the Teflon bags were opened, and the extracted cellulose was transferred to Eppendorf tubes. The yield of extracted cellulose was around 50% of the original sample weight. Then, 1 mL of deionized water was added to each tube, allowing the sample to soak for several hours. The samples then were homogenized using an ultrasonic transducer to ensure uniform consistency (Fig. 28). Following homogenization, the samples were frozen and subsequently freeze-dried for 3 days to prepare them for isotopic analysis. Finally, the freeze-dried cellulose was carefully folded into tin capsules for further isotopic measurements, ensuring compatibility with the analysis equipment. To avoid contamination, workspace and instruments were regularly disinfected, and all materials were handled only with gloves or tweezers. The cellulose was weighed before folding, targeting 1 mg ± 10% in each capsule to ensure consistent sample sizes.

Fig. 27: Cellulose extraction (own photo)

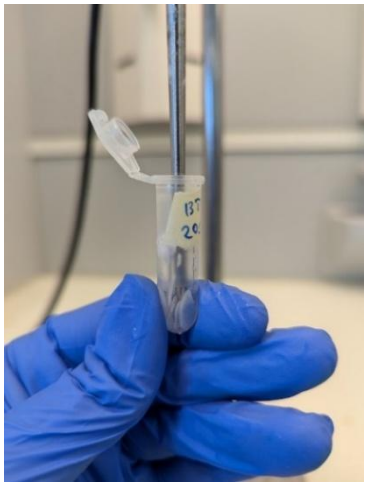

Fig. 28: Homogenization of cellulose with ultrasonic transducer (own photo)

2.6.2 Measuring $\delta^{13}C$

The isotopic composition of $\delta^{13}C$ in cellulose samples was measured using an Isotope Ratio Mass Spectrometer (IRMS), specifically the Sercon HS2022, coupled with the Sercon Iso-EA system. This setup enabled precise $\delta^{13}C$ measurements by combining an elemental analyzer with a mass spectrometer. The Sercon Iso-EA elemental analyzer combusted the cellulose samples into CO_2 gas. Each sample was automatically loaded into the combustion chamber, and the resulting gases processed through a chromatographic column to ensure purity before analysis. The purified gas then was transferred to the HS2022 IRMS for isotope analysis. The IRMS measured the ratio of $^{13}C/^{12}C$ in the CO_2 gas with high precision, separating isotopes based on their mass-to-charge ratio and thus quantified $\delta^{13}C$ for each sample (Sercon Ltd 2019b; Sercon Ltd 2019a). The IRMS generates raw $\delta^{13}C$ values which are expressed in per mil (‰) relative to the Vienna Pee Dee Belemnite (VPDB) standard, determined by analysis of a set of reference materials with known isotopic ratios. The precision of the analysis is ca. 0.1‰ (Saurer et al., 2024).

2.6.3 Correction and detrending of $\delta^{13}C$

To address the impact of declining atmospheric $\delta^{13}C$ values caused by fossil fuel emissions, an atmospheric correction was applied to the $\delta^{13}C$ data. This decline, known as the Suess effect, results from the release of CO_2 depleted in ^{13}C during fossil fuel combustion. Over time, this process has led to a gradual reduction in atmospheric $\delta^{13}C$, which subsequently affects $\delta^{13}C$ values in tree rings. As trees absorb CO_2 during photosynthesis, the decreasing $\delta^{13}C$ in atmospheric CO_2 is reflected in the $\delta^{13}C$ of tree-ring cellulose. To account for this, $\delta^{13}C$ values were adjusted using historical atmospheric $\delta^{13}C$ records obtained from ice core data and direct atmospheric measurements (Francey et al. 1999). This adjustment ensured that the corrected values reflected physiological responses of trees rather than shifts in atmospheric composition. After the atmospheric correction, $\delta^{13}C$ detrending was conducted in R. The same method used for TRW data was applied here, using a cubic smoothing 30-year spline. Furthermore, $\delta^{13}C$ chronologies and time series were generated and plotted for both corrected raw and detrended data, providing the basis for visual interpretation and analysis.

2.6.4 Statistical analysis of $\delta^{13}C$ responses to climate and pollution

This section extends TRW methods to $\delta^{13}C$, calculating EPS, Rbar, SNR, and mean values for reliability, coherence, and comparison. Chronologies with corrected raw data as well as indexed chronologies were examined. The relationship between $\delta^{13}C$ and drought was analyzed through SEA to identify responses to extreme climatic events, as well as Pearson correlation matrices to investigate correlation with climate variability. Scatterplots were used to visualize relationships, and linear regression was applied to undetrended $\delta^{13}C$ data to analyze the impact of air pollution. Both detrended and undetrended $\delta^{13}C$ data were used for climate correlations. The detrended data focused on isolating short-term climatic effects by removing long-term trends, such as those based on air pollution, while the undetrended data captured the combined effects of climate and longer trends.

To examine the combined effects of air pollution and climate on $\delta^{13}C$, multiple linear regression models were applied. This approach enabled the simultaneous evaluation of multiple independent variables, providing a more detailed understanding of their joint influence on $\delta^{13}C$. The models used $\delta^{13}C$ as the dependent variable, with SO_x and the climate variable showing the strongest correlations as independent variables. The analyses were conducted using the dyn package in R, which supports the incorporation of time-series data into regression models. The general structure of the models followed the format $lm(\delta^{13}C \sim SOx + climate)$, quantifying both individual and combined impacts of pollution and climate. This analysis offered insights into the strength and direction of these relationships and their interactions. To align with the $\delta^{13}C$ data, which were analyzed in 5-year blocks due to material constraints, corresponding blocks were constructed for air pollution and climate variables. Block averages were calculated for SO_x, NO_y, NH_x, and climate variables including temperature, precipitation, and SPEI. These blocks were aligned with the time periods showing the strongest correlations between $\delta^{13}C$ and climate variables, as identified in previous Pearson correlation analyses.

3. Results

3.1 Environmental conditions

3.1.1 Droughts

Calculating the SPEI from climate data obtained from the ClimateDT portal, aggregated over five months and filtered with a threshold of -1.5, identified the following years with severe drought conditions:

- **Swiss Central Plateau:** 2003, 2018, 2020, and 2022
- **Black Forest:** 1976, 2003, 2018, 2020, and 2022
- **Black Triangle:** 1976, 1990, 2003, 2018, 2019, 2020, and 2022

The five-month aggregation was selected as it aligned most closely with the most severe drought years documented in the literature (Schuldt et al. 2020; Hänsel et al. 2022; Spiecker and Kahle 2023). Focusing on two- or three-month aggregations during the growing season did not align with the known extreme drought years. Aggregations of five and six months produced better results, with the five-month aggregation providing the best match. However, comparisons showed that the classification of drought years also depended on the method used or the publication date of the studies. Older studies often emphasize droughts that, after the severe events of the past two decades, are no longer considered among the most extreme. Consequently, older studies identified more drought years in certain regions compared to the findings of this study (Brázdil et al. 2009). Furthermore, the years 2006, 2011, and 2015, often mentioned as drought years, were identified in this study only when using lower SPEI thresholds of -1 or -1.25 (Brunner et al. 2019; Klesse et al. 2022). The 2018/2019 period represents a prolonged two-year drought across all three regions, but 2019 is only identified as a drought year in the BT according to this

study's calculations. This suggests that the drought was particularly severe in the BT during the second year, potentially extending its effects and contributing to the 2020 drought. Finally, this study focused on the years 1976, 2003, 2018/2019, 2020, and 2022, as these are widely recognized as the most severe drought years in most studies and largely correspond with the SPEI calculations and are common across all three regions. The year 1976, although filtered with a threshold of -1.35 and not strictly meeting the -1.5 threshold for SCPA+B, was included as it falls within the 1970s, which belongs to the focus period of this study, and its SPEI value was very close to the threshold. It is also worth mentioning that when applying the lower thresholds of -1 and -1.25, moderate drought years during the 1980s, such as 1982 and 1989, as well as the more severe 1990, were identified for BT. When aggregating six months and using a threshold of -1 moderate droughts in the 1990s, specifically in 1991, 1993, and 1998 resulted for BF.

3.1.2 Pollution

Roughly calculated CLmaxS generally ranges from 800 to 1600 mg(S)/m²/year, with coniferous woodlands tolerating lower levels of 800–1200 mg(S)/m²/year, while broadleaved woodlands can withstand higher deposition levels of 1200–1600 mg(S)/m²/year. CLmaxN is estimated to range from 1400 to 2800 mg(N)/m²/year (Hettelingh et al. 2017; Geupel et al. 2022). In addition to these roughly estimated values, specific calculations have been performed for individual areas. The decades in which exceedances of these values occurred are summarized in Tab. 1 and further illuminated in the following sections.

Specifically calculated values for the Irchel area at SCPA+B are notable higher: CLmaxS is 4781 mg(S)/m²/year, and CLmaxN is 7435 mg(N)/m²/year (FOEN 2017). These elevated thresholds might be attributed to specific soil characteristics in the region. At SCPA+B, SO_x deposition peaked at 2854 mg(S)/m²/year in 1971, with the highest values occurring during the 1970s. By 2023, SO_x deposition had declined by 90%. NO_γ deposition peaked at 838 mg(N)/m²/year in 1988, while NH_x deposition reached 1202 mg(N)/m²/year in the same year. Combined N deposition at its peak totaled 2040 mg(N)/m²/year but never exceeded critical loads for N or S. By 2023, NO_γ deposition had decreased by 70%, and NH_x deposition declined slightly by 16%.

CLmaxS for the BF area were calculated to be 3200–4000 mg(S)/m²/year and are thus higher than the roughly calculated values from above (Augustin et al., 2005). CLmaxN derived from CCE status report 2017 are consistent with the roughly calculated values from above (Hettelingh et al. 2017). At BF, SO_x deposition peaked at 3626 mg(S)/m²/year in 1971. Critical loads for S exceeded the lower threshold during a few individual years in the 1970s; however, the upper threshold was never exceeded. By 2023, SO_x deposition had declined by 91%. NO_γ deposition peaked at 1001 mg(N)/m²/year in 1988, and NH_x deposition reached 1089 mg(N)/m²/year in the same year. Combined N deposition peaked at 2090 mg(N)/m²/year, exceeding lower critical loads from the 1970s to the 2000s but remaining below upper thresholds. By 2023, NO_γ deposition had decreased by 70%, and NH_x deposition declined by 21%.

For the Jizera Mountains, critical loads align with these roughly calculated values. CLmaxS ranges from 1154–1326 mg(S)/m²/year, and CLmaxN ranges from 2355 to 2568 mg(N)/m²/year, reflecting typical tolerance levels consistent with the estimated range above. At BT, SO_x deposition peaked at 6871 mg(S)/m²/year in 1975, exceeding upper and lower CLmaxS from the 1900s to the 2000s. By 2023, SO_x deposition had declined by 91%. NO_γ deposition peaked at 1169 mg(N)/m²/year in 1980, and NH_x deposition reached its maximum at 1221 mg(N)/m²/year in the same year. Combined N deposition peaked at 2390 mg(N)/m²/year in 1980, exceeded critical lower CLmaxN just during this year. By 2023, NO_γ deposition had decreased by 67% and NH_x deposition declined by 32%.

	SO_x exceeded lower CLmaxS	**SO_x exceeded upper CLmaxS**	**NO_γ+NH_x exceeded lower CLmaxN**	**NO_γ+NH_x exceeded upper CLmaxN**
SCPA+B	x	x	x	x
BF	1970s (few years)	x	1970s–2000s	x
BT	1900s–2000s	1900s–2000s	1980	x

Tab. 1: Exceedance of CLmaxS and CLmaxN

3.2 Tree-ring widths

3.2.1 Descriptive statistics of tree-ring width

Because five trees were available for each species from 1956 onward, descriptive statistical metrics were calculated for the entire dataset and for the period beginning in 1956. The values summarized in Tab. 2 highlight differences in growth patterns, environmental responses, and sensitivities across species and locations, as well as when comparing species within and across sites. The EPS of 0.85 was not achieved in all cases, but the values always exceeded 0.8, either for the entire dataset or for the period starting from 1956. Since these values are close to the reliability threshold, the chronologies still reliably represent the hypothetical "true" population signal of the sampled trees from each site.

	age range (years)	**mean age (years)**	**mean TRW (mm)**	**Rbar (all)**	**EPS (all)**	**SNR (all)**	**Rbar (1956)**	**EPS (1956)**	**SNR (1956)**
SCPAB	81–86	84	2.786	0.451	0.804	4.104	0.428	0.789	3.739
SCPAS	53–80	61	3.983	0.368	0.745	2.916	0.559	0.864	6.33
SCPBB	94–121	110	2.529	0.459	0.809	4.239	0.596	0.881	7.382
SCPBS	90–116	100	2.981	0.363	0.74	2.853	0.739	0.934	14.191
BFB	82–92	87	2.926	0.491	0.828	4.814	0.457	0.808	4.216
BFS	68–93	86	2.987	0.574	0.871	6.733	0.368	0.745	2.916
BTB	175–197	183	1.395	0.422	0.785	3.645	0.455	0.807	4.174
BTS	75–95	84	2.456	0.712	0.925	12.389	0.339	0.719	2.561

Tab. 2: Descriptive statistics of TRW for the entire dataset and 1956 onward

Beech generally showed lower growth rates and reduced sensitivity to year-to-year environmental variability compared to spruce, reflecting a more conservative growth strategy. This was evident in its lower Rbar, SNR, and EPS values in some cases. For example, at the SCPA site, where younger trees were growing, the EPS value for beech (SCPAB) decreased from 0.804 for the entire dataset to 0.789 for the post-1956 period. However, the corresponding Rbar values indicated moderate coherence in beech growth patterns, while the high SNR of 7.382 for SCPB beech (SCPBB) after 1956 demonstrated strong alignment with shared environmental signals. Spruce, in contrast, demonstrated higher growth rates and greater sensitivity to interannual environmental changes, which was reflected in its higher Rbar and EPS values across most sites. At the SCPA site, spruce (SCPAS) improved its EPS from 0.745 for the entire dataset to 0.864 after 1956. It is important to note that these are younger trees, which may have had less alignment with shared signals during the first years of growth. The corresponding increase in Rbar values further confirmed enhanced coherence in spruce growth after 1956. The exceptionally high SNR of 14.191 for the older spruces at SCPB (SCPBS) after 1956 highlighted its strong synchronization with shared environmental signals. At the BF site, spruce (BFS) showed higher Rbar (0.574) and EPS (0.871) for the entire dataset compared to beech (BFB) (Rbar 0.491 and EPS 0.828). However, from 1956 onwards, the differences between species became more pronounced at BF, as EPS of spruce declined to 0.745 while beech achieved a more stable EPS of 0.808. Spruce's continued sensitivity was reflected in its lower Rbar of 0.368, while the relative stability of beech was supported by its higher Rbar of 0.457. At the BT site, spruce (BTS) demonstrated the highest SNR of 12.389 for the entire dataset and an EPS of 0.925, reflecting robust environmental coherence. However, after 1956, its EPS decreased to 0.719, indicating some loss of shared signal. The corresponding Rbar of 0.339 confirmed reduced coherence, suggesting that intrinsic factors and external stressors during this period may have contributed to this decline. In contrast, beech (BTB) maintained an EPS of 0.807 with a Rbar of 0.455, indicating moderate alignment with shared environmental signals. Despite a slightly lower SNR of 4.174, beech showed stable growth patterns. The mean annual growth rates for both spruce and beech at BT were the only ones that increased during 2000–2023 compared to 1970–1999. At all other sites, mean growth rates declined over the same periods.

3.2.2 Cumulative radial growth

The CRG analysis showed differences between the sites and between the species. Except for BT, spruce indicated higher growth rates than beech, which suggested species-related differences in growth rate. Beech showed smoother CRG curves than spruce at all sites, indicating more stable growth compared to spruce. For instance, at BF and SCPA+B, spruce showed more pronounced dips during drought years than beech. At BF, recovery after droughts was slower for spruce than for beech. Differences between the species were further highlighted by the severe, long-lasting growth stagnation of BTS during periods of high pollution loads from the 1960s to 2000, followed by a fast recovery (Fig. 29). This could also be clearly seen as a long-term reduction in the plotted time series of the raw data (Fig. 30). In contrast, BTB showed only a small plateau from the late 1970s to the mid-1980s, coinciding with peak pollution of

SO_2, before it recovered to stable growth, which was also visible as a short-term dip in the raw data. Notably, there is no such plateau in the CRG curve at any of the other sites. For additional CRG plots and raw data, see Appendix A and B.

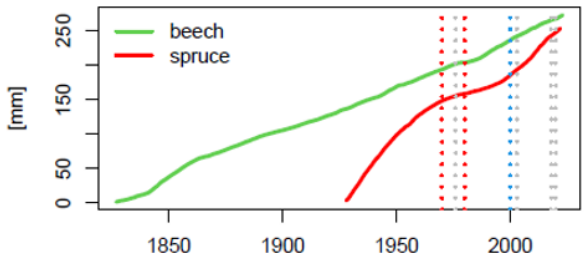

Fig. 29: BT spruce and beech mean CRG with marked droughts (grey), peak pollution plateau (red) and recovery of air quality (blue)

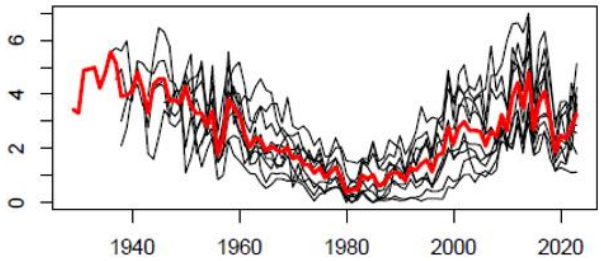

Fig. 30: BT spruce TRW raw data with average (red)

At SCPA, beech and spruce showed growth divergence beginning in the 1990s, with spruce exhibiting increased levels. This could indicate changes in conditions, such as reduced competition, suppression release, or superior growing conditions for some trees, possibly resulting from intervention, as this was a managed site. It should also be noted that the youngest trees of this study were growing at this site. Growth differences can also be attributed to age, with older trees showing slower growth trends compared to younger trees. This age effect was particularly visible in the beech curves, where older trees exhibited smoother curves, while younger trees had higher growth rates. Higher levels were observed for BTB, SCPBB, and SCPBS, which represented the oldest trees of this study. However, these differences may also reflect better growing conditions, varying site productivity, or competition levels, as the sites where the oldest trees were growing were unmanaged. For the younger trees at the managed sites, such as SCPA and BF, denser competition, nutrient limitations, or site-specific stressors could have played a role. When comparing CRG of the individual trees, beech showed relatively consistent levels across all sites until the 1990s, after which divergence became visible (Fig. 31). This change aligned with the increased occurrence and intensity of droughts during that time. In contrast, spruce showed greater variability in CRG levels across sites throughout the whole study period (Fig. 32). This was particularly visible at SCPA+B, where spruce showed site-dependent growth patterns, reflecting its sensitivity to local conditions.

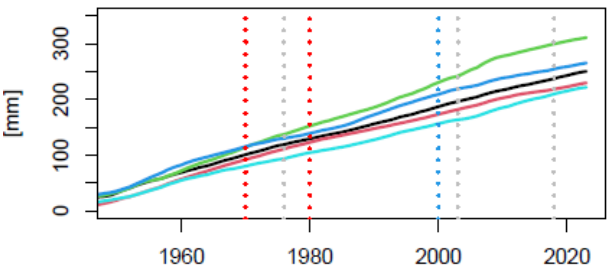

Fig. 31: BF beech CRG of the individual trees with marked droughts (grey), peak pollution plateau (red) and recovery of air quality (blue)

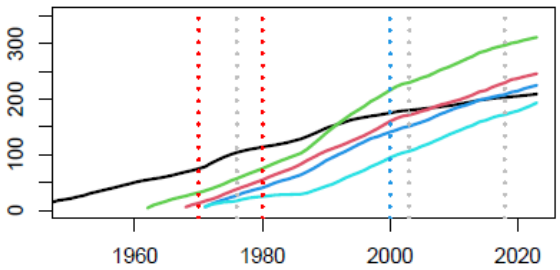

Fig. 32: SCPB spruce CRG of the individual trees with marked droughts (grey), peak pollution plateau (red) and recovery of air quality (blue)

3.2.3 Tree-ring width and drought events

The RWI analysis for spruce and beech during severe drought years highlighted site- and species-specific differences in growth response. During the 1976 drought, both spruce and beech experienced the most pronounced growth reductions at SCPB and BF, showing equally strong responses to the drought. In comparison, the growth reduction at BT was less pronounced. The SCPA site was excluded from this year's study because the trees were still in their juvenile age at that time. During the 2003 drought, spruce experienced the strongest growth reduction at SCPA+B, while beech was most affected at BT. During the prolonged drought of 2018–2019, spruce at BF and SCPA+B experienced the highest reduced growth in 2018, while spruce at BT showed the strongest growth reduction in 2019, the second year of the drought. Also, beech at BT exhibited a delayed response in 2019, with growth decreasing further in 2020. In contrast, beech at SCPA+B, and BF showed no growth reaction to the droughts of 2018 to 2020. Similarly, neither spruce nor beech at any site reacted to the drought of 2022. Tab. 3 summarizes the species-specific growth reductions during drought years at each site, complemented by RWI plots for all sites and species (Fig. 33 and 34) that illustrate the timing and magnitude of these reductions. Beyond the drought-related growth responses, a sustained period of growth decline was observed at the BT site for both beech and spruce. This decline began in 1978 for beech and in 1980 for spruce, lasting until 1983. Additionally, some spruce trees at BT exhibited missing rings in 1980 and 1981, and a notable growth reduction occurred in 1986/87. These declines aligned with episodes of harsh winters, frost events, cool summers, and heightened SO_x pollution. At the BF site, alongside the notable impact of the 1976 drought, a significant reduction in RWI was documented in 1986, coinciding with a cold winter and severe frost. At the SCPA+B site, beech exhibited its lowest relative growth values during the late frost event of 2017.

	1976	**2003**	**2018/2019**	**2020**	**2022**
SCPA	-	s<b	s<b (2018)	s<b	x
SCPB	s=b	s<b	s<b (2018)	s<b	x
BF	s=b	s<b	s<b (2018)	s<b	x
BT	s<b	b<s	s<b (2019)	b<s	x
spruce	SCPB & BF	SCPA+B	SCPA+B & BF (2018) BT (2019)	SCPA+B	x
beech	SCPB & BF	BT	x	BT	x

Tab. 3: Comparison of growth reactions of spruce (s) and beech (b) at different sites during drought years. Symbols indicate whether spruce or beech exhibited lower growth (s<b or b<s), equal growth (s=b), or no reaction (x). The sites with the highest growth reduction for each species are also noted.

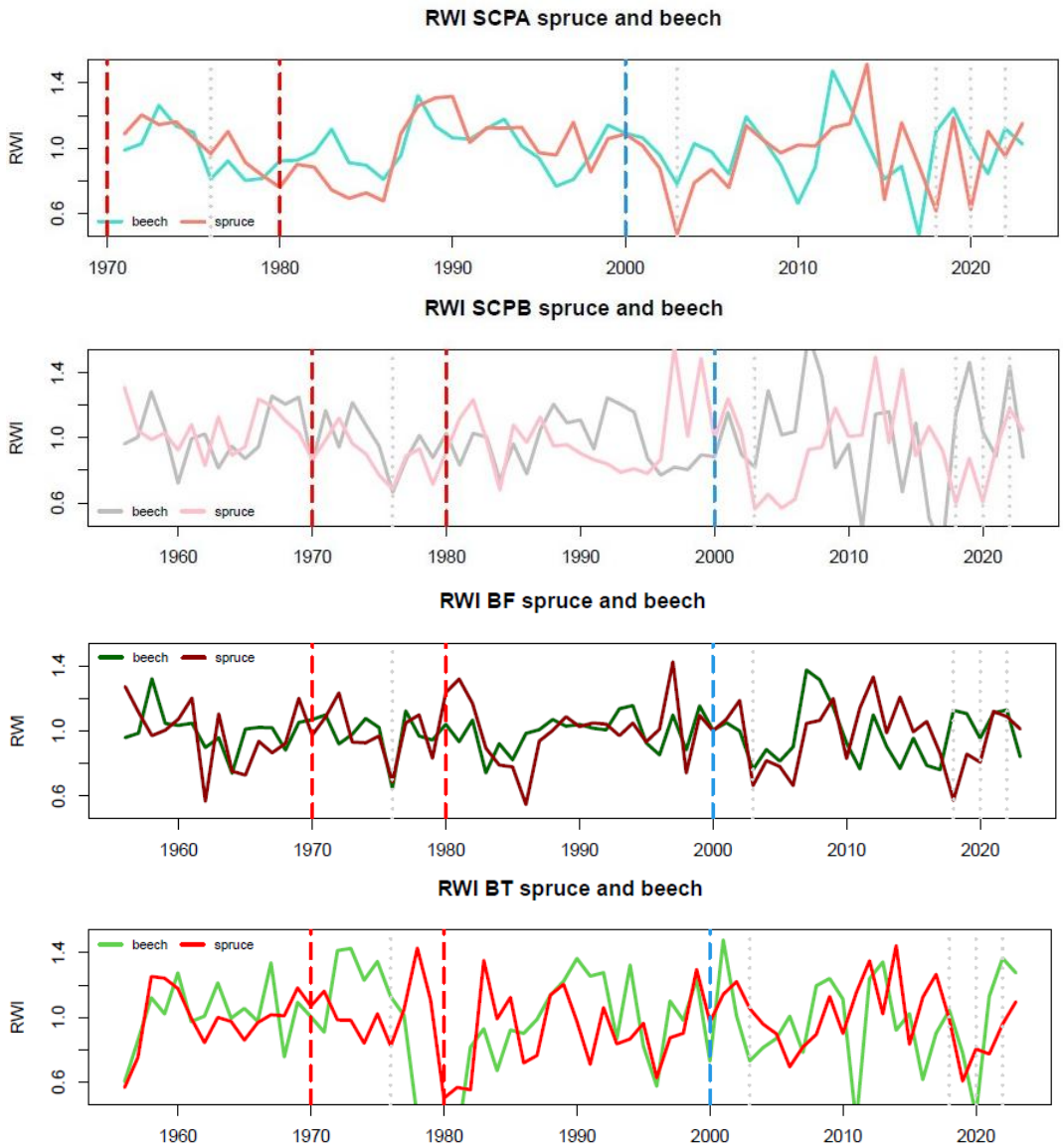

Fig. 33: RWI chronologies from each site with marked droughts (grey), peak pollution plateau (red) and recovery of air quality (blue)

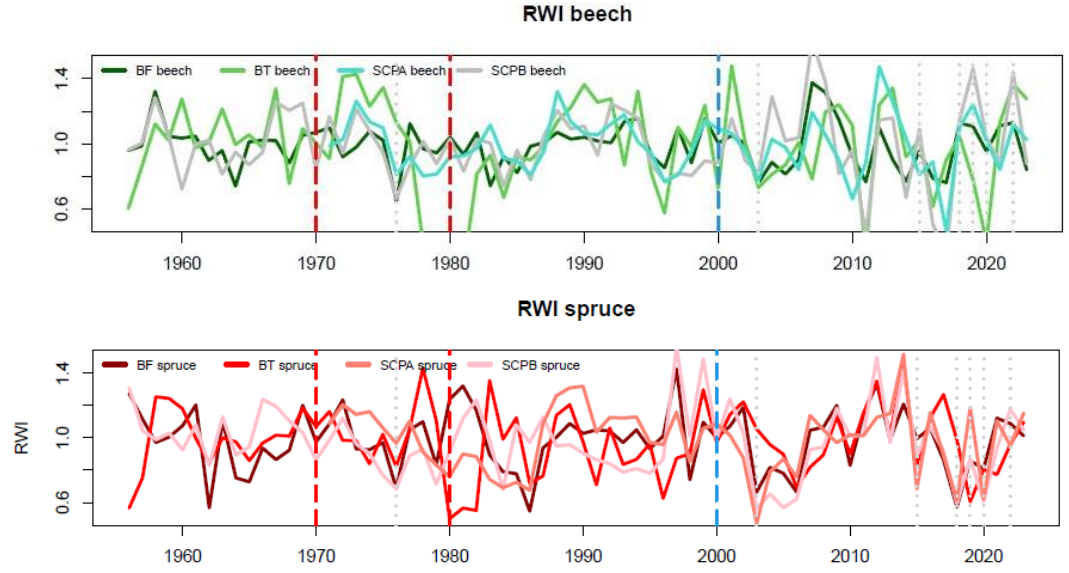

Fig. 34: RWI chronologies of spruce and beech with marked droughts (grey), peak pollution plateau (red) and recovery of air quality (blue)

The SEA analysis confirmed the findings obtained by comparing RWI chronologies. The average growth response during the selected drought years was exceptionally strong for spruce in BF and SCPA+B, with average TRW which were statistically significantly smaller during the drought events compared to all other years (Fig. 35). While an average growth decline of spruce at BT and beech at SCPA, BF, and BT during the drought events was observed, these reductions were not statistically significant and did not stand out as unique to the selected event years. Overall, beech showed a much smaller decline in growth during drought events, which indicated greater drought resistance compared to spruce. SCPA and BF exhibited the most pronounced growth reductions for spruce, which reflected higher sensitivity to drought conditions. In contrast, BT spruce showed minimal response to drought, differing from the trends observed at the other sites, which indicated less drought sensitivity of BT spruce compared to the other sites. Average RWI values for SCPA+B beech were notably lower in the year before the drought event, potentially indicating a pre-drought stress event, such as a prior drought or frost.

Fig. 35: SEA results, showing growth responses of spruce (salmon, pink, red) and beech (turquoise, grey, green) with ribbons representing 99% confidence intervals

3.2.4 Tree-ring width and climate variability

TRW sensitivity to climate varied by species and site. Tab. 4 summarizes species- and site-specific responses during peak growth, while Appendix C contains detailed $\delta^{13}C$-climate correlation matrices. At SCPA+B beech growth was most sensitive to June–July temperatures, indicating sensitivity to summer heat stress. Also previous year summer temperatures of July–August correlated negatively. Positive winter correlations at SCPA+B highlighted the benefits of mild winters. Negative correlations with July–August precipitation were observed, suggesting precipitation-related stress in late summer. Similar patterns were found for previous year rainfall during spring and early summer, with the older trees from SCPB additionally showing negative correlations with precipitation from previous autumn. For drought sensitivity (Fig. 36), weak positive correlations in May–June and the previous summer and autumn suggest that early summer and prior-year drought stress negatively affect tree-ring growth. However, negative correlations with SPEI for July–August suggested that beech growth was less adversely affected by drier conditions in late summer. Spruce growth at SCPA+B was sensitive to April–July temperatures, particularly in June–August, with positive winter and early spring correlations. Prior-year temperatures also influenced growth. Regarding precipitation, positive correlations with spring and summer precipitation, mainly June–July, indicated that water availability supported growth during the growing period. For drought sensitivity (Fig. 36), positive correlations with SPEI during spring and summer months, mainly June–July, showed that water balance strongly influenced spruce growth then.

Tree-ring growth of beech at BF showed negative correlations with temperature from March–July, with strongest in June–July. Regarding precipitation, beech showed the strongest positive response in June. In terms of drought sensitivity (Fig.37), positive correlations with SPEI in June indicated that beech suffered from drought during this critical period. Spruce growth in the Black Forest was strongly correlated with April–July temperatures. Precipitation had the strongest positive correlations with June–July precipitation, which highlighted the importance of sufficient water supply during summer. Thus, for drought sensitivity (Fig.37), also strong positive correlations with SPEI in June–July were observed.

At BT (Fig. 38), for beech was a weak negative correlation with RWI apparent in April and June, indicating that warm spring and early-summer temperatures may not favor growth. However, in July–August a positive correlation with temperature was visible, suggesting that warmer temperatures in late summer promote growth. A distinct pattern also emerged for precipitation, differing from the other sites, as beech seemed not to be precipitation sensitive. Similarly, no meaningful correlations with SPEI were found, indicating that TRW of beech was not sensitive to drought at this site. Spruce growth at BT (Fig. 38) also exhibited a very weak correlation pattern for temperature, with weak positive correlations for spring and summer temperatures and weak negative correlations only for June. Also, precipitation correlation patterns were very weak, showing positive correlation for August. Moreover, no meaningful correlations with SPEI were observed in the growing period just weak positive correlations for June and August–September were visible.

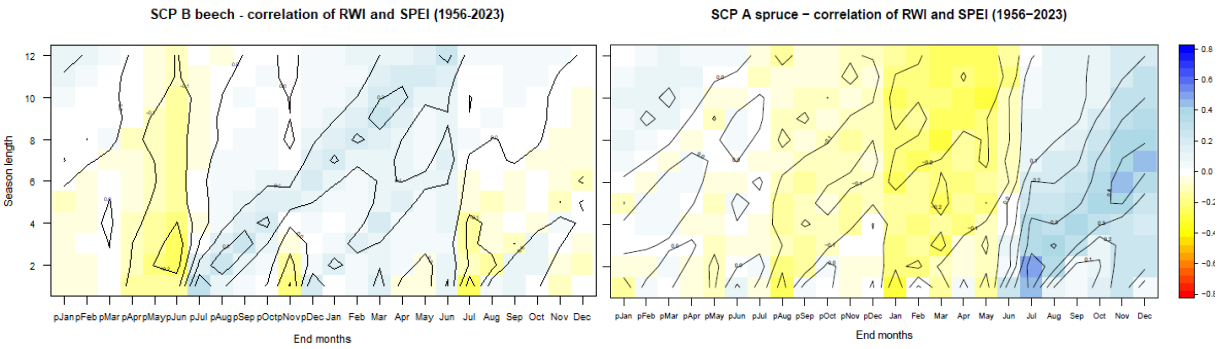

Fig. 36: Correlation matrices of RWI and SPEI for SCP beech and spruce

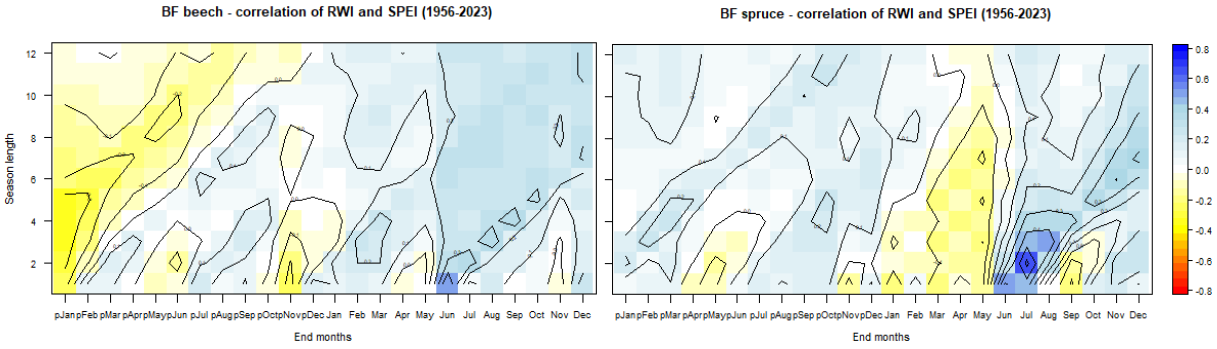

Fig. 37: correlation matrices of RWI and SPEI for BF beech and spruce

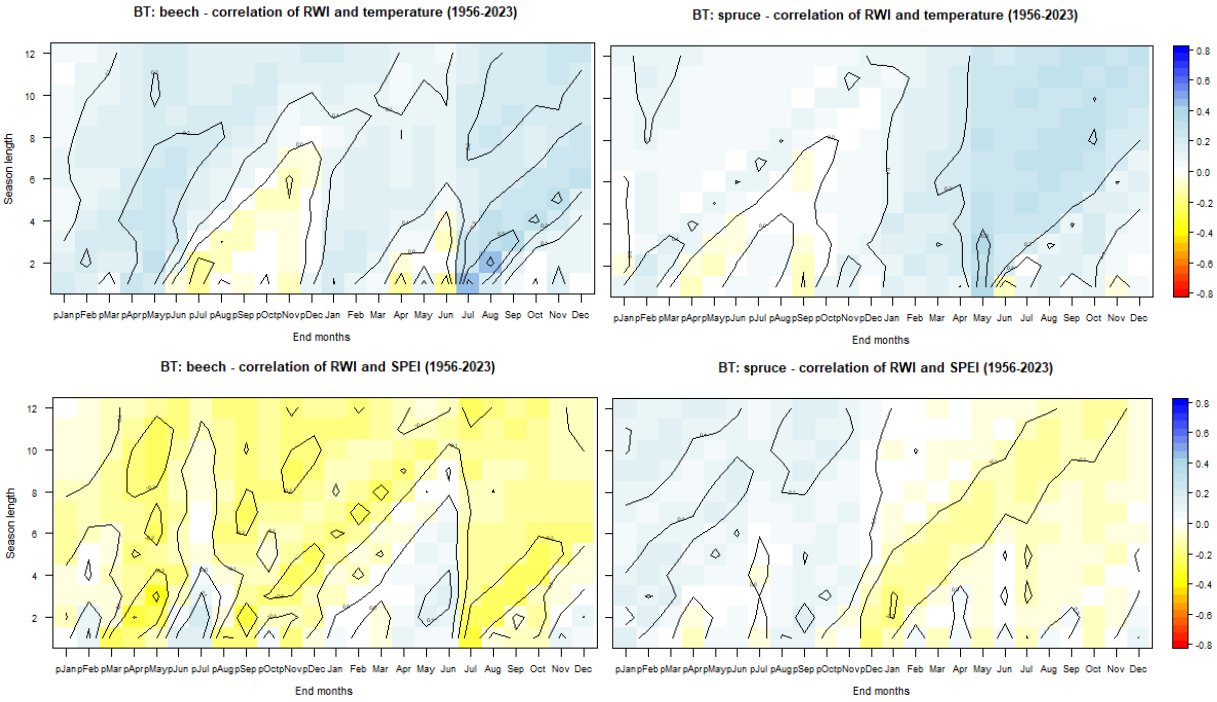

Fig. 38: Correlation matrices of RWI and temperature / RWI and SPEI for BT beech and spruce

	temperature	precipitation	SPEI
RWI - SCPA+B	s>b (-)	s>b (+)	s>b (+)
RWI - BF	s >b (-)	s>b (+)	s>b (+)
RWI - BT	b>s (+)	b>s (-)	x

Tab. 4: Comparison of TRW climate sensitivity of spruce (s) and beech (b) at different sites. Symbols indicate which species reacted more (s>b or b>s), or if there were no clear results visible (x) and the direction of the correlation (+/-)

3.2.5 Tree-ring width and air pollution

Single linear regression models across SCPB, BF, and BT showed weak relationships between air pollutants (SO_x, NO_γ, NH_x) and the RWI of beech and spruce. Beech generally exhibited positive coefficients for NH_x and SO_x, while spruce displayed negative coefficients for SO_x and NO_γ and positive coefficients for NH_x. However, the R^2 values were all very low, not exceeding 0.02, and none of the coefficients were statistically significant. Residual errors ranged from 0.16 to 0.23 at SCPB, 0.14 to 0.19 at BF, and 0.21 to 0.31 at BT, indicating considerable unexplained variability across sites. Beech showed less consistent growth patterns compared to spruce, as reflected in slightly higher residual errors, particularly at SCPB and BT. At BF, both species showed similarly weak and inconclusive relationships with pollutants. Overall, the models suggested that air pollutants had little to no measurable impact on the growth of beech and spruce, with growth variability probably driven by other ecological or climatic factors. Scatterplots of linear regression with corresponding metrics are provided in Appendix D.

3.3 Carbon isotope

3.3.1 Descriptive statistics of $\delta^{13}C$

The $\delta^{13}C$ analysis showed that BFB (Fig. 39) had overall weak metrics, with a Rbar of 0.152, an EPS of 0.472, and an SNR of 0.895, indicating poor coherence, low reliability, and a signal dominated by noise. A detailed temporal analysis using 20-year running windows with a 10-year overlap highlighted variability over time. The periods 1974–1993 and 2004–2023 showed moderate signal quality, with Rbar values around 0.36–0.38, EPS values around 0.74–0.76, and SNR values exceeding 2.8, which reflected improved coherence and reliability. In contrast, the period 1994–2013 showed a sharp decline, with a Rbar of 0.130, an EPS of 0.429, and an SNR of 0.750, causing the weak overall performance. During the study's focus period, the 1970s and 1980s, the metrics were considered sufficient for further analyses as they fluctuated around the minimum acceptable values. In contrast, all other datasets consistently demonstrated strong metrics, with Rbar values exceeding 0.62, EPS values above 0.85, and SNR values greater than 8 for the entire dataset (Tab. 5). Furthermore, the mean $\delta^{13}C$ values from both species were higher at the BT site, and at both sites they were also higher during 1970–1999 compared to 2000–2023. $\delta^{13}C$ series, chronologies and mean values are provided in Appendix E.

	Rbar	EPS	SNR
$\delta^{13}C$ BFB	0.152	0.472	0.895
$\delta^{13}C$ BFS	0.627	0.894	8.41
$\delta^{13}C$ BTB	0.774	0.945	17.094
$\delta^{13}C$ BTS	0.746	0.936	14.651

Tab. 5: Descriptive statistics for $\delta^{13}C$

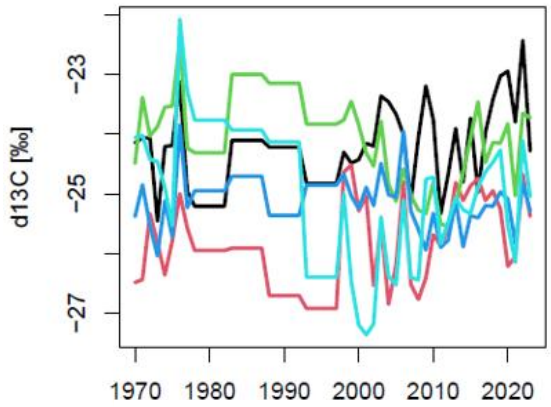

Fig. 39: $\delta^{13}C$ of individual beech trees at BF

3.3.2 $\delta^{13}C$ and drought

The $\delta^{13}C$ raw chronologies from spruce and beech at BF and BT, corrected for atmospheric ^{13}C of CO_2 (Fig. 40), showed that $\delta^{13}C$ values increased during drought events for both species at both sites. At BF, they decreased immediately after the 1976 drought event, indicating a fast recovery. In contrast, at BT, $\delta^{13}C$ values remained elevated for nearly two decades post-drought, with spruce even exhibiting a further increase during the 1980s while beech remained at a similarly elevated level. Unlike after the 2003 and 2019 droughts when both species at BT seemed to recover directly after the event. The hump in $\delta^{13}C$ values observed at BT during the 1970s and 1980s aligned well with the peak pollution levels recorded during that period. Also at BF, elevated values were visible then, but however, the increase was delayed compared to BT and was neither as strong nor as consistently high. The values at BF were also falling earlier and more gradually, compared to BT, where they fell abruptly at the end of the 1990s, along with the rapid reduction of air pollution. Beech at BF seemed to be more affected in the past few years than during the 1970s and 1980s. Similarly, at BT, $\delta^{13}C$ values of beech have been increasing again in recent years, indicating that beech has been experiencing greater stress from recent droughts. When comparing the detrended $\delta^{13}C$ index chronologies of the two species and sites (Fig. 41), differences in $\delta^{13}C$ increases during drought years became visible. The pooled year blocks could not be detrended, thus only values before and after were used to assess changes. In 1976, $\delta^{13}C$ values for both spruce and beech at BF were higher than at BT, with beech responding more strongly than spruce. In 2003, beech at BF also showed a greater increase, while at BT spruce exhibited higher $\delta^{13}C$. Spruce at BF fluctuated at higher levels after 2003, coinciding with milder droughts and heatwaves (2004, 2006, 2011, 2015), before peaking in 2020. Beech $\delta^{13}C$ at BF fluctuated at even higher levels than spruce after 2015, indicating it may have suffered more during this period, and peaked during the 2018/2019 drought. However, except for the period with higher fluctuating values in recent years, beech $\delta^{13}C$ values decreased more sharply after a drought event than spruce. At BT, both species showed their strongest increases in 2019 and responded more to the 2018/2019 drought than at BF, followed by sharp declines. During the 2020 drought spruce showed higher values at BF, and both species showed similar elevated values at BT. Unlike TRW, both species showed higher $\delta^{13}C$ values at BF during the 2022 drought, with the highest values in beech. Which species reacted more during which drought event is summarized in Tab. 6.

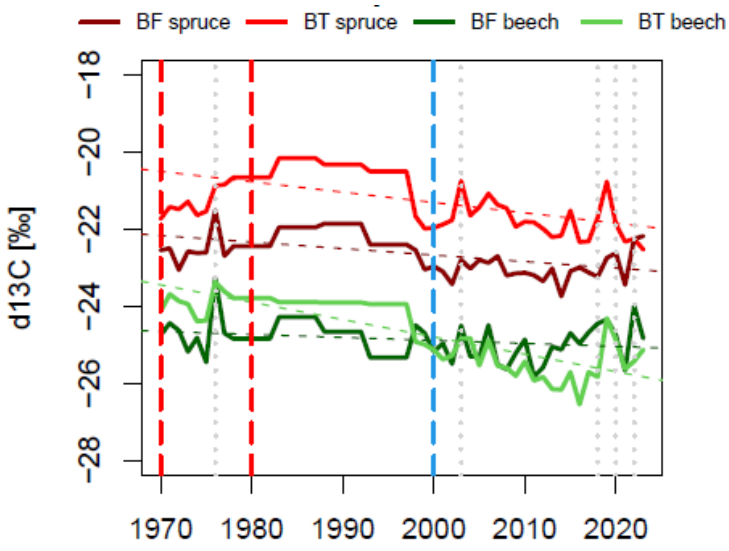

Fig. 40: Raw $\delta^{13}C$ chronologies with atmospheric correction for beech and spruce at BF and BT

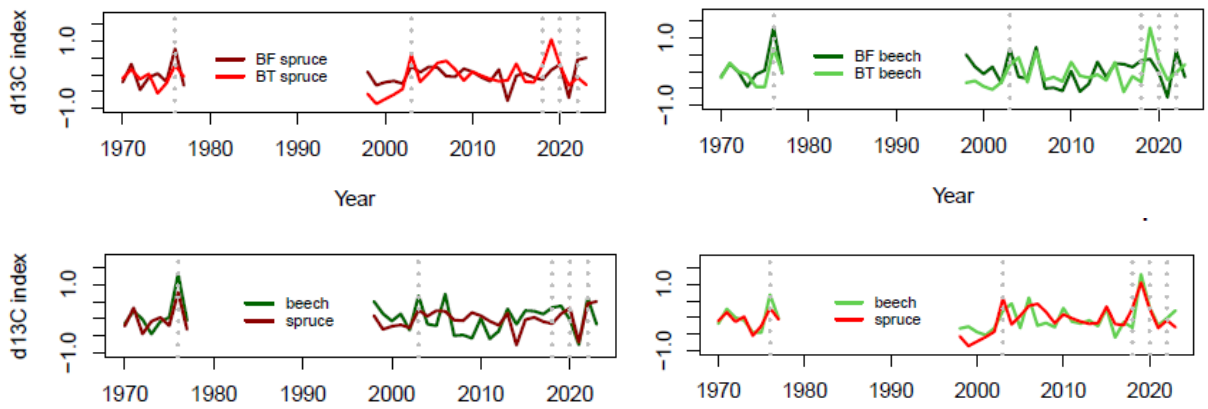

Fig. 41: δ¹³C index chronologies for spruce and beech at BF (bottom left) and BT (bottom right)

	1976	**2003**	**2018/2019**	**2020**	**2022**
BF	b>s	b>s	b>s (2018)	s>b	b>**s**
BT	b>s	s>b	b>s (2019)	s=b	x
spruce	BF	BT	BT (2019)	BF	BF
beech	BF	BF	BT (2019)	BT	BF

Tab. 6: Comparison of δ¹³C response of spruce (s) and beech (b) at BF and BT during drought years. Symbols indicate whether spruce or beech exhibited higher increases (s>b or b>s), equal increase (s=b), or no response (x). The sites with the highest δ¹³C increases for each species are also noted.

The SEA analysis (Fig. 42) was conducted using the drought years 2003, 2019, and 2020. The year 1976 could not be included because from 1978 on the years were pooled, and thus no average post-drought response would have been available for the analysis. Similarly, 2022 could not be included due to the lack of post-drought years for evaluation. The year 2019 was selected from this prolonged drought because the δ¹³C response was highest then. Both sites exhibited strong δ¹³C increases during the drought year, but the magnitude of the response differed between species and sites.

At BF, both beech and spruce δ¹³C showed a strong positive average response during the drought event, with spruce displaying a higher and statistically significant increase compared to beech. Post-drought, beech exhibited a steeper decline, indicating a faster recovery or reduced stress compared to spruce. In contrast, spruce maintained more consistently elevated δ¹³C levels, suggesting prolonged stress or slower recovery. Three years after the drought event, both species showed another pronounced increase in δ¹³C, probably reflecting the onset of the next drought. At the BT site, both species exhibited a sharp average increase in δ¹³C during the drought event, with beech reaching a slightly higher peak than spruce. However, only the increase observed in spruce was statistically significant. After the drought, spruce showed a steep decline in δ¹³C immediately following the drought year, followed by a gradual

recovery in subsequent years. In contrast, beech displayed a slower and more gradual decrease in $\delta^{13}C$ values post-drought, reflecting a less abrupt response compared to spruce. The peak $\delta^{13}C$ response at BT was stronger for both species compared to BF, suggesting that drought conditions at BT may have been more severe or that additional stressors amplified the response. Both species already showed elevated $\delta^{13}C$ values in the year before the drought event, which can be attributed to the two-year drought of 2018/2019, during which higher $\delta^{13}C$ values were already evident in the first year of the drought.

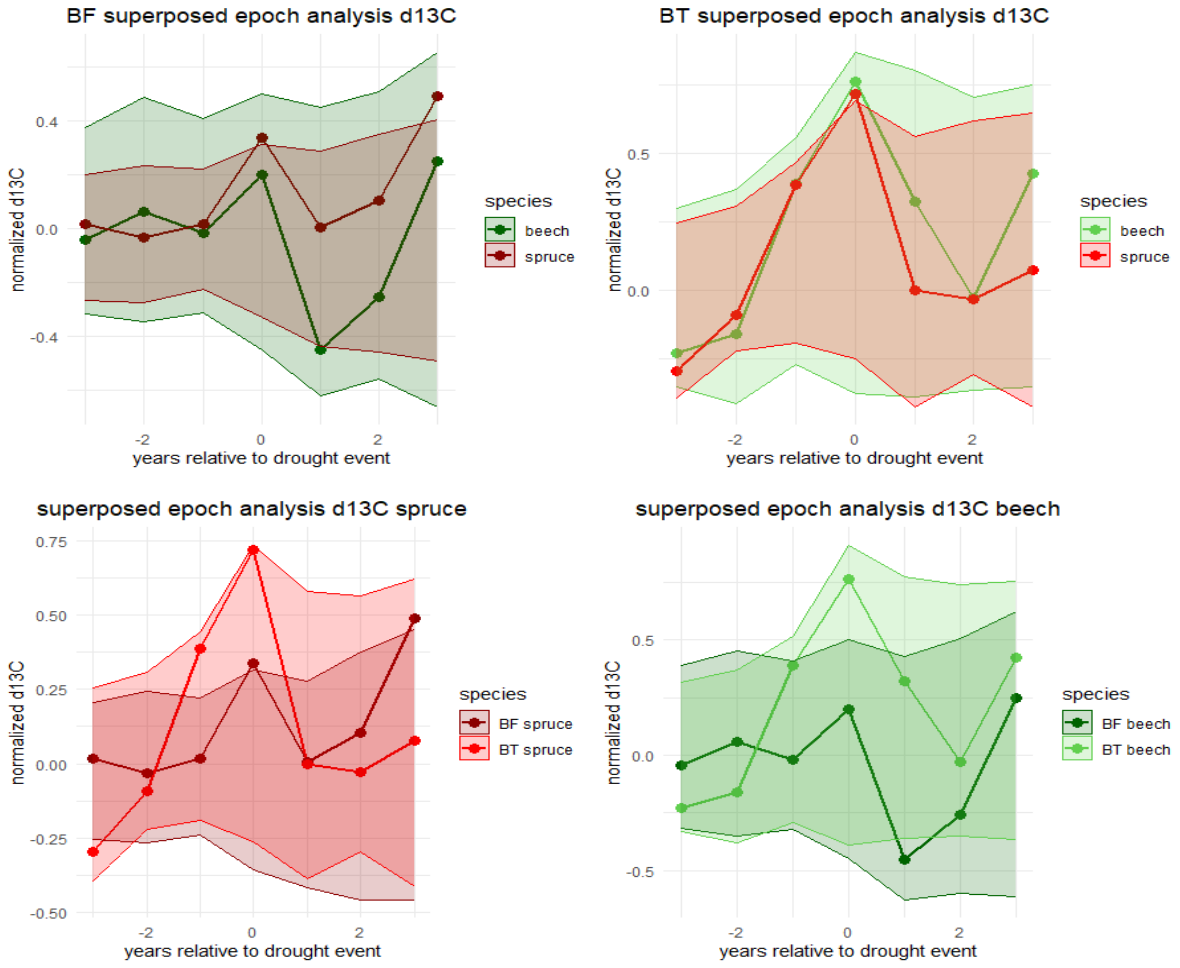

Fig. 42: SEA results, showing growth responses of spruce and beech with ribbons representing 99% confidence intervals

3.3.3 $\delta^{13}C$ and climate variability

The correlations between $\delta^{13}C$ and climate variables showed distinct patterns for temperature, precipitation, and SPEI across the two study sites and species, which are summarized in Tab. 7. Detailed correlation matrices of $\delta^{13}C$ and climate variables can be found in Appendix F. At the BT site, $\delta^{13}C$ showed strong positive correlations with temperature, precipitation, and SPEI, reflecting a clear response to climate variability. Beech exhibited strong correlations with temperature during late spring and early summer, particularly in May–July, while spruce responded most in June–August. Precipitation also showed strong negative correlations for both species during the growing season, especially June–July. SPEI (Fig. 43) also correlated negatively, mainly in May–July. Undetrended $\delta^{13}C$ data showed weaker

correlations overall, highlighting the importance of short-term variability in creating these responses. Overall, the Black Forest $\delta^{13}C$ patterns highlighted a strong response to climate variables, with beech and spruce showing similar trends but varying in the timing and strength of their responses.

At BT, $\delta^{13}C$ correlations were overall weaker than at BF. Beech $\delta^{13}C$ correlated positively with temperature during summer, mainly Jun–August and showed additional strong sensitivity to the previous spring and summer. Spruce also exhibited strong temperature correlations in summer, particularly June–August. However, when undetrended $\delta^{13}C$ values were considered, correlations for both beech and spruce exhibited strong negative trends, which seemed to contradict the patterns seen in the detrended data (Fig. 44). Precipitation and SPEI influenced $\delta^{13}C$ for both species during February–July, with summer peaks in June–July. Despite these weaker overall signals, $\delta^{13}C$ at the BT site still captured some drought-related impacts, with beech showing a stronger response during the summer months than spruce (Fig. 43). However, undetrended $\delta^{13}C$ data showed weaker, altered, and less consistent correlations, with beech also showing a response to precipitation from the previous year.

	temperature	**precipitation**	**SPEI**
$\delta^{13}C$ - BF	b>s (+)	b>s (-)	b>s (-)
$\delta^{13}C$ - BT	s>b (+)	b>s (-)	b>s (-)

Tab. 7: Comparison of $\delta^{13}C$ climate sensitivity of spruce (s) and beech (b) at different sites during periods of maximum growth activity. Symbols indicate whether spruce or beech reacted more (s>or b>s) and the direction of the correlation (+/-)

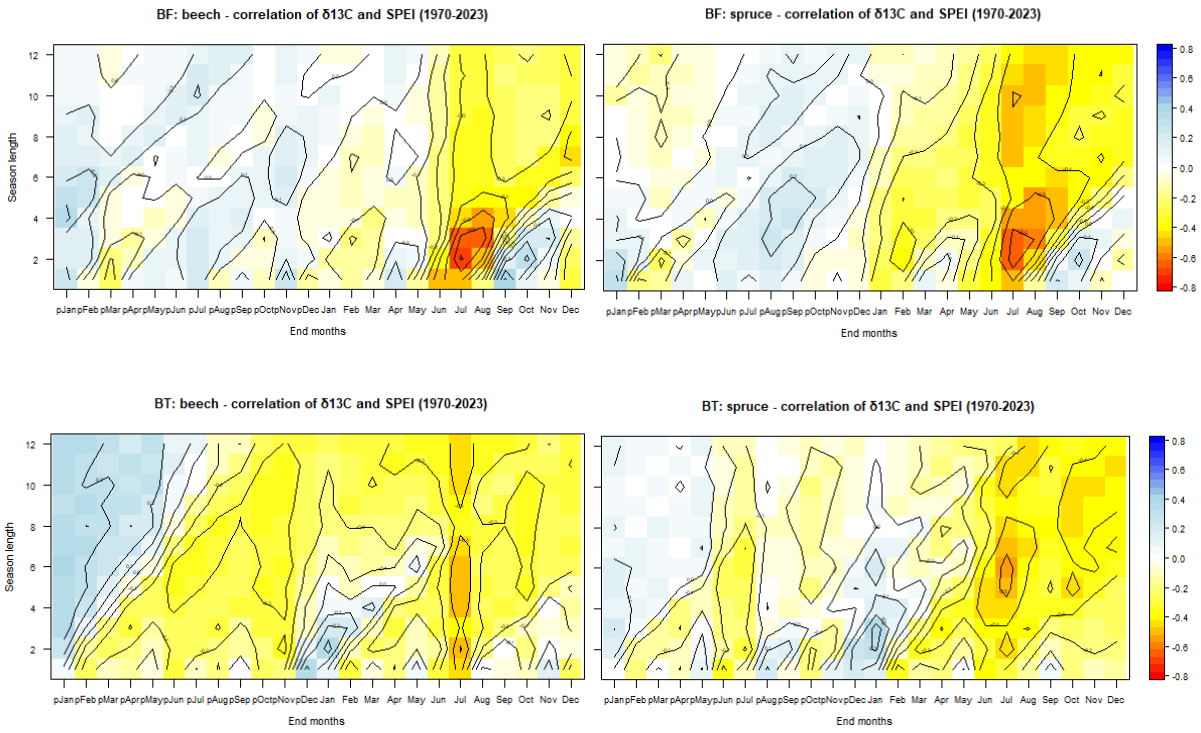

Fig. 43: Correlation matrices for $\delta^{13}C$ and SPEI for BF and BT beech and spruce

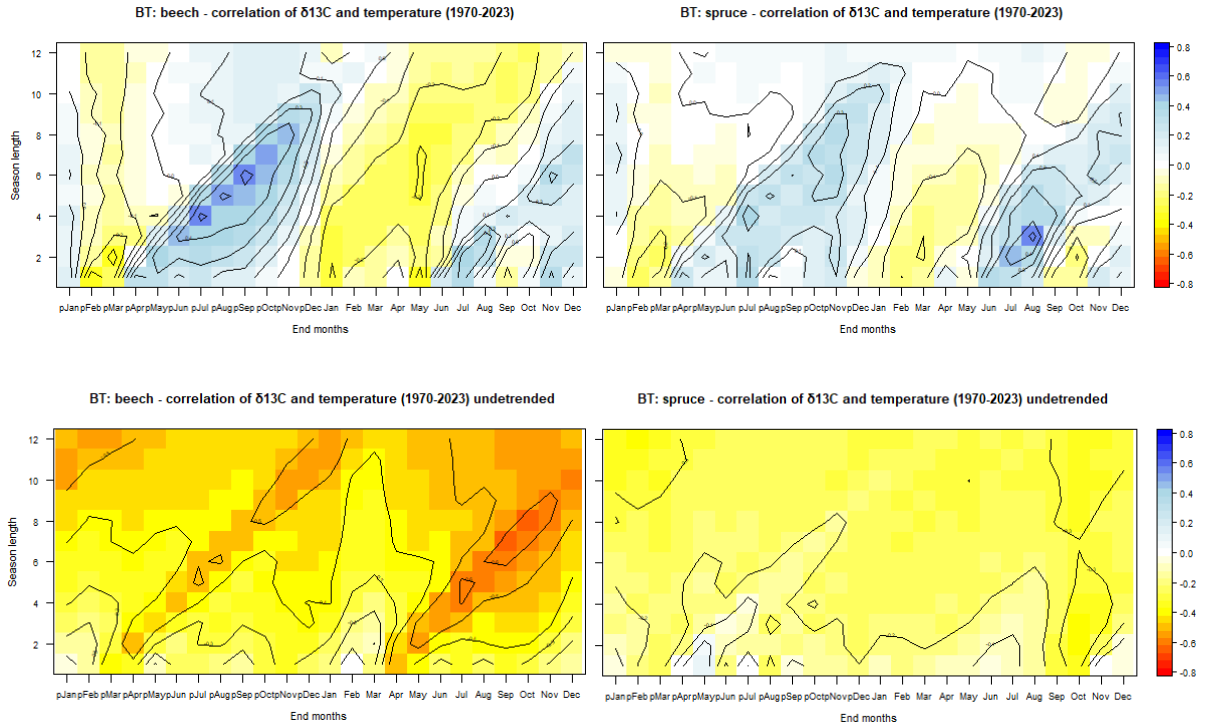

Fig. 44: Correlation matrices for δ¹³C and temperature for BT beech and spruce detrended and undetrended

3.3.4 δ¹³C and air pollution

Single linear regression models across BF and BT revealed positive relationships between air pollutants (SO_x, NO_γ, NH_x) and the δ¹³C of beech and spruce (Fig. 45), with stronger trends observed at BT compared to BF. Generally, δ¹³C of beech at BF exhibited weak relationships with pollutants. SO_x was moderately significant, NO_γ showed a non-significant influence, and NH_x showed a significant effect. Residual standard errors for beech ranged from 0.45 to 0.48, highlighting considerable unexplained variability. Spruce at BF showed moderate relationships, which were all highly significant. Residual errors for spruce were smaller compared to beech, ranging from 0.37 to 0.44, suggesting more stable δ¹³C responses to pollutants.

At BT, the δ¹³C of beech showed strong and highly significant relationships with all pollutants, with SO_x showing the strongest relationship. Residual errors for beech at BT are around 0.5, indicating robust model fits. For spruce at BT, NH_x and SO_x exhibited moderate positive relationships, whereas the relationship with NO_γ was strong. All three correlations were highly significant. Residual errors for spruce at BT ranged from 0.48 to 0.62, suggesting slightly greater unexplained variability compared to beech. Overall, pollutants had a greater impact on δ¹³C at BT compared to BF, with beech showing stronger responses than spruce. NH_x was the most influential factor at both locations, particularly for beech at BT. However, the unexplained variability, especially at BF, indicates that other factors also affected δ¹³C.

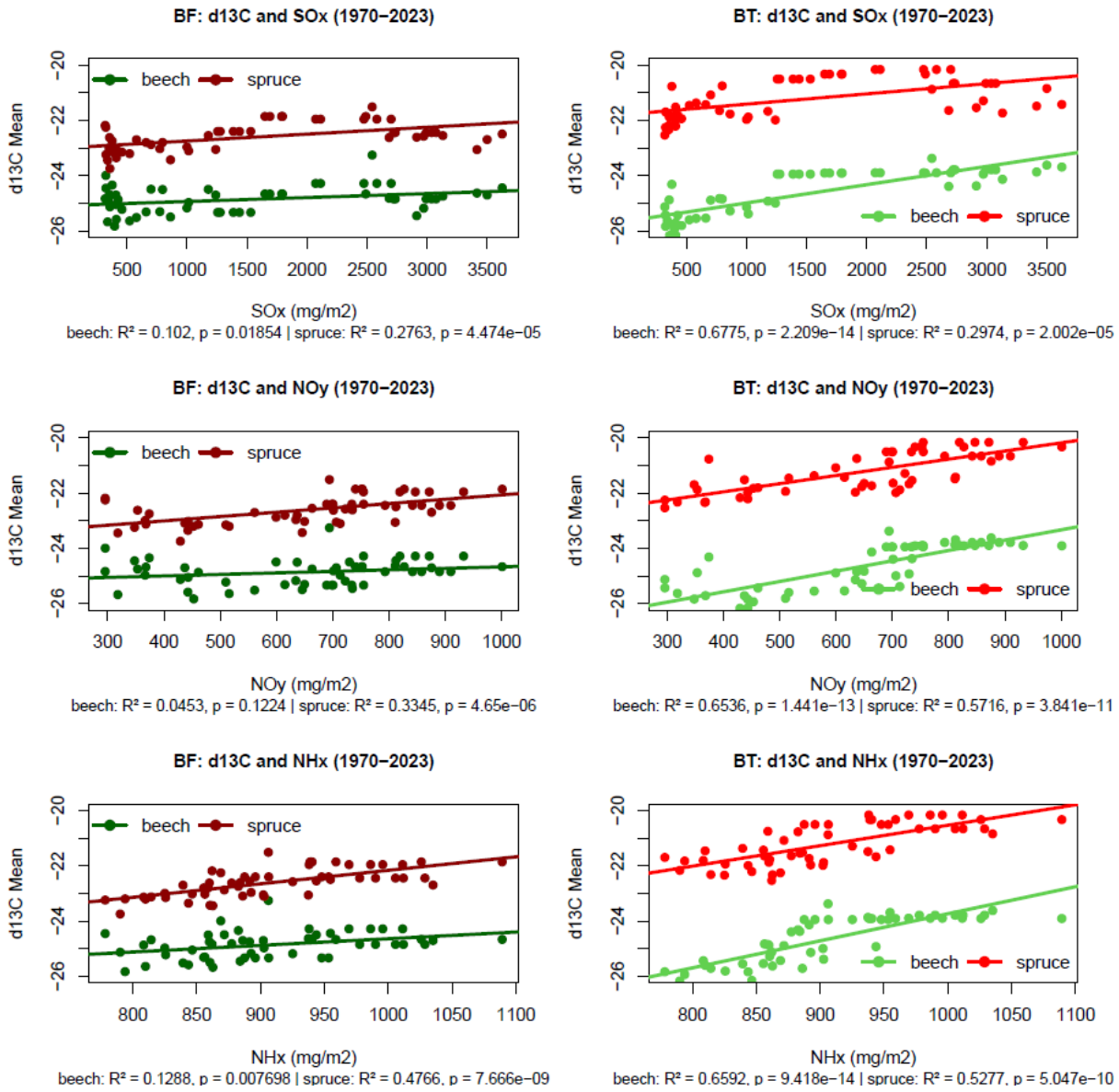

Fig. 45: Linear regression with δ¹³C and pollutants at BF and BT

As previously noted, Pearson correlation analysis for BT revealed a strong negative relationship between undetrended δ¹³C and temperature. This result was unexpected, as δ¹³C is generally anticipated to show a positive relationship with temperature (Gagen et al. 2022), a pattern also confirmed in this study by the analysis using detrended δ¹³C data. To investigate the cause of this discrepancy and identify potential driving factors affecting undetrended but atmospherically corrected δ¹³C data, a multiple linear regression was performed. In this analysis, δ¹³C was used as the dependent variable, while SO_x and June–July temperature, where the strongest positive correlations were observed, were included as independent variables. SO_x was included because CLmaxS was exceeded throughout the entire 20th century, while CLmaxN remained below critical levels during the same period. For beech, the combined effect of SO_x and temperature showed a moderate positive correlation (r = +0.377), while for spruce, the relationship was similarly positive but slightly stronger (r = +0.473). Although these findings were not statistically

significant, they suggest that the earlier negative correlation may have been influenced by the presence of SO_x. When both factors were considered together, the relationship between $\delta^{13}C$ and temperature shifted to align with expectations, returning to a positive correlation.

4. Discussion

4.1 Tree-ring widths

4.1.1 Contrasting growth strategies of spruce and beech

The analysis of growth metrics and CRG highlighted distinct responses of spruce and beech to environmental stressors, reflecting their contrasting growth strategies. Spruce exhibited higher sensitivity to environmental changes, as indicated by elevated SNR, EPS, and Rbar values. This high sensitivity allowed it to benefit from favorable conditions but also increased its susceptibility to stress, such as climatic extremes and pollution. Beech, on the other hand, displayed stable growth patterns, with moderate metrics and smoother CRG curves, reflecting its resilience under various environmental conditions (Kolář et al. 2017; Vacek et al. 2019). Although beech maintained consistent CRG levels within the same site until the 1980s, the increasing frequency and intensity of droughts in recent decades have caused greater physiological stress (Leuschner 2020). This likely led to a divergence in CRG trends among individual trees, as variability in microhabitats, soil conditions, and competition within the site probably also amplified differences in their growth responses to drought (Schmied et al. 2023). Still, its overall stability enabled faster recovery compared to spruce, which exhibited more variability throughout the study period. Site-specific CRG analyses revealed different growth responses for both species under varying environmental conditions and management practices.

At BT, spruce experienced prolonged growth stagnation during the 1970s and 1980s, coinciding with high pollution levels. It recovered only after pollution decreased, indicating that spruce might have suffered from pollution. Beech, in contrast, showed only a brief plateau during the same period and quickly returned to stable growth, demonstrating greater tolerance to pollution-related stress (Oulehle et al. 2024). However, linear regression models suggested that air pollutants had little to no measurable impact on the growth of both beech and spruce overall, indicating that their growth variability is probably also driven by other factors. At SCPA, young spruce trees exhibited improved growth over time, likely due to their adaptation to local conditions upon maturity and benefits from reduced competition and management practices (Popa et al. 2024). Meanwhile, beech at SCPA, growing within the same area, maintained steady growth with minimal responses to site-specific changes. At BF, beech demonstrated resilience to drought through stable growth and quicker recovery in CRG patterns, while spruce struggled with reduced coherence and slightly slower recovery from drought events, which might be explained by its higher drought sensitivity (Leuschner and Meier, 2018). Also, tree age probably influenced growth dynamics. Older trees, particularly beech, displayed smoother CRG curves and stable growth,

suggesting that they could better withstand stress. Younger trees showed faster but more variable growth. While age-related growth responses are subject to debate, this discrepancy may be explained by the advanced root systems of older trees, especially beech, which can provide better access to soil water reserves during drought. This enhanced water uptake likely reduced the impact of water deficits, contributing to the stability observed in older trees (Fung Au et al. 2022).

4.1.2 Drought sensitivity and site-specific growth patterns

The SEA analysis validated the patterns observed in the statistical metrics and CRG analyses, emphasizing the contrasting drought responses of spruce and beech (Fig. 35). Spruce exhibited the most pronounced growth reductions during drought events at BF and SCPA+B, with average TRW statistically significantly smaller during drought years compared to non-drought years. This finding aligns with its high sensitivity to environmental stressors, as reflected in elevated SNR, EPS, and Rbar values, as well as sharper declines and slower recovery observed in CRG patterns. Conversely, beech showed smaller and statistically insignificant average growth reductions during drought events across all sites, underscoring its greater resilience to drought stress. The higher drought sensitivity of Norway spruce compared to European beech can be attributed to differences in their root systems and the site-specific soil conditions. Whereas European beech has a deep-reaching heart root, Norway spruce has a shallower and only occasionally deeper-reaching tap root system (Ellenberg and Leuschner 2010). Deep rooting allows beech to access deeper water reserves, contributing to its higher drought resistance and resilience. This advantage is particularly beneficial in areas with soils that have a water-storing layer. The prevailing soils at BT and BF are acidic brown earth and para-brown earth with a potentially water-storing layer, probably providing better water availability during drought periods (Weber et al. 2013). However, the plateau location at SCPA+B reduces drainage and increases soil depth and soil water availability, and thus is more favorable for beech during droughts. By contrast, the BF and BT sampling locations lie on a slope, thus the steep terrain reduces soil depth and increases water runoff, limiting the water availability during extended droughts (Leuschner 2020; Klesse et al. 2022). Furthermore, the soil at BF is poor in carbonate compared to SCPA+B, which further increases the drought sensitivity of beech as this species reaches its drought limit more rapidly on base-poor soils compared to base-rich soils (Schmied et al. 2023).

However, neither spruce nor beech showed statistically significant growth decreases during drought events at BT (Fig. 35), suggesting a lower drought sensitivity of spruce at BT compared to SCPA+B and BF. This reduced sensitivity can likely be attributed to the cold and wet continental climate of the region, which helps mitigate the effects of drought. Additionally, the shorter growing season at BT, influenced by the site's elevation and continentality, further limits the period during which drought could negatively affect spruce growth. Positive correlations between spruce growth and July–August temperature support this, indicating that warmer temperatures during this period may actually benefit growth. This interpretation is further reinforced by the lack of strong positive correlations between spruce growth and SPEI

during the summer months, suggesting minimal drought impact. Similar findings have been reported in other studies from the region (Kroupová, 2002). Moreover, the growth optimum for spruce is typically between 550–900 m.a.s.l., placing the BT site at its upper limit, which may further influence the observed growth dynamics (Kolář et al. 2017). However, the weakening of the climate signal due to legacy effects of past pollution likely obscures the growth response to environmental stress rather than indicating reduced physiological sensitivity to drought (Kolář et al. 2015). Also for beech, correlation analysis with temperature at BT revealed a positive relationship with July and August temperatures. Comparing the RWI chronology of BT beech with a high-elevation chronology from Eastern Europe showed similar patterns, suggesting that the BT site exhibits characteristics typical of high-elevation environments (Klesse et al. 2024). Moreover, the growth optimum for beech generally ranges between 450 and 700 m.a.s.l., indicating that the BT site may be above its preferred range. This interpretation is further supported by BT's higher mean annual temperatures, which are 2.3°C and 3.2°C higher compared to BF and SCPA+B, respectively. Despite having a similar altitude, BT has a distinct climate classification, being Dfb (humid continental) compared to the Cfb (oceanic) classification of BF and SCPA+B. As European beech prefers a mild oceanic climate, this climatic difference, characterized by colder winters and more pronounced seasonal temperature fluctuations at BT, likely contributed to the growth dynamics observed in beech and probably also in spruce at this site (Pretzsch et al. 2014).

Overlapping droughts and heatwaves at all three sites might have impacted the SEA analysis by blurring distinct drought signals. There was evidence of pre-drought stress in beech at SCPA+B, with lower RWI values observed in the year preceding drought events. This pattern likely reflects the high frequency of severe droughts in recent years, where a year preceding a major drought might itself have experienced drought conditions. Additional factors, such as strong winter frosts and late frost events, made the interpretation of growth reductions for beech more complex. Its earlier leaf-out compared to evergreen spruce makes it vulnerable to damage from late frosts (Menzel et al. 2015; Leuschner and Meier 2018). This affected average growth in years before and after drought events, such as in 2017 at SCPA+B and 1978/79 at BT.

4.1.3 Species- and site-specific growth responses to extreme drought events

Defining and comparing extreme drought years proved to be a complex task due to the dependence on methodological choices, such as the selected drought index, the temporal aggregation of climate data, and the classification thresholds applied. The challenges became evident when shorter two- and three-month aggregations for the critical tree growth months of May, June, and July were used. While these methods captured water deficits during critical growth phases, they failed to correspond with extreme drought years documented in the literature, thereby underscoring their limitations. In contrast, longer aggregations of five or six months showed a stronger alignment with well-known severe drought years, reflecting the prolonged stress that often extends beyond the growing season. However, even with this approach, the results were still highly sensitive to the chosen SPEI threshold and differed between the

five- and six-month aggregations, making it harder to identify extreme drought years and showing how subjective drought classification can be. To address this issue, some studies have suggested focusing on analyzing sequences of multiple drought years, such as 2003–2006 and 2018–2020, rather than isolating and analyzing individual extreme drought events (Tresch et al. 2023). But this approach also raises the question of which method should be used to define and calculate these sequences. These methodological constraints created inconsistencies in defining extreme drought years, making direct comparisons of events across different regions questionable concerning their robustness. However, despite these challenges, if these concerns are set aside due to the lack of better alternatives, the comparison still highlight clear differences in responses between sites and species (Fig. 34).

In 1976, drought conditions were most pronounced in June across all three sites, aligning with the peak sensitivity periods of both spruce and beech. At SCPA+B and BF, both species exhibited equally strong growth reductions, with the impact most notable at these less continental sites. However, at BT, beech did not exhibit any negative growth reaction, and spruce showed only a weak negative response. This confirms that beech at BT is not highly sensitive to drought, while spruce exhibits only mild drought sensitivity, as already indicated by the correlation between RWI and SPEI. This also align with a study from the Carpathians, which suggests that the drought sensitivity of spruce decreases in this region at elevations above 800 m.a.s.l. (Popa et al., 2024). In 2003, drought conditions were concentrated in June and August across all three sites, though at BT the drought was notably more severe in August. At SCPA+B and BF, its intensity was relatively equal in June and August, aligning with the periods of greatest drought sensitivity for spruce. As a result, spruce showed a more pronounced growth reduction than beech at SCP A+B and BF. In contrast, at BT, beech experienced a stronger growth reduction than spruce, likely because the drought effects began as early as February and intensified in August, exacerbating the cumulative drought stress on beech, which is more sensitive to dry spring conditions at BT.

The 2018/2019 drought was characterized by distinct temporal and spatial patterns across the three sites. In 2018, the drought was most severe in April and July at SCPA+B and BF, whereas at BT it peaked in May, June, and especially August, extending into 2019 with additional dry conditions in April, June, and July. Spruce showed the strongest growth reductions across all sites, although the timing differed. At SCPA+B and BF, the most significant reductions occurred in 2018, aligning with peak drought severity there. At BT, spruce responded most strongly in 2019 due to the prolonged character of the drought and cumulative stress (Tresch et al. 2023). Beech at SCPA+B and BF did not show strong growth reductions in 2018 or 2019, indicating its resilience under these conditions. At SCPA+B, beech demonstrated negative correlations with precipitation, suggesting potential sensitivity to waterlogging or precipitation-related stresses. This may explain its negative correlation with SPEI during certain spring and summer months. It is also the reason why beech at SCPA+B probably had enough water available due to a waterlogging soil layer and deeper reserves. At BF, spruce was more affected by the 2018 drought than beech, due to its greater sensitivity to drought in July. At BT, spruce's higher drought sensitivity and the

increased severity in 2019 led to its most pronounced growth reduction that year compared to all other drought years. In contrast, beech, lacking notable drought sensitivity at BT, showed no response to the 2018 drought but experienced weak growth reductions in 2019. This was likely due to its sensitivity to prolonged droughts and previous summer conditions, combined with the greater drought severity at this site in 2019.

The 2020 drought occurred in April and July at SCPA+B and BF, and in April at BT. Timing strongly influenced species responses. At SCPA+B and BF, drought-sensitive spruce showed growth reductions, while beech exhibited no reaction, reflecting its higher drought resilience. However, at BT, beech exhibited a strong growth reduction, which was much more pronounced than at the other sites and unexpected given its typical lack of drought sensitivity at this location. This decline could be attributed to additional stress factors, such as reduced snow cover in the preceding winter, which may have exposed the roots of the frost sensitive species to freezing damage due to reduced insulation, while also limiting soil water recharge. This would have further reduced its ability to access water and nutrients combined with the ongoing severe and prolonged 2018–2020 drought series (Stjepanović et al. 2018; Arnič et al. 2021). During the 2022 drought, neither beech nor spruce showed a growth response at any site. The drought peaked in March, followed by a dry May, and peaked again in July. Although the dry conditions during the vegetation period could have affected at least the growth of drought-sensitive spruce, the overall impact of the 2022 drought was weak and did not cause measurable reductions for both species. Because 2021 was relatively cool and wet, trees and soil water reserves likely recovered, reducing the impact of the 2022 drought. This is further supported by the correlations of TRW with climate conditions from the previous year.

4.1.4. Exceedance of critical loads

When examining the impact of pollution on TRW, both species showed similarly weak and statistically non-significant relationships with pollutants across all sites. Therefore, the presented results do not provide sufficient evidence to establish a clear cause-and-effect relationship between pollution and growth reduction based solely on TRW data. This suggests that the observed growth reductions might probably be influenced by other environmental or climatic factors, even if they coincided with periods of high pollution levels. To further investigate this, the exceedance of critical loads (Tab. 1) must be considered, as these thresholds offer more insight into the levels at which stress occurs in forests. At SCPA+B, neither CLmaxS nor CLmaxN were exceeded, indicating that acidification likely did not occur at this site, and forests were not stressed by it. At BF, the lower CLmaxS was exceeded during a few individual years, while the lower CLmaxN was continuously exceeded from the 1970s to the 2000s. This pattern suggests that light soil acidification may have occurred during this period. Management practices at the site, which include recommendations for lime application, support this interpretation (Chair of Forest Growth and Dendroecology UFR, 2024). These practices likely aimed to address potential pH imbalances and calcium deficiencies in the local soil, as the absence of free lime indicates slightly acidic

conditions (Hruška et al. 2023). However, the lack of continuous exceedance of the lower CLmaxS, along with the absence of any exceedance of the upper CLmaxS, suggests that S deposition was unlikely a central stress factor at BF. The fact that critical loads for acidification at BF were rarely or minimally exceeded aligns with these findings, reinforcing the conclusion that acidification at the site was not a significant issue. This interpretation is also supported by the results of linear regression models, which do not indicate significant acidification stress due to S deposition.

A closer look at CLmaxS and CLmaxN at SCPA+B site reveals that the local soil can tolerate relatively high levels of S and N deposition before experiencing acidification. This is because, despite their acidic character, the soils have carbonate-rich bedrock, and the negative effects of acidification are therefore mitigated (Geoportal Kanton Zürich, 2024; Hopf et al., 2020). Thus, they can effectively neutralize incoming acid inputs, minimizing the risk of CLmaxS and CLmaxN limits being exceeded, even during times of elevated deposition in the past. However, while these soils are well-protected against acidification, CLmaxN is only relevant to assessing N deposition's impact on soil acidification. It does not account for the ecological impacts of N deposition. These impacts are better assessed using different thresholds, such as CLnutN (critical nutrient load for N) and CLempN (empirical critical load for N), which focus specifically on the effects of N enrichment on ecosystems. CLempN are determined from field studies, N application experiments, and long-term monitoring that link N deposition to ecological impacts. CLempN provides a threshold above which N deposition has been empirically shown to cause measurable harm to ecosystems, and thus is particularly interesting for this study. CLnutN, on the other hand, are theoretical thresholds based on nutrient requirements and imbalances in ecosystems. They estimate the maximum N deposition that can occur before causing problems such as nutrient saturation or eutrophication (Bobbink et al. 2015; Bobbink et al. 2022). CLnutN and CLempN are generally lower than CLmaxN. This means that while soils may buffer against acidification, N levels could still harm ecosystems through nutrient saturation or eutrophication.

The overall CLempN for European mixed Abies-Picea-Fagus woodland is estimated at 1000–2000 mg(N)/m²/year (Bobbink et al. 2015). Other calculations suggest an upper limit of CLempN of 1500 mg(N)/m²/year and CLnutN of 1400–1600 mg(N)/m²/year (Rihm and Künzle 2023). CLempN exceeded depending on the threshold applied. If the lower threshold is considered, CLempN was exceeded from the 1970s to the 2000s, similar to the CLempN, whereas CLempN was never exceeded at any of the three sites under the higher threshold. When CLempN is not exceeded, N deposition can stimulate growth in both beech and spruce under favorable conditions, particularly when paired with elevated CO_2 levels. However, at BT, these growth-stimulating effects may have been moderated by the high S deposition (Oulehle et al. 2024). A study on long-term forest observation plots in Switzerland indicated that beech experienced greater growth reductions than spruce when N deposition exceeded species-specific thresholds. Beech growth declined more strongly above 2600 mg(N)/m²/year, while spruce was affected at levels above 2000–2200 mg(N)/m²/year (Braun et al. 2017). Neither of these

thresholds were exceeded at any of the sites, supporting the assumption that N deposition likely did not play a major role in the observed forest stress, although the exceeding of the CLnutN indicates nutrient saturation and eutrophication. However, the lasting effects of high N deposition likely continue to pose ecological challenges (LUBW 2010; Bobbink et al. 2015; Brady and Weil 2017; Hopf et al. 2020).

Studies have shown that increased N deposition can heighten forest sensitivity to drought and other stress factors (Braun et al. 2017). Consequently, the effects of drought at SCPA+B and BF may have been further intensified by these cumulative impacts, leading to increased tree mortality (Tresch et al. 2023). The reappearance of the same symptoms at these sites during the severe droughts of the past two decades, as seen during the forest dieback of the 1970s and 1980s, strongly suggests that drought was the main driver of forest decline in both periods (Cherubini et al. 2021). Climate-driven spruce mortality has also been confirmed in studies from the BF region, identifying drought and heat as the key drivers of declining radial growth rates from 1900 to 2020 and tree mortality due to desiccation over the past 68 years. This trend extends into the late 20th century when forest dieback in Germany was largely attributed to acid rain. Following the hot and dry summers from 1972 to 1976, tree mortality in the Black Forest surged to levels unprecedented in the previous 24 years, triggering discussions about forest decline as a newly emerging phenomenon. Although climatic conditions temporarily improved, reducing mortality, extreme July temperatures in 1983, combined with low precipitation from June to August and snow breakage from 1981/82, created favorable conditions for bark beetle infestations (Spiecker and Kahle 2023). Given that SCPA+B had lower S deposition but a comparable climate, drought and bark beetle-driven tree mortality were likely similar at this site (Tresch et al. 2023).

Studies from Switzerland suggest that beech suffered more during the droughts of the last two decades, which is also consistent with patterns observed in other regions (Klesse et al. 2022; Neycken et al. 2024). Severe droughts, such as those in 1976, 2003, and 2018/2019, have been associated with widespread crown defoliation, significant radial growth declines, and delayed mortality in beech. For example, following the 2018 drought, many beech trees experienced crown dieback and bark damage, with mortality rates increasing strongly in subsequent years. These findings underscore the vulnerability of beech to past and recent drought events (Braun et al. 2017; Leuschner 2020). The decline in mean growth rates from 2000 to 2023 compared to 1970–1999 for both species at SCPA+B confirms rising stress in the past two decades. During drought, tree mortality is caused by the combined effects of impaired water transport and reduced energy availability. Prolonged water loss can lead to hydraulic failure, where the xylem, responsible for water transport, becomes dysfunctional because of tissue dehydration, which disrupts the normal physiological functions of the trees. Simultaneously, drought-induced reductions in photosynthesis limit the tree's ability to assimilate C, forcing reliance on stored carbohydrates. As trees deplete their energy reserves, C starvation reduces their capacity to maintain essential functions. Hydraulic failure intensifies the problem by restricting photosynthesis, starting a cycle that accelerates tree decline and increases susceptibility to pests and other stressors (Schuldt et al. 2020).

While the strong decrease in SO_x and NO_y deposition across all regions demonstrates the success of air quality regulations in recent decades, the prolonged exceedance of CLmaxS during the whole 20th century, combined with extremely high pollution levels in the 1970s and 1980s at the BT site, caused soil acidification and lasting changes in soil chemistry. These legacy effects continue to influence forest health to this day (Akselsson et al. 2004; Rydval and Wilson 2012). Furthermore, air pollution, particularly SO_2, may have had a more immediate and direct effect on forest decline than soil acidification alone. Studies indicate that high SO_2 levels caused chlorophyll degradation, needle loss, and reduced photosynthesis in trees, effects which are independent of soil acidification (Hruška et al. 2023). This dual impact, direct physiological stress from pollutants and slower-acting soil acidification, may explain why pollution effects were not strongly reflected in TRW data from BT, as growth reductions were likely influenced by multiple interacting factors, including climatic stressors (Kroupová 2002; Rydval and Wilson 2012; Vacek et al. 2020; Hruška et al. 2023). However, there is a conceptual uncertainty in the critical loads concept, as it does not account for the time factor and therefore cannot predict when effects on trees will occur (Akselsson et al. 2004). Nevertheless, it can be assumed that the extremely high pollution levels and persistent exceedance of CLmaxS at BT likely contributed to the observed forest decline. Air pollution effects often outweighed the slower impacts of soil acidification, particularly during periods of peak deposition coinciding with unfavorable climatic conditions (Kroupová 2002; Muzika et al. 2004; Lomský et al. 2012; Rydval and Wilson 2012; Kolář et al. 2015; Vejpustková et al. 2017; Putalová et al. 2019; Vacek et al. 2020; Shetti et al. 2024). The increase in mean TRW from 2000 to 2023 compared to 1970–1999 suggests a recovery in growth rates, coinciding with improved air quality. However, as forest health is influenced by many interacting factors, it is impossible to quantify the specific contribution of pollution without also analyzing other factors (Akselsson et al. 2004).

4.1.5 Pollution effects and long-term growth recovery

Focusing on the 1970s and 1980s at BT, beech and spruce experienced significant growth depression in 1978-1983 and 1980-1983, respectively (Fig. 34), aligning with extreme environmental stress at this site. This stress coincided with peak SO_2 deposition, exacerbated by frequent winter smog inversion layers that trapped pollutants near the ground. These inversions prolonged exposure to SO_2 and other pollutants, disrupting tree physiology by reducing photosynthesis, impairing stomatal function, and causing nutrient imbalances (Kroupová 2002; Rydval and Wilson 2012; Vejpustková et al. 2017; Vacek et al. 2020). The differing rooting systems of beech and spruce likely influenced their responses to pollution. Beech, with its deeper roots, may have had better access to more stable nutrient reserves in lower soil layers, potentially buffering it against the effects of acid deposition and nutrient leaching. This could have contributed to its relatively higher resilience under pollution stress (Oulehle et al. 2024). In contrast, spruce's shallower root system made it more reliant on surface-level nutrients, which are more susceptible to leaching under acidified conditions. As a result, spruce may have been more affected by deficiencies in calcium and magnesium, which are important for tree health and stress tolerance (Vacek et al. 2020). Limited access to deeper, less disturbed nutrient pools could have contributed to spruce's

higher sensitivity to both pollution and drought (Vacek et al. 2020; Oulehle et al. 2024). Additionally, some studies suggest that soil acidification can impair root elongation, which might have further affected spruce's ability to cope with environmental stress (Šantrůčková et al. 2019).

In addition to pollution, cold summers during the late 1970s and early 1980s likely contributed to the observed growth reductions. Reduced summer temperatures slow metabolic processes, delay leaf development, and shorten the active photosynthetic period (Stjepanović et al. 2018). They added to the physiological stress caused by pollution and nutrient imbalances, worsening growth declines, particularly at the BT site where nutrient deficiencies were more severe due to acidification (Oulehle et al. 2024). The cold and wet summer of 1978 was particularly challenging for temperature-sensitive beech trees at this high elevation site, thus marking the onset of their growth decline. The situation worsened during the winter of 1978/79 when a sudden temperature drop from +10°C to -20°C within 15 hours initiated a ten-day period of severe frost in January. Beech, which is more frost-sensitive than spruce, displayed strong physiological stress, exacerbated by the preceding cold summer (Kroupová 2002; Leuschner and Meier 2018; Stjepanović et al. 2018). At the same time, beech trees in the Jizera Mountains were heavily infested by beech scale, which added to the stress of already weakened trees (Vacek et al. 2019). The pest damages the bark, disrupts the flow of nutrients and increased the risk of secondary infections by fungi. Combined with other stressors, it can severely reduce tree growth and, in severe cases, lead to mortality (Gora et al. 1996; Houston 1998). Environmental challenges persisted into 1980, characterized by an unusually cold growing season, which further stressed both species. The winter of 1980/81 compounded these issues, with low temperatures coinciding with high SO_2 concentrations. For spruce, the stress was particularly severe, which is reflected in the missing rings during 1980 and 1981, indicating halted cambial activity. A heavy frost in January 1982 and similarly harsh winters in 1984/85 and 1986/87 added to the cumulative stress, with a heavy late frost event in April 1987, characterized by a rapid temperature drop from 10°C to -7°C, which further stressed both species. Frost can damage buds and needles, impair osmotic balance, and reduce frost hardiness, especially in trees already weakened by pollutants. Moreover, the impact of SO_2 was further exacerbated by mechanical injury to needle surfaces caused by frost. The combination of freezing temperatures and high levels of SO_2 often led to chlorophyll damage and needle withering, which occurred when high concentrations of SO_2 came into contact with the assimilatory organs of spruce (Kroupová 2002; Rydval and Wilson 2012; Kolář et al. 2015). Between 1979 and 1987, defoliation was a major contributor to growth depression, driven by a combination of air pollution, winter desiccation, and frost events. High SO_2 levels damaged stomatal function and chloroplasts, directly causing needle loss and impairing photosynthesis. Simultaneously, acid deposition depleted base cations, further weakening the trees. During harsh winters, desiccation occurred as needles lost water while the soil remained frozen, preventing water uptake. This stress was compounded by severe frost events that caused additional damage to needles and buds. Weakened by pollution and climatic stress, many spruce trees became highly susceptible to bark beetle infestations, further exacerbating defoliation and contributing to delayed recovery (Vacek et al. 2019; Vacek et al. 2020).

The severe drought of 1976, along with the moderate droughts of the 1980s, probably compounded the physiological damage caused by pollution by further limiting water availability and the uptake of essential nutrients, which were already depleted due to acid deposition (Vacek et al. 2020). The deposition of pollutants on plant leaves caused damage to the waxy protective layer on the surface, which resulted in increased water loss through transpiration and heightened vulnerability to dry conditions (Huttunen and Laine 1983; Shetti et al. 2024). However, while drought might also have contributed to increased stress, it may not have been the central cause of the observed growth declines during this period, as air pollution and nutrient imbalances combined with cold summers and hard winters played a more dominant role in suppressing tree growth at BT (Kroupová 2002). Recovery from these growth depressions began in the 1990s with significant reductions in SO_2 emissions following stricter environmental regulations. However, spruce recovery was slower because even after SO_2 emissions were significantly reduced in the 1990s, the recovery of nutrient balances in forest soils was slow due to the severity of prior acidification. Trees continued to struggle with nutrient deficiencies, particularly calcium and phosphorus, which limited their recovery and growth potential (Rydval and Wilson 2012). While beech showed more stable growth, benefiting from its physiological flexibility and deeper rooting system which allows it to adapt more effectively to the changing environmental conditions (Oulehle et al., 2024; Siegwolf et al., 2022). But as all spruces sampled in this study survived the forest dieback of the 1970s and 1980s, they were probably also able to withstand the effects of acidification. Norway spruce has demonstrated several adaptations to cope with acidified soils. For instance, it alters root distribution by increasing root growth in the organic-rich humic layer, where acidity is lower, while reducing root growth in the deeper mineral soil (Jentschke et al. 2001). Additionally, spruce trees, along with their mycorrhizal fungi, reduce aluminum toxicity in the root zone by binding aluminum with organic compounds and enhancing nutrient uptake to counteract the acidic conditions (Collignon et al. 2012).

4.2 Stable isotope $\delta^{13}C$

4.2.1 Variability in $\delta^{13}C$ series

At BF, the weak $\delta^{13}C$ metrics for beech (Tab. 5 and Fig. 39) suggest that the $\delta^{13}C$ signal was dominated by noise, likely influenced by both climatic and site-specific factors. They were characterized by poor coherence and low reliability, which may have partly reflected local microenvironmental heterogeneity, such as variability in light availability, soil moisture access or microclimatic conditions. Competition for light and water can reduce the ability of a tree to respond optimally to favorable conditions (Belmecheri et al. 2022). The period of lowest signal quality, which had the most significant impact on overall performance, coincided with varying precipitation patterns and moderate droughts during the 1990s and 2000s. Notable years include 1991, 1993, 1998, 2006, 2011, as well as the severe drought of 2003. The weak signal quality probably reflected variations in precipitation and forest stand dynamics. It is possible that not all trees experienced the same level of stress during moderate droughts, leading to varying physiological responses. For instance, neighboring trees can mitigate the effects of drought and

heat by lowering the vapor pressure deficit through their transpiration, which may result in diverse reactions among individual trees to drought conditions (Talbott et al. 2003). Although direct data on tree neighborhood structure at BF is not available, also competition with allospecific neighbors could have resulted in lower $\delta^{13}C$ values in beech, potentially reflecting better water access due to reduced intraspecific competition (Mölder et al. 2011). This dynamic may partly explain some of the $\delta^{13}C$ variability observed in BF beech during periods of heightened drought frequency. Additionally, the decreased variability in the $\delta^{13}C$ signal observed after the severe 2003 drought suggests that soil moisture across the site may have been more uniformly reduced during this and the following intense drought events. Consequently, the influence of local environmental heterogeneity probably diminished as trees experienced comparable levels of drought stress.

Legacy effects of prolonged N levels exceeding critical loads likely increased drought sensitivity of some individual trees, leading to varying drought responses among them. As beech reacts more sensitively to N deposition than spruce, this could also explain why spruce metrics were more stable at the same site (Braun et al. 2017; Gharun et al. 2021; Paligi et al. 2024). Because spruce is generally more sensitive to drought than beech, it may have exhibited more uniform stress responses to drought events across the site, contributing to more stable $\delta^{13}C$ metrics (Hartl-Meier et al. 2015a; Leuschner and Meier 2018). Additional factors, such as the influence of previous-year C storage and reallocation, may also have affected the isotopic signal, which is often the case for deciduous tree species such as beech (Belmecheri et al. 2022; Kagawa et al. 2022). Additionally, research has shown that the tolerance of beech trees to extreme environmental conditions is partly governed by genetic factors, which also influence the growth rates of different genotypes (Leuschner 2020). However, this aspect was not examined in the present study. Whole-ring analyses average out intra-annual $\delta^{13}C$ variations, which may obscure seasonal signals or stress responses. In cases where intra-ring variability is high, noise could be introduced, potentially resulting in low metrics (Belmecheri et al. 2022). Sampling and laboratory biases might have further exacerbated the variability. Inconsistencies in tree-ring processing, such as non-uniform extraction of cellulose or improper homogenization, could have introduced noise into the dataset. Potential contamination during laboratory preparation, such as the presence of residual chemicals or environmental contaminants, could also have distorted the $\delta^{13}C$ values (Belmecheri et al. 2022).

4.2.2 General $\delta^{13}C$ responses and drought sensitivity

The results of the SEA (Fig. 42) showed strong positive $\delta^{13}C$ increases during drought years in both species at both sites, indicating stomatal closure as a response to reduced water availability. These findings align with the theory of physiological adjustment, where stress-induced reductions in internal CO_2 concentrations result in elevated $\delta^{13}C$ values (Cernusak et al. 2022). Additionally, the analysis revealed species- and site-specific variations in $\delta^{13}C$ responses to drought, driven by differences in water-use efficiency (WUE), recovery strategies, and site conditions. The contrasting responses between BT and BF highlight how these factors influence how trees adjust to cope with stress (Hartl-Meier et al. 2015a).

The statistically significant increase in $\delta^{13}C$ of spruce during drought years, compared to beech, can be attributed to its shallow root system, which limits access to deeper soil moisture and increases reliance on near-surface water sources, as also discussed for TRW. This response aligns with spruce's isohydric strategy, where rapid stomatal closure during drought minimizes water loss and prevents hydraulic failure. However, it also reduces photosynthesis and C assimilation. While this strategy effectively reduces stress during droughts, it can limit growth, as reflected in the lower TRW of spruce during drought events. This is because wood production is closely linked to stomatal conductance, which is reduced under this water-saving strategy (Saurer et al. 1995; Hartl-Meier et al. 2015a). However, it also allowed spruce to recover more quickly after a drought because its hydraulic system remained largely intact. Beech used its anisohydric strategy by keeping its stomata open longer during drought, which helped to continue photosynthesis and growth. However, this also led to more water loss and a higher risk of damage to its water transport system. This strategy is supported by the efficient water transport of beech trees and their deep-rooting system. Nevertheless, it often resulted in slower recovery because hydraulic damage needed to be repaired, contributing to carry-over effects that prolonged the impact of drought and explained the elevated $\delta^{13}C$ values (Hartl-Meier et al. 2015a). This is particularly evident for BFB, which exhibited increased $\delta^{13}C$ levels that remained elevated for several years during the 2010s (Fig. 40 and Fig. 41), coinciding with a high frequency of moderate and severe droughts. The intra-species differences in mean $\delta^{13}C$ values further confirm these contrasting strategies. Spruce consistently exhibited higher $\delta^{13}C$ values than beech, not only during drought but also under favorable moisture conditions. This is due to spruce's generally lower stomatal conductance, which reduces the c_i/c_a ratio and limits discrimination against ^{13}C (Paligi et al. 2024). Additionally, during drought, spruce relies more on enriched stored C reserves formed during periods of reduced discrimination, further elevating $\delta^{13}C$ values. Beech allocates more C to growth, maintains photosynthesis, and discriminates more against ^{13}C, leading to lower $\delta^{13}C$ values (Schäfer et al. 2017).

Both species showed their highest values at BT (Tab. 6 and Fig. 40), indicating that additional stressors such as air pollution probably enhanced stress at this site (Andreu-Hayles et al. 2022; Siegwolf et al. 2022). Across both sites, $\delta^{13}C$ values decreased when comparing 1970–1999 with 2000–2023. The decrease was more pronounced at BT, potentially due to the reduction of stress from pollution and soil acidification. At BT, the strongest decrease between the two periods was observed in beech, likely reflecting the slower recovery of spruce due to its higher vulnerability to pollution and persistent legacy effects (Oulehle et al. 2024). At BF, spruce $\delta^{13}C$ values decreased stronger than those of beech when comparing 1970–1999 with 2000–2023, potentially due to the already mentioned drought-induced elevation of $\delta^{13}C$ in recent years. This rise in $\delta^{13}C$ may be connected to increased drought sensitivity, which was likely exacerbated by the high N deposition rates that peaked during the 1980s. These elevated N levels may have negatively impacted root systems and mycorrhizal associations, reducing the capacity of spruce to efficiently absorb water under drought conditions (Paligi et al. 2024). Gharun et al. (2021) studied beech at Lägern, a site near the SCPA+B location, and found that high N inputs initially enhanced

photosynthesis by increasing the activity of RuBisCO, the enzyme responsible for C fixation. Increased N boosted RuBisCO production, making leaves more efficient at using CO_2, which resulted in higher C assimilation rates. This enhanced photosynthesis also improved intrinsic water-use efficiency (WUE_i), the balance between C uptake and water loss, by enabling higher photosynthetic activity relative to water use. Enhanced photosynthesis lowers c_i within the leaves and thus reduces the discrimination against ^{13}C, resulting in higher $\delta^{13}C$ values. After the 1980s, declining N deposition reduced its fertilizing effect and caused photosynthesis to decrease compared to water loss. This change led to lower $\delta^{13}C$ values over time. As mentioned before, prolonged high N levels also left lasting effects, further lowering the ability of beech to photosynthesize efficiently. While rising atmospheric CO_2 after 1980 could have helped trees by increasing C uptake, stress from soil degradation and lower N inputs made it harder for trees to fully benefit from the extra CO_2. The repeated severe droughts after 2000 added further stress to beech trees already weakened by these lasting effects of N deposition (Paligi et al. 2024). This pattern was also reflected in the decreasing growth rates observed at SCPA+B and BF. However, at BT, growth was likely enhanced due to stress reduction associated with lower SO_x levels.

When comparing the beech chronologies from the study by Gharun et al. (2021) and BF, strong similarities can be observed (Fig. 46). The initial increase due to N fertilization, followed by a decline related to N saturation, indicates that trees at both sites reacted similarly to N inputs. Additionally, similar climate conditions at both sites suggest comparable increases in $\delta^{13}C$ values due to drought stress. This can be seen in the temporarily higher $\delta^{13}C$ values during moderate droughts in the 1980s and 1990s. At the BT site, N input was comparable to that at BF and SCPA+B. Therefore, the strong increase in $\delta^{13}C$ values observed at BT during the peak pollution period of the 1970s and 1980s can be primarily attributed to S deposition rather than N deposition. If N deposition had been the dominant factor, the $\delta^{13}C$ increase at BF would have been similarly pronounced, supporting the same conclusion discussed earlier in relation to TRW. Although BFS and BFB also showed elevated $\delta^{13}C$ values during the 1980s and 1990s, the stress was probably due to droughts, as highlighted in the TRW analysis and supported by previous studies (Leuschner 2020; Spiecker and Kahle 2023). This is further supported by the $\delta^{13}C$ data (Fig. 40), where BFS and BFB increased during the 1976 drought, decreased rapidly thereafter, rose again in the mid-1980s and then just stayed elevated briefly before gradually declining again. Since the years were pooled into 5-year blocks, it is not possible to say exactly in which year the increase was highest. However, the fact that the period of elevated values aligns with the droughts of the mid-1980s and early 1990s, while lower values correspond to a phase of favorable climate, strongly supports droughts as the primary stressor during this time. The observation that the next increase occurred

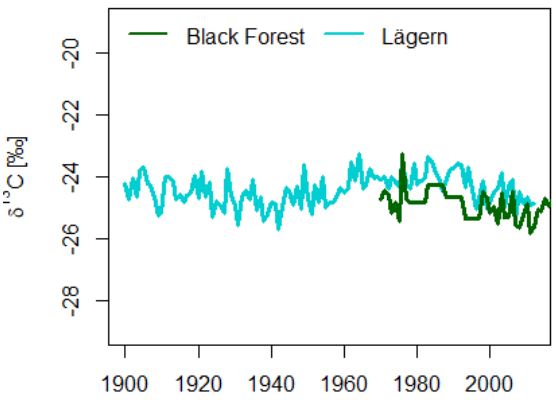

Fig. 46: $\delta^{13}C$ chronologies from beech of BF and Lägern (based on data from Gharun et al., 2021)

again during the drought years of the late 1990s further reinforces this conclusion. If pollution were the main cause of stress, the values would have remained consistently high and would not have recovered immediately following the droughts. In contrast, BTS and BTB $\delta^{13}C$ values remained elevated after the 1976 drought, and BTS even continued to increase over the subsequent decades. Moderate droughts during the 1980s and 1990s likely added to the stress experienced at BT during this period.

Looking at the average $\delta^{13}C$ response during extreme drought years (Fig. 42), the elevated values observed in both species at BT before the event reflect the continuing effects of the prolonged 2018/2019 drought. This underscores the impact of sequential stress events in influencing physiological responses. Moreover, isotopic composition in tree rings is usually affected by multiple interacting environmental factors, especially in temperate forests, which complicates the interpretation of SEA results (Hartl-Meier et al. 2015a). Overlapping time windows analyzed due to repeated drought events, such as 2018/2019 and 2020, or the 2006 heatwave following the 2003 drought, probably affected the SEA results and reduced their statistical significance. Choosing only three event years to analyze the average response to extreme droughts probably does not fully capture the complexity of drought responses but can provide a useful overview, showing basic patterns. Thus, focusing on individual extreme drought years could offer deeper insights into drought impacts, as average responses may obscure important year-specific variations.

4.2.3 $\delta^{13}C$ responses to extreme drought events

Looking at $\delta^{13}C$ values during specific extreme drought years, distinct patterns highlight the varying responses of species and sites to severe water stress (Fig. 41). Comparing these responses with individual sensitivity to climatic variations (Fig. 43 and Fig. 44) helps identify the underlying causes for the differing reactions observed during drought years. In 1976, when drought conditions were most severe in June at both sites, beech showed higher $\delta^{13}C$ values than spruce, with the highest increases at BF, where the drought was more severe. This also aligns with the strongest correlations between beech $\delta^{13}C$ and SPEI for June–July at both sites. Also during the 2003 drought, beech showed a stronger response at BF, reflecting its sensitivity to June–August drought conditions, when the drought was most severe. At BT, however, spruce exhibited a stronger reaction because the drought had already started in February. Combined with its sensitivity to winter and spring drought, with highest $\delta^{13}C$ correlations occurring for February–July, it suffered more than beech. Additionally, higher temperatures from June to August added to the stress due to their positive correlations with $\delta^{13}C$ in spruce. During the prolonged 2018/2019 drought, $\delta^{13}C$ values increased only in beech at BF. The strongest drought impacts occurred from April to July, coinciding with the highest correlation of its $\delta^{13}C$ with SPEI. Additionally, higher temperatures from April onwards had a stronger effect on beech $\delta^{13}C$ than on spruce. In contrast, spruce at BF had consistently slightly elevated $\delta^{13}C$ values compared to beech since the 2003 drought, probably due to the impact of repeated moderate droughts. Beech began to exhibit elevated $\delta^{13}C$ values after the moderate 2015 drought, even exceeding those of spruce. These values rose further during the 2018 drought and

remained elevated throughout 2019. This pattern again highlights the combined effects of previously discussed physiological adjustments to drought stress. Beech can cope with single droughts due to its anisohydric strategy, but repeated droughts can cause more damage to its water transport system and overall health. This cumulated damage made it harder for beech to recover (Pflug et al. 2018; Frei et al. 2022). At BT, both beech and spruce showed extremely high $\delta^{13}C$ values in 2019 due to the more intense and prolonged drought at this site. Dry conditions began in February 2018, persisted from April to November, and returned in spring 2019 after a moderately wet December and January. This led to minimal water availability causing severe stress for both species. Additionally, beech $\delta^{13}C$ showed a strong correlation with the previous year's summer temperatures, which were already high in 2018, leading to further increases in $\delta^{13}C$ values in 2019. The 2020 drought, which mainly affected April and July, had a greater impact on spruce $\delta^{13}C$ at BF, while at BT beech reacted more to it due to its stronger correlation with SPEI for April–July. In 2022, mainly trees at BF reacted to the drought, with beech showing slightly higher values than spruce. This could be attributed to the strong correlations of both species with May and July, when the drought was most severe. At BT, both species showed only small increase, likely due to the previous year's wet conditions and heavy snowfall during winter, which resulted in more water availability and thus reduced drought stress.

4.2.4 $\delta^{13}C$ responses to pollution

As shown by the analysis of extreme drought years, short-term $\delta^{13}C$ variations are primarily controlled by climatic variables that impact stomatal conductance. Sunlight and photosynthesis also play a role, but stomatal behavior is a central driver of high-frequency $\delta^{13}C$ changes (Gagen et al. 2022). This has also been demonstrated by the analysis of $\delta^{13}C$ in relation to climate variability. These variations occur over short time scales, such as months or seasons, and are generally independent of long-term pollution trends, which act more gradually over decades (Wagner and Wagner 2006). Interestingly, the relationship between $\delta^{13}C$ and climate variability generally showed relatively weak correlations at the BT site. This weakened climate signal in the isotopes can be attributed to pollution. Studies have found that high levels of SO_2 emissions during peak pollution periods caused stomatal closure and thus reduced the sensitivity of $\delta^{13}C$ to climatic variability and masked the influence of short-term climate fluctuations. However, after the reduction of SO_2 emissions after the 1980s, the climate signal in $\delta^{13}C$ partially recovered as stomatal conductance increased and the isotopic response to climate became more pronounced again (Boettger et al. 2014).

To explore this further, correlations with climate factors were also analyzed using undetrended $\delta^{13}C$ data that had been corrected for atmospheric $\delta^{13}C$ changes. Since these data are influenced by other factors, the correlations visualized in correlation matrices seemed unusual. At the BF site, the correlations were similar to those observed with the detrended data but were noticeably weaker, likely due to non-climatic factors that damped the $\delta^{13}C$ signal, such as age trend or general temperature increase (Belmecheri et al. 2022). At the BT site, the correlations were not only weakened but also showed notable differences to

those with the correlated data. For instance, temperature showed negative correlations with $\delta^{13}C$ (Fig. 44) instead of the expected positive correlations typically associated with stomatal conductance (Saurer et al. 2008). This unexpected relationship suggests that another strong factor might be interfering with or changing the $\delta^{13}C$-climate signal, which has a bigger impact than climate alone. In contrast, correlations at the BF site were only slightly weaker, indicating that the trend influencing the data at BF is less pronounced or significant than the one affecting BT. Differences in S deposition, with much higher levels at BT compared to BF, likely played a major role in driving the $\delta^{13}C$ signal at BT, in addition to the influence of climate factors. Thus, the influence of SO_x at BT was further investigated through multiple linear regression, which included both SO_x and June–July temperatures, when the positive correlation with detrended data is strongest, and undetrended $\delta^{13}C$ data. Instead of the unexpected negative relationship observed earlier in the Pearson correlation analysis, positive correlations resulted. Although these were not statistically significant, the results suggest that S deposition at BT had a considerable impact on $\delta^{13}C$ values, potentially masking the typical positive relationship between $\delta^{13}C$ and temperature.

The results of the linear regression analyses of $\delta^{13}C$ with pollutants (Fig. 45) further confirmed impacts from pollution. Moreover, they revealed notable differences between BF and BT. Positive correlations between $\delta^{13}C$ and pollutants were observed at both sites, but these relationships were statistically significantly stronger at BT than at BF. At BF, the significant correlation between $\delta^{13}C$ and NH_x reflects the previously discussed role of N inputs in enhancing photosynthesis and WUE_i (Gharun et al. 2021). The weaker correlation with SO_x at BF compared to BT indicates that S deposition had less impact at this site, which is consistent with the lower deposition level compared to BT. Prolonged SO_2 exposure can disrupt the balance between C assimilation and stomatal conductance, leading to elevated $\delta^{13}C$ values. However, this effect was likely minimal at BT due to its lower S deposition levels, which explains the weaker $\delta^{13}C$ response at this site (Rinne et al. 2010).

At BT, beech $\delta^{13}C$ demonstrated strong and highly statistically significant relationships with all three pollutants, with SO_x showing the strongest correlation. This aligns with the persistent exceedance of CLmaxS throughout the 20th century, which caused stomatal closure and elevated $\delta^{13}C$ values (Savard 2010; Siegwolf et al. 2022). Prolonged SO_2 exposure at BT likely elevated $\delta^{13}C$ values through mechanisms such as increased dark respiration, where trees use more energy for basic metabolic processes, and altered C allocation between growth and storage. This led to reduced discrimination against ^{13}C, which resulted in $\delta^{13}C$ enrichment (Wagner and Wagner, 2006). Additionally, SO_2 exposure can cause oxidative stress in trees by generating harmful molecules that damage important components of the photosynthetic system, such as chloroplasts. This disruption reduces the efficiency of C assimilation and thus leads to raised $\delta^{13}C$ values. Furthermore, SO_2 can lead to acidification within plant cells, which alters their internal pH. This acidic environment impairs the function of important enzymes involved in photosynthesis, such as RuBisCO, further compounding the impact on $\delta^{13}C$ values (Dhir et al., 2022).

Significant correlations were also observed for spruce at BT, with NH_x and SO_x showing moderate positive relationships, while NO_γ demonstrated the strongest correlation. The influence of NO_γ likely reflected its dual role as a nutrient at moderate levels but as a stress inducer at higher concentrations (Savard 2010). However, spruce $\delta^{13}C$ at BT did not fully align with expected trends under pollution stress. This discrepancy may result from the combined effects of pollution and climatic conditions, such as unusually cold summers or repeated moderate droughts, both of which occurred during the 1970s and 1980s (Kroupová 2002; Rydval and Wilson 2012; Andreu-Hayles et al. 2022; Gagen et al. 2022). These factors likely contributed to increased $\delta^{13}C$ variability during the peak pollution period (Rinne et al. 2010). Additionally, legacy effects of prolonged SO_2 exposure, such as reduced photosynthetic efficiency and altered nutrient dynamics, could have delayed spruce recovery even after reductions in SO_2 emissions post-1980 (Rinne et al. 2010). The greater $\delta^{13}C$ variability in spruce at BT probably reflected its higher drought sensitivity and isohydric water-saving strategy. Repeated droughts at BT during the peak pollution period may have caused cumulative stress, leading to inconsistent stomatal responses. In contrast, beech exhibited more stable $\delta^{13}C$ responses, supported by its anisohydric strategy, which maintains higher stomatal conductance under moderate stress (Savard et al. 2020).

Other studies conducted in the Bohemian Forest mountains in the Czech Republic, near the BT site, which were also exposed to heavy atmospheric pollution in the last century, found a strong impact of air pollution on $\delta^{13}C$ (Santruckova et al. 2007; Píšová et al. 2008). They investigated the influence of SO_x and NO_x deposition on tree physiology, primarily using $\Delta^{13}C$ of spruce. $\Delta^{13}C$ represents C isotope discrimination during photosynthesis and reflects the balance between stomatal conductance and C assimilation, which makes it a valuable indicator of environmental stress on trees. It is calculated from the ratio of stable C isotopes (^{13}C /^{12}C) in plant biomass relative to the atmospheric ^{13}C content, corrected for temporal changes in atmospheric $\delta^{13}C$ due to fossil fuel emissions and other factors (Saurer et al. 2004). These studies confirmed that acid deposition led to significant reductions in soil pH and an increase in aluminum toxicity, which impaired nutrient uptake and water availability by forcing roots into upper soil layers. The isotopic signal in the tree rings reflected these physiological stresses, with $\Delta^{13}C$ values showing a sharp decline between the 1950s and 1980s, coinciding with the peak of pollution. This decline was attributed to stomatal closure caused by SO_2 exposure, which disrupted the balance between C assimilation and WUE. It was observed that the assimilation organs were damaged by pollution, which resulted in reduced photosynthetic efficiency. Then a gradual recovery of $\Delta^{13}C$ values was observed since the 1990s, which corresponding to the reduction of S and N depositions and the associated partial recovery of biological processes within the trees. When transforming $\delta^{13}C$ from BT to $\Delta^{13}C$ and averaging the values in 10-year blocks for comparison with the $\Delta^{13}C$ chronology from Píšová et al. (2008) (Fig. 47), the patterns observed at BT closely align with those reported in the Bohemian Forest Mountains. While the trends are consistent, differences in the absolute values can be attributed to methodological variations, such as the use of whole wood versus cellulose, as well as site-specific conditions. Despite these differences, the overall similarity in trends and their temporal

agreement confirm that pollution was the dominant driver of $\Delta^{13}C$, respectively, $\delta^{13}C$ variability at both sites during the peak pollution period. Moreover, the Bohemian Forest studies also reported weakened correlations between $\Delta^{13}C$ and climatic factors during the peak pollution period, a phenomenon similar to the already discussed observations at the BT site. Although the Bohemian Forest Mountain studies focused just on spruce, the trends are comparable to the ones observed in beech at BT, further highlighting the consistent regional impact of pollution on tree physiology.

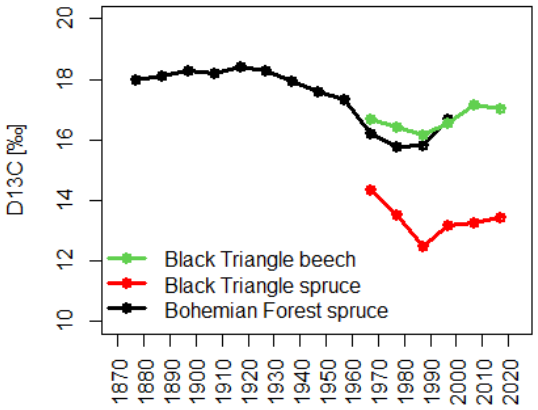

Fig. 47: $\Delta^{13}C$ chronologies from BT and Bohemian Forest (based on data from Píšová et al., 2008)

4.2.5 Methodological considerations

When analyzing undetrended $\delta^{13}C$ data in relation to N and S deposition and climate, it is important to consider autocorrelation. Autocorrelation means that $\delta^{13}C$ values from one year are influenced by conditions from previous years. Undetrended data, which include long-term trends, such as tree aging or atmospheric changes, show stronger autocorrelation compared to detrended data. This can reduce the independence of the observations and lead to overestimating the strength of statistical results. This is especially an issue in smaller datasets, where fewer effective observations can make it harder to draw reliable conclusions about the relationships between $\delta^{13}C$, pollution, and climate (Fritts and Swetnam 1989; Manzanedo and Pederson 2019). As mentioned earlier, short-term changes in $\delta^{13}C$ are strongly influenced by climate factors, especially those that affect stomatal conductance, like drought. However, pollution can have a long-term impact that overlaps with these short-term effects. For example, at the BT site, high levels of SO_2 emissions during peak pollution periods caused stomatal closure, which weakened the $\delta^{13}C$ response to climate changes. After SO_2 emissions decreased in the 1980s, the $\delta^{13}C$ signal started to recover, showing stronger responses to climate again (Boettger et al. 2014). To better understand how $\delta^{13}C$ is influenced by pollution and climate, Principal Component Analysis (PCA) could be a useful method. PCA simplifies complex datasets by grouping related variables into a smaller number of components, helping to identify major patterns. This could provide insight into how $\delta^{13}C$ responds to S and N deposition and drought in spruce and beech. PCA is useful for distinguishing common trends caused by pollution from species-specific responses, which is especially relevant at sites like BT, where the impact of pollution was more pronounced (Guerrieri et al. 2020).

Additionally, common trends and co-integration are valuable tools for understanding long-term $\delta^{13}C$ responses. A common trend shows shared $\delta^{13}C$ patterns across spruce and beech caused by widespread environmental factors like pollution or regional climate changes. Co-integration focuses on long-term connections between the $\delta^{13}C$ of different species, even when their short-term responses differ due to the already discussed physiological differences (Haugen et al. 2015). These methods are particularly

useful for studying undetrended $\delta^{13}C$ data, as they help separate the long-term impacts of pollution from short-term climate variability. Although this study does not use PCA, common trends, or co-integration analyzes due to the scope of a MSc thesis, these methods are discussed to highlight their potential. Future research using these approaches could provide deeper insights into how air pollution and climate interact to influence $\delta^{13}C$ in spruce and beech. This thesis focuses on simpler methods to analyze and interpret the data, while acknowledging the value of these advanced techniques for further studies.

5. Conclusion

This thesis investigated the causes of forest dieback during the 1970s and 1980s in Central Europe, focusing on Norway spruce and European beech in three regions with varying pollution histories: SCPA+B, BF, and BT, using TRW and $\delta^{13}C$ data. It was analyzed how climate, air pollution, site-specific conditions, and species-specific traits influenced tree responses and forest decline. The findings revealed that forest dieback during the 1970s and 1980s was caused by a combination of region-specific stressors with different impacts across sites. At SCPA+B and BF, which are areas with low to moderate diffuse pollution, drought was identified as the primary stressor leading to tree mortality and forest dieback during the 1970s and 1980s. Severe droughts, such as the one in 1976, caused strong growth reductions, particularly in spruce, which showed higher sensitivity to drought. The deeper rooting system of beech enabled a better access to water reserves and thus enhanced its resilience to drought-induced stress. However, the cumulative drought effects in recent decades have challenged its stability, as seen in slower recovery following repeated drought events. Besides the fact that drought was the dominant driver of stress in regions with diffuse light or moderate pollution, bark beetle infestations also added to the stress in spruce at SCPA+B and BF, amplifying the impact of drought and leading to increased mortality.

In contrast, at the heavily polluted BT, forest dieback was primarily caused by air pollution, with S deposition playing a more central role than at the other two sites. The combined prolonged deposition of S and N caused severe soil acidification, magnesium depletion, and aluminum toxicity, weakening trees and increasing their sensitivity to other stressors. Winter inversion layers trapped pollutants near the ground, increasing exposure to SO_2 and compounding its direct physiological effects, such as damage to assimilatory organs and impaired photosynthesis. Extreme frost events and cold summers increased tree stress at BT, especially in beech, which is more frost-sensitive than spruce. Beech suffered more directly from frost damage, with a faster decline in growth when combined with pollution. However, it recovered more quickly than spruce due to its physiological flexibility. Spruce, in contrast, experienced more severe and prolonged stress due to its higher sensitivity to pollution. The combined effects of extreme winter frost events, late frosts, cold summers, moderate droughts, and pollution were particularly detrimental to spruce, leading to prolonged growth stagnation. Bark beetle infestations also contributed to forest decline in spruce at BT, while beech scale infestations added stress to beech trees during this period. N deposition contributed to nutrient saturation and subsequent stress at all three sites.

Initially, N deposition acted as a growth stimulant by enhancing photosynthesis. However, prolonged exposure led to imbalances in nutrient cycling, making trees more vulnerable to other stressors. Similar levels of N deposition across SCPA+B, BF, and BT suggest that N-related stress was comparable at all three sites. The heightened tree stress observed at BT can therefore be attributed to the substantially higher S deposition levels during the peak pollution period at this site compared to SCPA+B and BF. Once the fertilizing effect of N deposition ended at SCPA+B and BF, drought sensitivity increased, contributing to intensified drought stress in recent years. At BT, the weaker climate signal in $\delta^{13}C$ data reflected the legacy effects of pollution, which masked typical $\delta^{13}C$-climate responses. The distinct climate at BT, characterized by colder winters, a shorter growing season, and higher continentality, made both spruce and beech less responsive to drought compared to SCPA+B and BF. However, in recent years, trees at BT have also been affected more by drought, with events such as the prolonged 2018/2019 drought that caused significant stress. Although trees at BT have recovered following the reduction of air pollution in the 1990s, legacy effects of pollution, combined with the increasing frequency of severe droughts, continue to affect tree responses and forest health.

The study also revealed notable differences in tree responses to drought events. Spruce exhibited sharper growth declines and higher $\delta^{13}C$ values, reflecting its isohydric strategy of rapid stomatal closure, which conserves water but limits photosynthesis and C assimilation. Beech, with its anisohydric strategy, maintained photosynthesis during drought but faced a higher risk of hydraulic failure. These contrasting strategies were further shaped by site conditions such as soil depth, water-holding capacity, and topography. Ranking drought events from tree perspective was challenging due to differences in drought timing, intensity, duration, and the cumulative impacts of prior and subsequent stressors. Nonetheless, the results suggest that prolonged and frequent severe droughts, such as those in 2018/2019/2020, cause greater stress. Thus, the rising frequency of severe droughts poses a major challenge, especially for beech, which recovers more slowly from repeated drought stress. Spruce, with its high drought sensitivity, will also face increasing pressure, and drought-weakened trees will be more susceptible to mortality, particularly due to bark beetle infestations.

Overall, this thesis highlights how tree stress and mortality during the 1970s and 1980s were impacted by the interplay of climatic extremes, air pollution, site-specific factors, and species-specific traits. While drought was the main driver in regions with low and moderate diffuse pollution, stress at BT was primarily linked to air pollution, compounded by extreme frost, late frost, cold summers, and occasional moderate droughts. The lasting effects of acidification at BT highlight the importance of pollution legacy effects in influencing forest health, even decades after emissions have been reduced. At the BT site, high S deposition had a greater role in pollution stress than N deposition, which, after an initial fertilization effect, caused similar stress across all sites. These findings are important for managing forests. Knowing how different sites and tree species react to stress is crucial for species selection and forest management strategies to make forests more resilient. Future research could include also other species and focus on

separating the effects of drought, frost, and specific pollutants through advanced statistical analysis and long-term monitoring. Addressing the long-term impacts of past pollution and dealing with the growing threat of more severe and frequent droughts due to climate change will be central to protecting Central European forests and the ecological, economic, and cultural services and benefits they provide.

Literature

Akselsson, C., Ardö, J. and Sverdrup, H. 2004. Critical loads of acidity for forest soils and relationship to forest decline in the northern Czech Republic. *Environmental Monitoring and Assessment* (98), pp. 363–379.

Allen, C.D. et al. 2010. A global overview of drought and heat-induced tree mortality reveals emerging climate change risks for forests. *Forest Ecology and Management* 259(4), pp. 660–684. doi: 10.1016/J.FORECO.2009.09.001.

Andreu-Hayles, L. et al. 2022. Limits and Strengths of Tree-Ring Stable Isotopes. *Tree Physiology* 8, pp. 399–428. Available at: https://link.springer.com/chapter/10.1007/978-3-030-92698-4_14 [Accessed: 26 December 2024].

Arnič, D., Gričar, J., Jevšenak, J., Božič, G., von Arx, G. and Prislan, P. 2021. Different Wood Anatomical and Growth Responses in European Beech (Fagus sylvatica L.) at Three Forest Sites in Slovenia. *Frontiers in Plant Science* 12, p. 669229. Available at: www.frontiersin.org [Accessed: 26 January 2025].

Augustin, S., Bolte, A., Holzhausen, M. and Wolff, B. 2005. Exceedance of critical loads of nitrogen and sulphur and its relation to forest conditions. *European Journal of Forest Research* 124(4), pp. 289–300. Available at: https://link.springer.com/article/10.1007/s10342-005-0095-1 [Accessed: 23 December 2024].

Belmecheri, S., Wright, W.E. and Szejner, P. 2022. Sample Collection and Preparation for Annual and Intra-annual Tree-Ring Isotope Chronologies. pp. 103–134. doi: 10.1007/978-3-030-92698-4_4.

Bobbink, R. et al. 2015. Effects and Empirical Critical Loads of Nitrogen for Europe. In: De Vries, W., Hettelingh, J.-P., and Posch, M. eds. *Critical Loads and Dynamic Risk Assessments. Nitrogen, Acidity and Metals in Terrestrial and Aquatic Ecosystems.* pp. 85–127. doi: 10.1007/978-94-017-9508-1_4.

Bobbink, R., Loran, C. and Tomassen, H. 2022. *Review and revision of empirical critical loads of nitrogen for Europe*. German Environment Agency.

Boden, S., Kahle, H.P., Wilpert, K. von and Spiecker, H. 2014. Resilience of Norway spruce (Picea abies (L.) Karst) growth to changing climatic conditions in Southwest Germany. *Forest Ecology and Management* 315, pp. 12–21. doi: 10.1016/j.foreco.2013.12.015.

Boettger, T., Haupt, M., Friedrich, M. and Waterhouse, J.S. 2014. Reduced climate sensitivity of carbon, oxygen and hydrogen stable isotope ratios in tree-ring cellulose of silver fir (Abies alba Mill.) influenced by background SO2 in Franconia (Germany, Central Europe). *Environmental Pollution* 185, pp. 281–294. doi: 10.1016/j.envpol.2013.10.030.

Bosela, M. et al. 2018. Contrasting effects of environmental change on the radial growth of co-occurring beech and fir trees across Europe. *Science of the Total Environment* 615, pp. 1460–1469. doi: 10.1016/j.scitotenv.2017.09.092.

Bosela, M., Kulla, L., Roessiger, J., Šebeň, V., Dobor, L., Büntgen, U. and Lukac, M. 2019. Long-term effects of environmental change and species diversity on tree radial growth in a mixed European forest. *Forest Ecology and Management* 446, pp. 293–303. doi: 10.1016/j.foreco.2019.05.033.

Bottero, A. et al. 2021. Growth resistance and resilience of mixed silver fir and Norway spruce forests in central Europe: Contrasting responses to mild and severe droughts. *Global Change Biology* 27(18), pp. 4403–4419. doi: 10.1111/gcb.15737.

Brady, N. and Weil, R. 2017. *Nature and Properties of Soils*. Pearson Education Limited. pp. 375–376. Available at: https://www.researchgate.net/publication/301200878_The_Nature_and_Properties_of_Soils_15th_edition [Accessed: 23 January 2025].

Braun, S., Schindler, C. and Rihm, B. 2017. Growth trends of beech and Norway spruce in Switzerland: The role of nitrogen deposition, ozone, mineral nutrition and climate. *Science of The Total Environment* 599–600, pp. 637–646. doi: 10.1016/J.SCITOTENV.2017.04.230.

Brázdil, R., Trnka, M., Dobrovolný, P., Chromá, K., Hlavinka, P. and Žalud, Z. 2009. Variability of droughts in the Czech Republic, 1881-2006. *Theoretical and Applied Climatology* 97(3–4), pp. 297–315. doi: 10.1007/s00704-008-0065-x.

Brooks, J.R., Rugh, W.D., Werner, R.A., Brooks, J.R., Rugh, W.D. and Werner, R.A. 2022. Tree-Ring Stable Isotope Measurements: The Role of Quality Assurance and Quality Control to Ensure High Quality Data. *Tree Physiology* 8, pp. 191–213. Available at: https://link.springer.com/chapter/10.1007/978-3-030-92698-4_6 [Accessed: 26 December 2024].

Brunner, M.I., Liechti, K. and Zappa, M. 2019. Extremeness of recent drought events in Switzerland: Dependence on variable and return period choice. *Natural Hazards and Earth System Sciences* 19(10), pp. 2311–2323. doi: 10.5194/NHESS-19-2311-2019.

Büntgen, U. et al. 2021. Recent European drought extremes beyond Common Era background variability. *Nature Geoscience 2021 14:4* 14(4), pp. 190–196. Available at: https://www.nature.com/articles/s41561-021-00698-0 [Accessed: 25 December 2024].

Cernusak, L.A., Ubierna, N., Cernusak, L.A. and Ubierna, N. 2022. Carbon Isotope Effects in Relation to CO2 Assimilation by Tree Canopies. *Tree Physiology* 8, pp. 291–310. Available at: https://link.springer.com/chapter/10.1007/978-3-030-92698-4_9 [Accessed: 26 December 2024].

Cherubini, P., Battipaglia, G. and Innes, J.L. 2021. Tree Vitality and Forest Health: Can Tree-Ring Stable Isotopes Be Used as Indicators? *Current Forestry Reports* 7, pp. 69–80. Available at: https://doi.org/10.1007/s40725-021-00137-8.

Cienciala, E., Altman, J., Doležal, J., Kopáček, J., Štěpánek, P., Ståhl, G. and Tumajer, J. 2018. Increased spruce tree growth in Central Europe since 1960s. *Science of the Total Environment* 619(620), pp. 1637–1647. Available at: https://doi.org/10.1016/j.scitotenv.2017.10.138 [Accessed: 4 October 2023].

ClimateDT. 2024. *Climate Downscaling Tool - Institute of Biosciences and Bioresources*. Available at: https://www.ibbr.cnr.it/climate-dt/ [Accessed: 26 December 2024].

Collignon, C., Boudot, J.P. and Turpault, M.P. 2012. Time change of aluminium toxicity in the acid bulk soil and the rhizosphere in Norway spruce (Picea abies (L.) Karst.) and beech (Fagus sylvatica L.) stands. *Plant and Soil* 357(1–2), pp. 259–274. Available at: https://hal.science/hal-01268312 [Accessed: 21 January 2025].

Cook, E., Briffa, K., Shiyatov, S., Mazepa, V. and Jones, P.D. 1990. Data Analysis. *Methods of dendrochronology*, pp. 97–162. Available at: https://link.springer.com/chapter/10.1007/978-94-015-7879-0_3 [Accessed: 30 January 2025].

Von Detten, R., Metzger, B. and Brüggemeier. Franz-Josef. 2012. Der Wald stirbt?! Eine westdeutsche Debatte der 1980er Jahre. *Freiburger Universitätsblätter* 196, pp. 115–137.

Dhir, B. 2016. Air pollutants and photosynthetic efficiency of plants. *Plant Responses to Air Pollution*, pp. 71–84. Available at: https://link.springer.com/chapter/10.1007/978-981-10-1201-3_7 [Accessed: 26 December 2024].

Dulamsuren, C., Hauck, M., Kopp, G., Ruff, M. and Leuschner, C. 2017. European beech responds to climate change with growth decline at lower, and growth increase at higher elevations in the center of its distribution range (SW Germany). *Trees - Structure and Function* 31(2), pp. 673–686. doi: 10.1007/s00468-016-1499-x.

Earth Science Australia. 2024. *Dendrochronology*. Available at: https://earthsci.org/space/space/geotime/dendro/dendro.html [Accessed: 26 December 2024].

Ellenberg, H. and Leuschner, C. 2010. *Vegetation Mitteleuropas mit den Alpen in ökologischer, dynamischer und historischer Sicht*. 6th ed. Verlag EUgen Ulmer Stuttgart.

Engardt, M., Simpson, D., Schwikowski, M. and Granat, L. 2017. Deposition of sulphur and nitrogen in Europe 1900–2050. Model calculations and comparison to historical observations. *Tellus, Series B: Chemical and Physical Meteorology* 69(1). doi: 10.1080/16000889.2017.1328945.

ETH Library. [no date]. *Waldsterben Demonstration in Switzerland, 1984*. Available at: https://ba.e-pics.ethz.ch/#detail-asset=5a8c496c-8342-4a76-95ff-ad4d080a6285 [Accessed: 9 January 2025].

FOEN. 2017. *National Focal Centre Report - Switzerland. In: Hettelingh et al. 2017 (CCE Final Report). p. 177-190*. Available at: https://www.umweltbundesamt.de/en/cce-status-reports [Accessed: 20 January 2025].

FOEN, F.O. for the E. 2016. *Critical Loads of Nitrogen and their Exceedances. Swiss contribution to the effects-oriented work under the Convention on Long-range Transboundary Air Pollution (UNECE)*.

Francey, R.J. et al. 1999. A 1000-year high precision record of δ13C in atmospheric CO2. *Tellus B: Chemical and Physical Meteorology* 51(2), p. 170. Available at: https://www.tandfonline.com/doi/abs/10.3402/tellusb.v51i2.16269 [Accessed: 10 January 2025].

Frank, D., Fang, K. and Fonti, P. 2022. Dendrochronology: Fundamentals and Innovations. pp. 21–59. doi: 10.1007/978-3-030-92698-4_2.

Frei, E.R. et al. 2022. European beech dieback after premature leaf senescence during the 2018 drought in northern Switzerland. *Plant Biology (Stuttgart, Germany)* 24(7), p. 1132. Available at: https://pmc.ncbi.nlm.nih.gov/articles/PMC10092601/ [Accessed: 25 January 2025].

Fritts, H.C. 1976. *Tree Rings and Climate*. London, New York and San Francisco: Academic Press.

Fritts, H.C. and Swetnam, T.W. 1989. Dendroecology: A Tool for Evaluating Variations in Past and Present Forest Environments. *Advances in ecological research* 19, pp. 111–188.

Fung Au, T. et al. 2022. Younger trees in the upper canopy are more sensitive but also more resilient to drought. *Nature Climate Change* 12, pp. 1168–1174.

Gagen, M. et al. 2022. Climate Signals in Stable Isotope Tree-Ring Records. pp. 537–579. doi: 10.1007/978-3-030-92698-4_19.

Gärtner, H. and Nievergelt, D. 2010. The core-microtome: A new tool for surface preparation on cores and time series analysis of varying cell parameters. *Dendrochronologia* 28(2), pp. 85–92. doi: 10.1016/j.dendro.2009.09.002.

Gärtner, H., Schneider, L. and Cherubini, P. 2024. A New Workflow for Sampling and Digitizing Increment Cores. *Journal of Visualized Experiments (JoVE)* (211), p. e67098. Available at: https://app.jove.com/t/67098/a-new-workflow-for-sampling-and-digitizing-increment-cores [Accessed: 29 December 2024].

Geoportal Kanton Zürich. 2024. *GIS-Browser*. Available at: https://maps.zh.ch/ [Accessed: 27 December 2024].

Geupel, M., Loran, C., Scheuschner, T. and Wohlgemuth, L. 2022. *CCE Status Report 2022*.

Gharun, M. et al. 2021. Effect of nitrogen deposition on centennial forest water-use efficiency. *Environmental Research Letters* 16(11). doi: 10.1088/1748-9326/ac30f9.

Google Maps. 2024. *GeoBasis-DE/BKG*. Available at: https://www.google.com/maps/dir/?entry=wc [Accessed: 27 December 2024].

Gora, V., König, J. and Lunderstädt, J. 1996. Population dynamics of beech scale (Cryptococcus fagisuga) (Coccina, Pseudococcidae) related to physiological defence reactions of attacked beech trees (Fagus sylvatica). *Chemoecology* 7(2), pp. 112–120. Available at: https://link.springer.com/article/10.1007/BF01239488 [Accessed: 26 January 2025].

Grennfelt, P., Engleryd, A., Forsius, M., Hov, Ø., Rodhe, H. and Cowling, E. 2020. Acid rain and air pollution: 50 years of progress in environmental science and policy. *Ambio* 49(4), pp. 849–864. doi: 10.1007/s13280-019-01244-4.

Guerrieri, R., Vanguelova, E., Pitman, R., Benham, S., Perks, M., Morison, J.I.L. and Mencuccini, M. 2020. Climate and atmospheric deposition effects on forest water-use efficiency and nitrogen availability across Britain. *Scientific Reports 2020 10:1* 10(1), pp. 1–16. Available at: https://www.nature.com/articles/s41598-020-67562-w [Accessed: 28 January 2025].

Hájek, V. et al. 2021. Effect of climate change on the growth of endangered scree forests in krkonoše national park (Czech Republic). *Forests* 12(8). doi: 10.3390/f12081127.

Hänsel, S., Hoy, A., Brendel, C. and Maugeri, M. 2022. Record summers in Europe: Variations in drought and heavy precipitation during 1901–2018. *International Journal of Climatology* 42(12), pp. 6235–6257. doi: 10.1002/joc.7587.

Hartl-Meier, C. et al. 2015a. Uniform climate sensitivity in tree-ring stable isotopes across species and sites in a mid-latitude temperate forest. *Tree Physiology* 35(1), pp. 4–15. Available at: https://dx.doi.org/10.1093/treephys/tpu096 [Accessed: 24 December 2024].

Hartl-Meier, C., Büntgen, U. and Esper, J. 2015b. How is drought affecting forest growth and how can stable isotopes contribute to answer this question?

Haugen, M.A., Rajaratnam, B. and Switzer, P. 2015. Extracting Common Time Trends from Concurrent Time Series: Maximum Autocorrelation Factors with Application to Tree Ring Time Series Data. Available at: https://arxiv.org/abs/1502.01073v3 [Accessed: 28 January 2025].

Helle, G. et al. 2022. Stable Isotope Signatures of Wood, its Constituents and Methods of Cellulose Extraction. *Tree Physiology* 8, pp. 135–190. Available at: https://link.springer.com/chapter/10.1007/978-3-030-92698-4_5 [Accessed: 26 December 2024].

Hemmerle, H., May, J.-H., Preusser, F., Vergletscherungen, S. and Anschriften Der Verfasser, S. 2016. *Übersicht über die pleistozänen Vergletscherungen des Schwarzwaldes*.

Hettelingh, J.-P.., Posch, M.. and Slootweg, J.. 2017. *CCE Final Report 2017. European critical loads: database, biodiversity and ecosystems at risk*. National Institute for Public Health and the Environment.

Hopf, S.-E., Tresch, S. and Braun, S. 2020. *Rekonstruktion der Bodenversauerung in Schweizer Wäldern - Einblick in Prozesse der Bodenversauerung in Schweizer Wäldern anhand der historischen Entwicklungen von Elementkonzentrationen in Stammscheiben von Buchen, Fichten und Eichen*. Available at: www.iap.ch.

Houston, D.R. 1998. Exotic pests of eastern forests conference proceedings. In: Britton, K. O. ed. Forest Service and Tennessee Exotic Pest Plant Council, pp. 29–41.

Hruška, J., Oulehle, F., Chuman, T., Kolář, T., Rybníček, M., Trnka, M. and McDowell, W.H. 2023. Forest growth responds more to air pollution than soil acidification. *PLOS ONE* 18(3), p. e0256976. Available at: https://journals.plos.org/plosone/article?id=10.1371/journal.pone.0256976 [Accessed: 30 December 2024].

Hughes, M.K., Swetnam, T.W. and Diaz, H.F. 2011. *Dendroclimatology. Progress and Prospects*. Available at: http://www.springer.com/series/5869.

Hůnová, I., Maznová, J. and Kurfürst, P. 2014. Trends in atmospheric deposition fluxes of sulphur and nitrogen in Czech forests. *Environmental Pollution* 184, pp. 668–675. doi: 10.1016/j.envpol.2013.05.013.

Huttunen, S. and Laine, K. 1983. Effects of air-borne pollutants on the surface wax structure of Pinus sylvestris needles. *Annales Botanici Fennici* 20(1), pp. 79–86.

Jentschke, G. et al. 2001. Does soil acidity reduce subsoil rooting in norway spruce (picea abies)? *Plant and Soil* 237(1), pp. 91–108. Available at: https://link.springer.com/article/10.1023/A:1013305712465 [Accessed: 21 January 2025].

Kagawa, A., Battipaglia, G., Kagawa, A. and Battipaglia, G. 2022. Post-photosynthetic Carbon, Oxygen and Hydrogen Isotope Signal Transfer to Tree Rings—How Timing of Cell Formations and Turnover of Stored Carbohydrates Affect Intra-annual Isotope Variations. *Tree Physiology* 8, pp. 429–462.

Available at: https://link.springer.com/chapter/10.1007/978-3-030-92698-4_15 [Accessed: 26 December 2024].

Kahle, H. and Spiecker, H. 1996. Adaptability of radial growth of Norway spruce to climate variations: results of a site specific dendroecological study in high elevations of the Black Forest (Germany). In: *Tree Rings, Environment, and Humanity*. pp. 785–801.

Kandler, O. and Innes, J.L. 1995. Air pollution and forest decline in Central Europe. *Environmental Pollution* 90(2), pp. 171–180.

Keller, T. 1984. *Direct effects of sulphur dioxide on trees*. Available at: https://about.jstor.org/terms.

Klesse, S. et al. 2022. Long-term soil water limitation and previous tree vigor drive local variability of drought-induced crown dieback in Fagus sylvatica. *Science of the Total Environment* 851. doi: 10.1016/j.scitotenv.2022.157926.

Klesse, S. et al. 2024. No Future Growth Enhancement Expected at the Northern Edge for European Beech due to Continued Water Limitation. *Global Change Biology* 30(10). Available at: https://onlinelibrary.wiley.com/doi/10.1111/gcb.17546.

Kolář, T. et al. 2015. Pollution control enhanced spruce growth in the 'Black Triangle' near the Czech-Polish border. *Science of the Total Environment* 538, pp. 703–711. doi: 10.1016/j.scitotenv.2015.08.105.

Kolář, T., Čermák, P., Trnka, M., Žid, T. and Rybníček, M. 2017. Temporal changes in the climate sensitivity of Norway spruce and European beech along an elevation gradient in Central Europe. *Agricultural and Forest Meteorology* 239, pp. 24–33. doi: 10.1016/j.agrformet.2017.02.028.

Kopáček, J. and Veselý, J. 2005. Sulfur and nitrogen emissions in the Czech Republic and Slovakia from 1850 till 2000. *Atmospheric Environment* 39(12), pp. 2179–2188. doi: 10.1016/j.atmosenv.2005.01.002.

Köppen, W. 1918. Klassifikation der Klimate nach Temperatur, Niederschlag und Jahresablauf. *Petermanns Geographische Mitteilungen* (64), pp. 193–203.

Křeček, J. and Hořická, Z. 2006. Forests, air pollution and water quality: influencing health in the headwaters of Central Europe's "Black Triangle".

Krejza, J. et al. 2021. Evidence of climate-induced stress of Norway spruce along elevation gradient preceding the current dieback in Central Europe. *Trees - Structure and Function* 35(1), pp. 103–119. doi: 10.1007/s00468-020-02022-6.

Kroupová, M. 2002. Dendroecological study of spruce growth in regions under long-term air pollution load. *Journal of Forest Science* 48(12), pp. 536–548. doi: 10.17221/11921-jfs.

Kuneš, I. et al. 2024. The history of the Jizera Mts forests in the former heavily polluted area of Central Europe. *Anthropocene Review* 11(2), pp. 463–487. doi: 10.1177/20530196231204344.

Lábusová, J. et al. 2019. Patterns of forest dynamics in a secondary old-growth beech-dominated forest in the jizera mountains beech forest reserve, Czech republic. *IForest* 12(1), pp. 17–26. doi: 10.3832/ifor2702-011.

Landolt, W. and Keller, T. 1985. Uptake and effects of air pollutants on woody plants. *Experientia* 41(3), pp. 301–310. doi: https://doi.org/10.1007/BF02004490.

Leuschner, C. 2020. Drought response of European beech (Fagus sylvatica L.)—A review. *Perspectives in Plant Ecology, Evolution and Systematics* 47. doi: 10.1016/j.ppees.2020.125576.

Leuschner, C. and Meier, I.C. 2018. The ecology of Central European tree species: Trait spectra, functional trade-offs, and ecological classification of adult trees. *Perspectives in Plant Ecology, Evolution and Systematics* 33, pp. 89–103. doi: 10.1016/j.ppees.2018.05.003.

LGRB. 2024. *Kartenviewer*. Available at: https://maps.lgrb-bw.de/ [Accessed: 27 December 2024].

Lindner, M. et al. 2010. Climate change impacts, adaptive capacity, and vulnerability of European forest ecosystems. *Forest Ecology and Management* 259(4), pp. 698–709. doi: 10.1016/j.foreco.2009.09.023.

Lomský, B., Šrámek, V. and Novotný, R. 2012. Changes in the air pollution load in the Jizera Mts.: Effects on the health status and mineral nutrition of the young Norway spruce stands. *European Journal of Forest Research* 131(3), pp. 757–771. doi: 10.1007/s10342-011-0549-6.

LUBW. 2010. *Bericht zur Versauerung der Umwelt*.

Manzanedo, R.D. and Pederson, N. 2019. Towards a More Ecological Dendroecology. *Tree-Ring Research* 75(2), pp. 152–159. Available at: https://dx.doi.org/10.3959/1536-1098-75.2.152 [Accessed: 28 January 2025].

Marchi, M., Bucci, G., Iovieno, P. and Ray, D. 2024. ClimateDT: A Global Scale-Free Dynamic Downscaling Portal for Historic and Future Climate Data. *Environments - MDPI* 11(4). doi: 10.3390/environments11040082.

Maxwell, R.S. and Larsson, L.A. 2021. Measuring tree-ring widths using the CooRecorder software application. *Dendrochronologia* 67, p. 125841. doi: 10.1016/J.DENDRO.2021.125841.

McDowell, N. et al. 2008. Mechanisms of plant survival and mortality during drought: Why do some plants survive while others succumb to drought? *New Phytologist* 178(4), pp. 719–739. doi: 10.1111/j.1469-8137.2008.02436.x.

Mckee, T.B., Doesken, N.J. and Kleist, J. 1993. The relationship of drought frequency and duration to time scales. In: *Eighth Conference on Applied Climatology*. Boston: American Meteorological Society, pp. 179–184.

Menzel, A., Helm, R. and Zang, C. 2015. Patterns of late spring frost leaf damage and recovery in a European beech (Fagus sylvatica L.) stand in south-eastern Germany based on repeated digital photographs. *Frontiers in Plant Science* 6(FEB), p. 116555. Available at: www.frontiersin.org [Accessed: 18 January 2025].

Mitwelt Stiftung Oberrhein. [no date]. *Waldsterben & Klimawandel in Deutschland aktuell: Hitze, Trockenheit*. Available at: https://www.mitwelt.org/waldsterben-klimawandel-aktuell.html [Accessed: 26 December 2024].

Mölder, I., Leuschner, C. and Leuschner, H.H. 2011. δ13C signature of tree rings and radial increment of Fagus sylvatica trees as dependent on tree neighborhood and climate. *Trees - Structure and Function* 25(2), pp. 215–229. doi: 10.1007/s00468-010-0499-5.

Muzika, R.M., Guyette, R.P., Zielonka, T. and Liebhold, A.M. 2004. The influence of O3, NO2 and SO2 on growth of Picea abies and Fagus sylvatica in the Carpathian Mountains. In: *Environmental Pollution*. pp. 65–71. doi: 10.1016/j.envpol.2003.10.021.

Neycken, A., Wohlgemuth, T., Frei, E.R., Klesse, S., Baltensweiler, A. and Lévesque, M. 2024. Slower growth prior to the 2018 drought and a high growth sensitivity to previous year summer conditions predisposed European beech to crown dieback. *Science of the Total Environment* 912. doi: 10.1016/j.scitotenv.2023.169068.

Nilsson, J. and Grennfelt, P. 1988. *Critical Loads for Sulphur and Nitrogen, Report from a workshop held at Skokloster, Sweden*.

Oulehle, F., Kolář, T., Rybníček, M., Hruška, J., Büntgen, U. and Trnka, M. 2024. Complex imprint of air pollution in the basal area increments of three European tree species. *Science of the Total Environment* 951. doi: 10.1016/j.scitotenv.2024.175858.

Paligi, S.S. et al. 2024. Water status dynamics and drought tolerance of juvenile European beech, Douglas fir and Norway spruce trees as dependent on neighborhood and nitrogen supply. *Tree Physiology* 44(5). doi: 10.1093/treephys/tpae044.

Pflug, E.E., Buchmann, N., Siegwolf, R.T.W., Schaub, M., Rigling, A. and Arend, M. 2018. Resilient Leaf Physiological Response of European Beech (Fagus sylvatica L.) to Summer Drought and Drought Release. *Frontiers in Plant Science* 9, p. 187. Available at: https://pmc.ncbi.nlm.nih.gov/articles/PMC5825912/ [Accessed: 25 January 2025].

Píšová, L., Svoboda, M., Šantrůček, J. and Šantrůčková, H. 2008. Can 13C stable isotope record of Norway spruce tree rings display the effect of environmental conditions. *Journal of Forest Science* 54(6), pp. 255–261.

Popa, A., van der Maaten-Theunissen, M., Popa, I., Badea, O. and van der Maaten, E. 2024. Spruce suffers most from drought at low elevations in the Carpathians, though shows high resilience. *Forest Ecology and Management* 571. doi: 10.1016/j.foreco.2024.122201.

Pretzsch, H. et al. 2014. Mixed Norway spruce (Picea abies [L.] Karst) and European beech (Fagus sylvatica [L.]) stands under drought: from reaction pattern to mechanism. *Trees - Structure and Function* 28(5), pp. 1305–1321. doi: 10.1007/s00468-014-1035-9.

Pretzsch, H., Grams, T., Häberle, K.H., Pritsch, K., Bauerle, T. and Rötzer, T. 2020. Growth and mortality of Norway spruce and European beech in monospecific and mixed-species stands under natural episodic and experimentally extended drought. Results of the KROOF throughfall exclusion experiment. *Trees - Structure and Function* 34(4), pp. 957–970. doi: 10.1007/s00468-020-01973-0.

Putalová, T., Vacek, Z., Vacek, S., Štefančík, I., Bulušek, D. and Král, J. 2019. Tree-ring widths as an indicator of air pollution stress and climate conditions in different Norway spruce forest stands in the Krkonoše Mts. *Central European Forestry Journal* 65(1), pp. 21–33. doi: 10.2478/forj-2019-0004.

Rao, M.P., Cook, E.R., Cook, B.I., Anchukaitis, K.J., D'Arrigo, R.D., Krusic, P.J. and LeGrande, A.N. 2019. A double bootstrap approach to Superposed Epoch Analysis to evaluate response uncertainty. *Dendrochronologia* 55, pp. 119–124. doi: 10.1016/j.dendro.2019.05.001.

Rathgeber, C.B.K. et al. 2022. Anatomical, Developmental and Physiological Bases of Tree-Ring Formation in Relation to Environmental Factors. *Tree Physiology* 8, pp. 61–99. Available at: https://link.springer.com/chapter/10.1007/978-3-030-92698-4_3 [Accessed: 26 December 2024].

Rihm, B. and Künzle, T. 2023. *Nitrogen deposition and exceedances of critical loads for nitrogen in Switzerland 1990-2020*.

Rinne, K.T., Loader, N.J., Switsur, V.R., Treydte, K.S. and Waterhouse, J.S. 2010. Investigating the influence of sulphur dioxide (SO2) on the stable isotope ratios (δ13C and δ18O) of tree rings. *Geochimica et Cosmochimica Acta* 74(8), pp. 2327–2339. doi: 10.1016/j.gca.2010.01.021.

Roberts, L. 1983. *Is Acid Deposition Killing West German Forests?*

Rukh, S., Sanders, T.G.M., Krüger, I., Schad, T. and Bolte, A. 2023. Distinct Responses of European Beech (Fagus sylvatica L.) to Drought Intensity and Length—A Review of the Impacts of the 2003 and 2018–2019 Drought Events in Central Europe. *Forests* 14(2). doi: 10.3390/f14020248.

Rydval, M. and Wilson, R. 2012. The impact of industrial SO2 pollution on North Bohemia conifers. *Water, Air, and Soil Pollution* 223(9), pp. 5727–5744. doi: 10.1007/s11270-012-1310-6.

Šantrůčková, H., Cienciala, E., Kaňa, J. and Kopáček, J. 2019. The chemical composition of forest soils and their degree of acidity in Central Europe. *Science of The Total Environment* 687, pp. 96–103. doi: 10.1016/J.SCITOTENV.2019.06.078.

Santruckova, H., Šantrůček, J., Šetlík, J., Svoboda, M. and Kopáček, J. 2007. Carbon isotopes in tree rings of Norway spruce exposed to atmospheric pollution. *Environmental Science and Technology* 41(16), pp. 5778–5782. doi: 10.1021/es070011t.

Saurer, M., Cherubini, P., Reynolds-Henne, C.E., Treydte, K.S., Anderson, W.T. and Siegwolf, R.T.W. 2008. An investigation of the common signal in tree ring stable isotope chronologies at temperate sites. *Journal of Geophysical Research: Biogeosciences* 113(4). doi: 10.1029/2008JG000689.

Saurer, M., Oettli, M. and Lehmann, M.M. 2024. A Simple Method for Triple Stable Isotope Analysis of Cellulose, Sugar, and Bulk Organic Matter—Advances and Limitations. *Rapid Communications in Mass Spectrometry* 39(4), p. e9957. Available at: https://onlinelibrary.wiley.com/doi/full/10.1002/rcm.9957 [Accessed: 7 January 2025].

Saurer, M., Siegenthaler, U. and Schweingruber, F. 1995. The climate-carbon isotope relationship in tree rings and the significance of site conditions. *Tellus, Series B* 47 B(3), pp. 320–330. doi: 10.3402/TELLUSB.V47I3.16051.

Saurer, M., Siegwolf, R.T.W. and Schweingruber, F.H. 2004. Carbon isotope discrimination indicates improving water-use efficiency of trees in northern Eurasia over the last 100 years. *Global Change Biology* 10(12), pp. 2109–2120. doi: 10.1111/j.1365-2486.2004.00869.x.

Savard, M.M. 2010. Tree-ring stable isotopes and historical perspectives on pollution - An overview. *Environmental Pollution* 158(6), pp. 2007–2013. doi: 10.1016/j.envpol.2009.11.031.

Savard, M.M., Bégin, C. and Marion, J. 2020. Response strategies of boreal spruce trees to anthropogenic changes in air quality and rising pCO2. *Environmental Pollution* 261. doi: 10.1016/j.envpol.2020.114209.

Schäfer, C., Grams, T.E.E., Rötzer, T., Feldermann, A. and Pretzsch, H. 2017. Drought Stress Reaction of Growth and Δ13C in Tree Rings of European Beech and Norway Spruce in Monospecific Versus

Mixed Stands Along a Precipitation Gradient. *Forests 2017, Vol. 8, Page 177* 8(6), p. 177. Available at: https://www.mdpi.com/1999-4907/8/6/177/htm [Accessed: 18 January 2025].

Schmied, G. et al. 2023. Rapid beech decline under recurrent drought stress: Individual neighborhood structure and soil properties matter. *Forest Ecology and Management* 545. doi: 10.1016/j.foreco.2023.121305.

Schuldt, B. et al. 2020. A first assessment of the impact of the extreme 2018 summer drought on Central European forests. *Basic and Applied Ecology* 45, pp. 86–103. doi: 10.1016/j.baae.2020.04.003.

Schütt, P. 1977. Das Tannensterben. Der Stand unseres Wissens über eine aktuelle und gefährliche Komplexkrankheit der Weißtanne (Abies alba Mill.). *Forstwissenschaftliches Centralblatt* 96(3), pp. 177–186.

Schütt, P. and Cowling, E.B. 1985. Waldsterben, a general decline of forest in Central Europe. symptoms, development and possible causes. Plant Dis. *Plant Disease* 69, pp. 548–558. doi: 10.1094/PD-69-548.

Schwarz, J., Skiadaresis, G., Kohler, M., Kunz, J., Schnabel, F., Vitali, V. and Bauhus, J. 2020. Quantifying Growth Responses of Trees to Drought—a Critique of Commonly Used Resilience Indices and Recommendations for Future Studies. *Current Forestry Reports* 6(3), pp. 185–200. doi: 10.1007/S40725-020-00119-2.

Schweingruber, F.H. 1988. *Tree Rings*. Springer Netherlands. doi: 10.1007/978-94-009-1273-1.

Schweingruber, F.H. 1996. *Tree Rings and Environment Dendroecology*. Paul Haupt.

Schweingruber, F.H., Kontic, R. and Winkler-Seifert, A. 1983. *Eine jahrringanalytische Studie zum Nadelbaumsterben in der Schweiz. Bericht 253*. Birmensdorf.

Schweizerisches Sozialarchiv. [no date]. *Vogler Gertrud*. Available at: https://www.bild-video-ton.ch/bestand/objekt/Sozarch_F_5107-Na-08-105-029 [Accessed: 26 December 2024].

Sercon Ltd. 2019a. *HS2022 Isotope Ratio Mass Spectrometer*. Available at: www.sercongroup.com.

Sercon Ltd. 2019b. *The Sercon iso EArth and iso EArth +*. Available at: www.sercongroup.com.

Shetti, R., Boonen, K., Smiljanić, M., Tejnecký, V., Drábek, O. and Lehejček, J. 2024. Do trees respond to pollution? A network study of the impact of pollution on spruce growth from Europe. *Environmental Pollution* 350, p. 124012. doi: 10.1016/J.ENVPOL.2024.124012.

Siegwolf, R.T.W. et al. 2022. Impact of Increasing CO2, and Air Pollutants (NOx, SO2, O3) on the Stable Isotope Ratios in Tree Rings. pp. 675–710. Available at: https://link.springer.com/chapter/10.1007/978-3-030-92698-4_24 [Accessed: 26 December 2024].

Šimůnek, V., Vacek, Z., Vacek, S., Králíček, I. and Vančura, K. 2019. Growth variability of European beech (Fagus sylvatica L.) natural forests: Dendroclimatic study from Krkonoše National Park. *Central European Forestry Journal* 65(2), pp. 92–102. doi: 10.2478/forj-2019-0010.

Skelly, J.M. and Innes, J.L. 1994. Waldsterben in the Forests of Central Europe and Eastern North America: Fantasy or Reality? *Plant Disease* 78(11), pp. 1021–1032.

Sousa-Silva, R. et al. 2018. Tree diversity mitigates defoliation after a drought-induced tipping point. Available at: https://onlinelibrary.wiley.com/doi/10.1111/gcb.14326 [Accessed: 4 October 2023].

Speer, J.H. 2009. *Fundamentals of Tree-Ring Research*. University of Arizona Press.

Spiecker, H. and Kahle, H.P. 2023. Climate-driven tree growth and mortality in the Black Forest, Germany—Long-term observations. *Global Change Biology* 29(20), pp. 5908–5923. doi: 10.1111/gcb.16897.

Stjepanović, S., Matović, B., Stojanović, D., Lalić, B., Levanič, T., Orlović, S. and Gutalj, M. 2018. The Impact of Adverse Weather and Climate on the Width of European Beech (Fagus sylvatica L.) Tree Rings in Southeastern Europe. *Atmosphere 2018, Vol. 9, Page 451* 9(11), p. 451. Available at: https://www.mdpi.com/2073-4433/9/11/451/htm [Accessed: 26 January 2025].

swisstopo. 2024. *Maps of Switzerland*. Available at: https://map.geo.admin.ch [Accessed: 27 December 2024].

Talbott, L.D., Rahveh, E. and Zeiger, E. 2003. Relative humidity is a key factor in the acclimation of the stomatal response to CO2. *Journal of Experimental Botany* 54(390), pp. 2141–2147. Available at: https://dx.doi.org/10.1093/jxb/erg215 [Accessed: 23 January 2025].

Thomas Daphne, Reinds Gert Jan, Posch Maximilian and Slootweg Jaap. 2021. *Critical loads for eutrophication and acidification for European terrestrial ecosystems Final report*.

Tresch, S., Roth, T., Schindler, C., Hopf, S.E., Remund, J. and Braun, S. 2023. The cumulative impacts of droughts and N deposition on Norway spruce (Picea abies) in Switzerland based on 37 years of forest monitoring. *Science of the Total Environment* 892. doi: 10.1016/j.scitotenv.2023.164223.

UBA. 2024. *Final report Manual on Methodologies and Criteria for Modelling and Mapping Critical Loads and Levels and Air Pollution Effects, Risks, and Trends. Update 2024.* Coordination Centre for Effects (CCE) ed. German Environment Agency.

Vacek, Z. et al. 2019. Adaption of Norway spruce and European beech forests under climate change: From resistance to close-to-nature silviculture. *Central European Forestry Journal* 65(2), pp. 129–144. doi: 10.2478/forj-2019-0013.

Vacek, Z. et al. 2020. Long-term effect of climate and air pollution on health status and growth of Picea abies (L.) Karst. peaty forests in the Black Triangle region. *Dendrobiology* 83, pp. 1–19. doi: 10.12657/denbio.083.001.

Vejpustková, M., Čihák, T., Samusevich, A., Zeidler, A., Novotný, R. and Šrámek, V. 2017. Interactive effect of extreme climatic event and pollution load on growth and wood anatomy of spruce. *Trees - Structure and Function* 31(2), pp. 575–586. doi: 10.1007/s00468-016-1491-5.

Vicente-Serrano, S.M., Beguería, S. and López-Moreno, J.I. 2010. A Multiscalar Drought Index Sensitive to Global Warming: The Standardized Precipitation Evapotranspiration Index. *Journal of Climate* 23(7), pp. 1696–1718. Available at: https://journals.ametsoc.org/view/journals/clim/23/7/2009jcli2909.1.xml [Accessed: 24 October 2024].

De Vries, W., Hettelingh, J.-P. and Posch, M. 2015. The history and current state of critical loads and dynamic modelling assessments. pp. 1–11. Available at: https://research.wur.nl/en/publications/the-history-and-current-state-of-critical-loads-and-dynamic-model [Accessed: 23 December 2024].

Wagner, R. and Wagner, E. 2006. Influence of air pollution and site conditions on trends of carbon and oxygen isotope ratios in tree ring cellulose. In: *Isotopes in Environmental and Health Studies*. pp. 351–365. doi: 10.1080/10256010600991078.

Wandeler, H. 1982. *Das Ausmass der Waldschäden - Ihre ökologische und wirtschaftliche Bedeutung in der Schweiz, in: Waldschäden durch Immissionen? Ausmass bereits sichtbarer Schäden. Erste Forschungsergebnisse. Mögliche Massnahmen*. Rüschlikon/Zürich: Gottlieb Duttweiler-Institut für wirtschaftliche und soziale Studien.

Wang, P., Xu, D., Lakshmanan, P., Deng, Y., Zhu, Q. and Zhang, F. 2024. Mitigation strategies for soil acidification based on optimal nitrogen management. *Frontiers of Agricultural Science and Engineering* 11(2), pp. 229–242. Available at: https://journal.hep.com.cn/fase/EN/10.15302/J-FASE-2024562 [Accessed: 21 January 2025].

Weber, P., Bugmann, H., Pluess, A.R., Walthert, L. and Rigling, A. 2013. Drought response and changing mean sensitivity of European beech close to the dry distribution limit. *Trees - Structure and Function* 27(1), pp. 171–181. Available at: https://link.springer.com/article/10.1007/s00468-012-0786-4 [Accessed: 26 December 2024].

Werner, R.A. and Cormier, M.-A. 2022. Isotopes—Terminology, Definitions and Properties. *Tree Physiology* 8, pp. 253–289. Available at: https://link.springer.com/chapter/10.1007/978-3-030-92698-4_8 [Accessed: 26 December 2024].

Wikimedia Commons/Anna Uciechowska. 2024. *Turow Coal Mine*. Available at: https://commons.wikimedia.org/wiki/File:Turow.jpg [Accessed: 29 December 2024].

Wikimedia Commons/Lovecz. 2024. *Jizera Mountains*. Available at: https://commons.wikimedia.org/wiki/File:Acid_rain_woods1.JPG [Accessed: 28 January 2025].

Wikimedia Commons/Werni1. 2024. *Turow Powerstation*. Available at: https://commons.wikimedia.org/wiki/File:Turow-powerstation.jpg#filelinks [Accessed: 28 December 2024].

Wu, X. et al. 2022. Timing and Order of Extreme Drought and Wetness Determine Bioclimatic Sensitivity of Tree Growth. *Earth's Future* 10(7), p. e2021EF002530. Available at: https://onlinelibrary.wiley.com/doi/full/10.1029/2021EF002530 [Accessed: 24 December 2024].

Zang, C., Hartl-Meier, C., Dittmar, C., Rothe, A. and Menzel, A. 2014. Patterns of drought tolerance in major European temperate forest trees: Climatic drivers and levels of variability. *Global Change Biology* 20(12), pp. 3767–3779. doi: 10.1111/gcb.12637.

Zimmermann, S., Luster, J., Blaser, P., Walthert, L. and Lüscher, P. 2006. Waldböden der Schweiz. Band 3: Regionen Mittelland und Voralpen. WSL, E. F. ed. p. 848. Available at: https://www.ott-verlag.ch/titel/waldböden-der-schweiz-3/ [Accessed: 23 January 2025].

Appendix

Appendix A: TRW raw data

A1: TRW raw data of cores with average

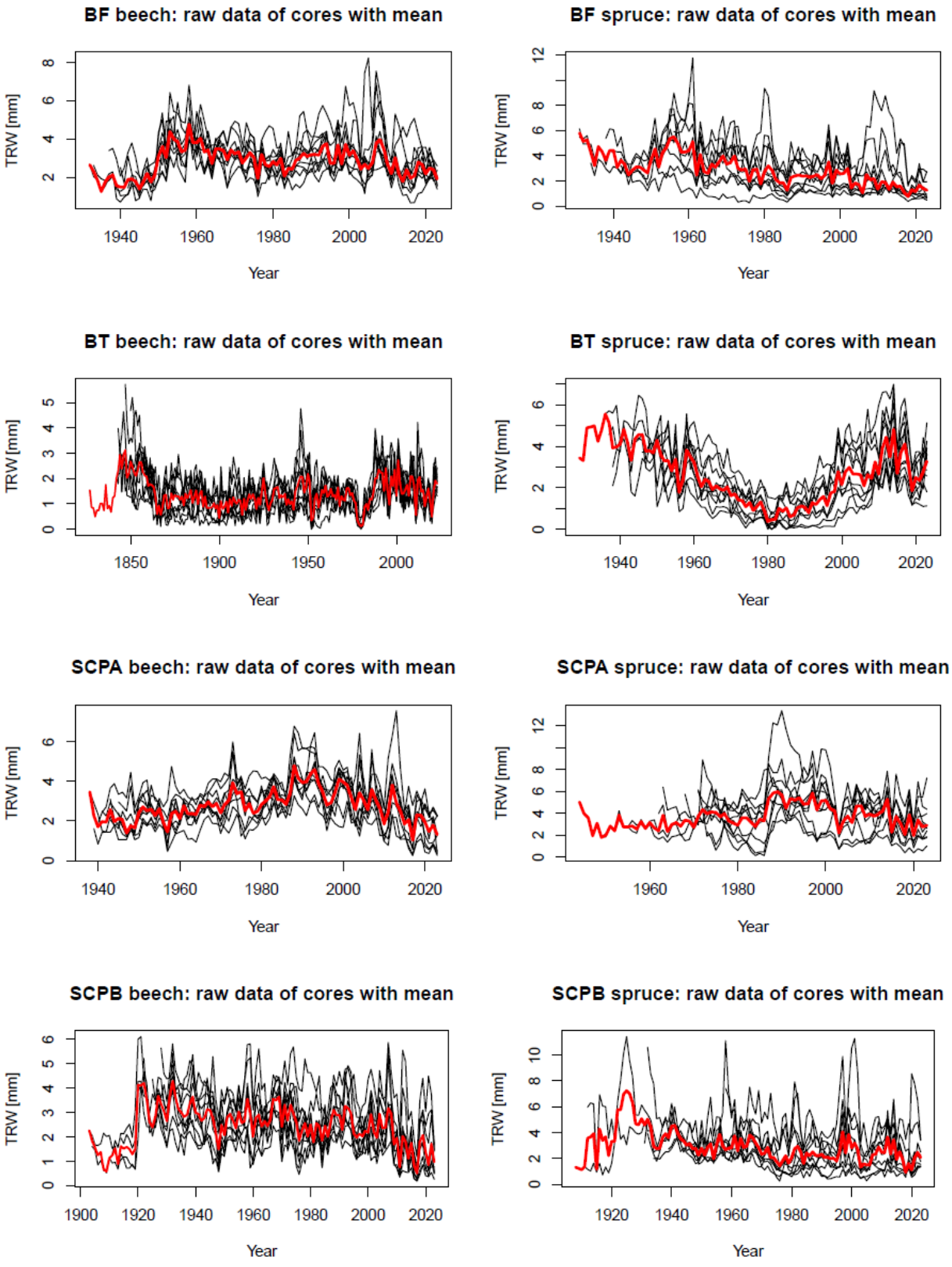

A2: TRW raw data of trees

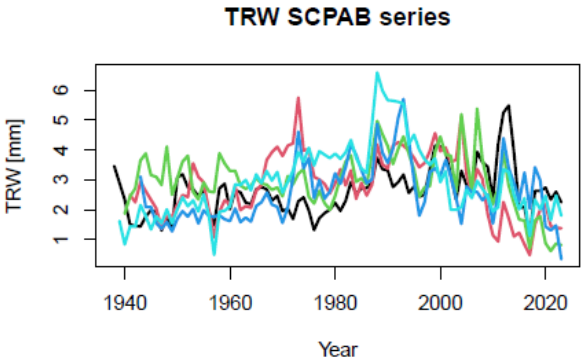

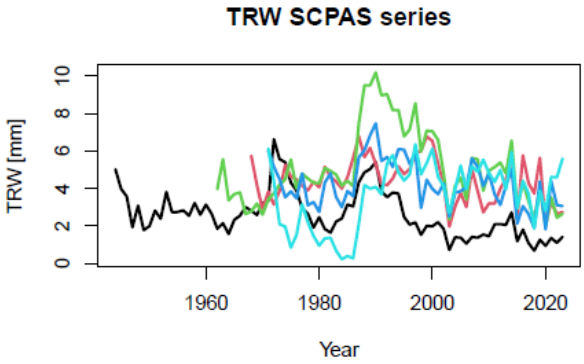

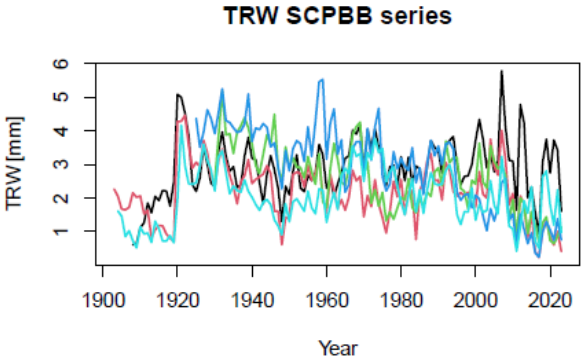

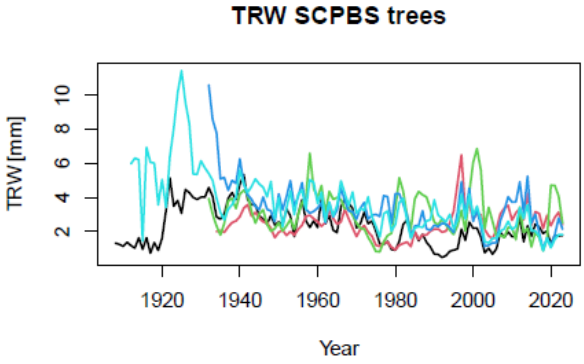

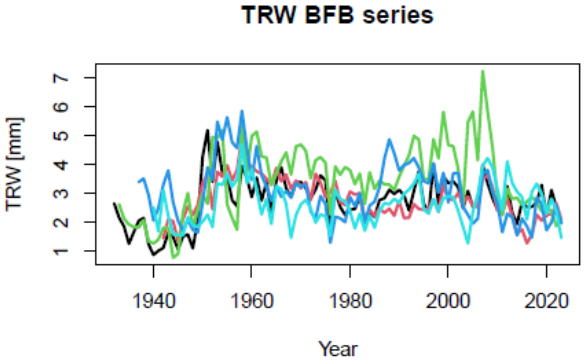

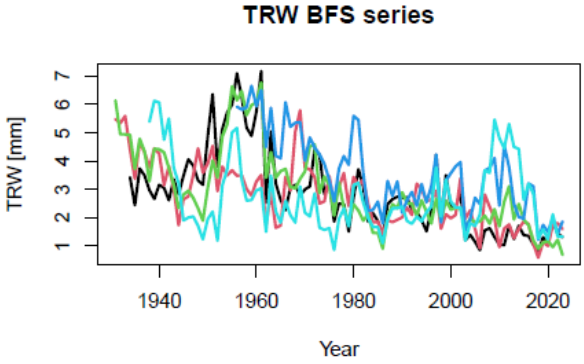

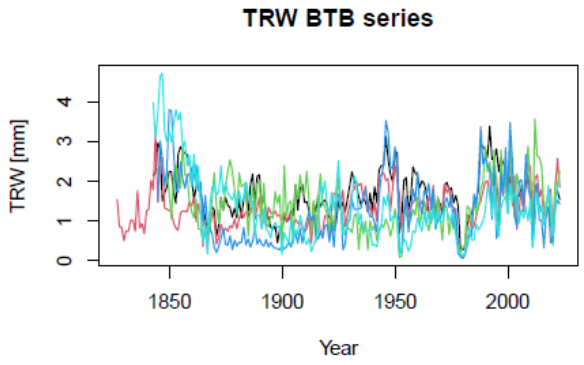

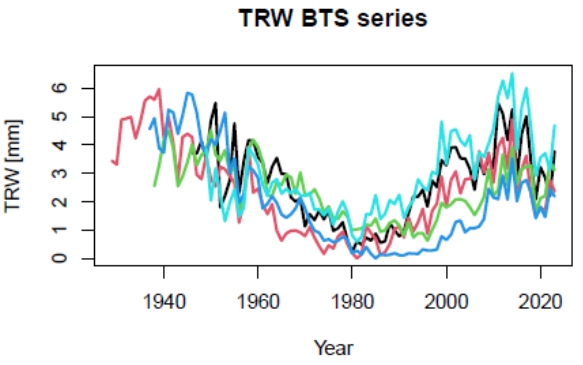

Appendix B: Cumulative radial growth

B1: CRG series

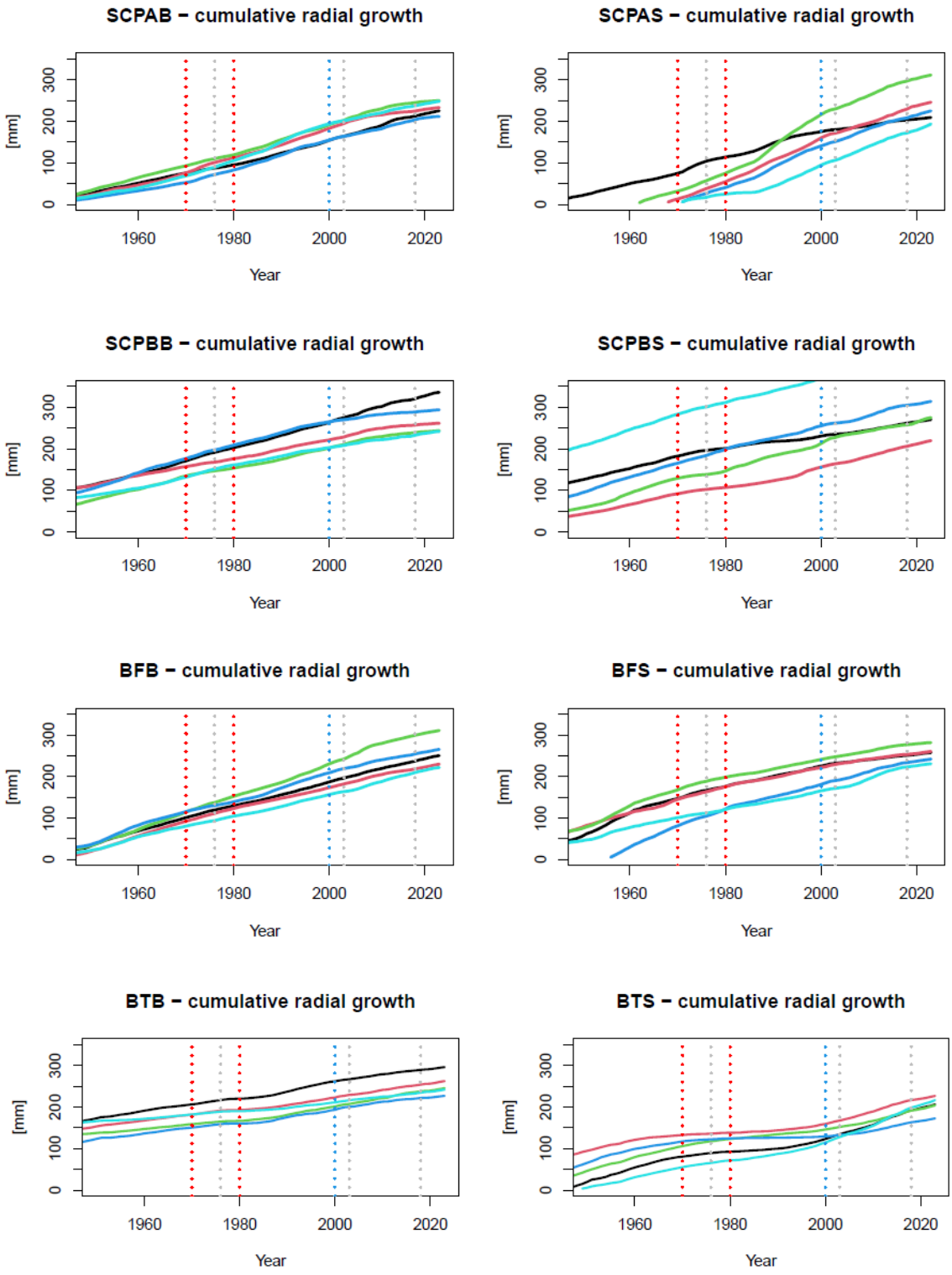

B2: CRG means

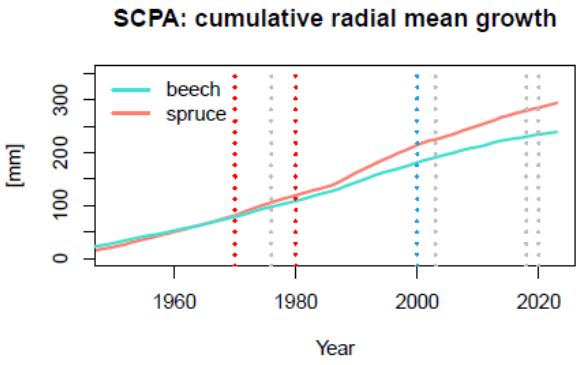
SCPA: cumulative radial mean growth
beech
spruce
[mm]
0
100
200
300
1960
1980
2000
2020
Year

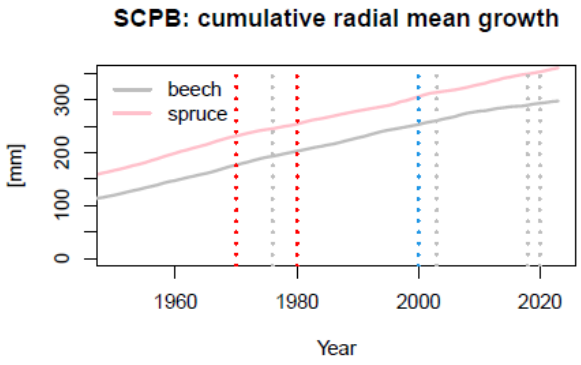
SCPB: cumulative radial mean growth
beech
spruce
[mm]
0
100
200
300
1960
1980
2000
2020
Year

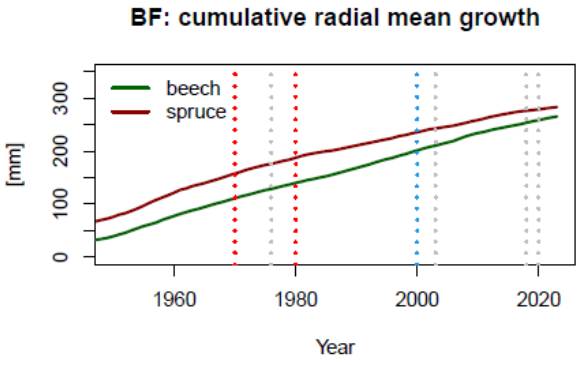
BF: cumulative radial mean growth
beech
spruce
[mm]
0
100
200
300
1960
1980
2000
2020
Year

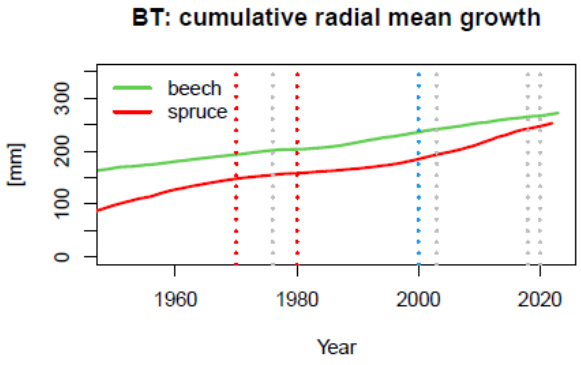
BT: cumulative radial mean growth
beech
spruce
[mm]
0
100
200
300
1960
1980
2000
2020
Year

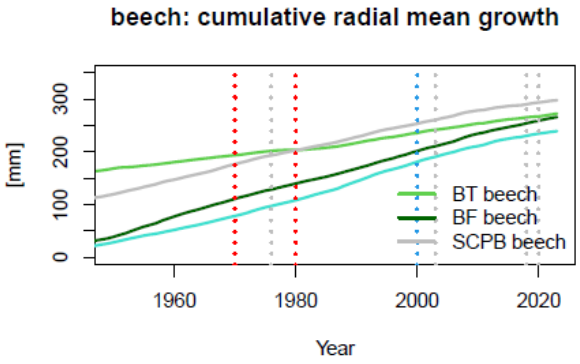
beech: cumulative radial mean growth
BT beech
BF beech
SCPB beech
[mm]
0
100
200
300
1960
1980
2000
2020
Year

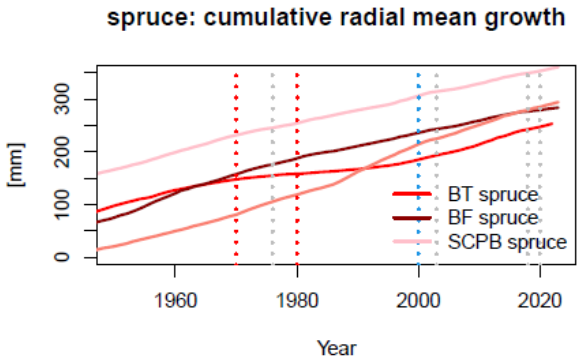
spruce: cumulative radial mean growth
BT spruce
BF spruce
SCPB spruce
[mm]
0
100
200
300
1960
1980
2000
2020
Year

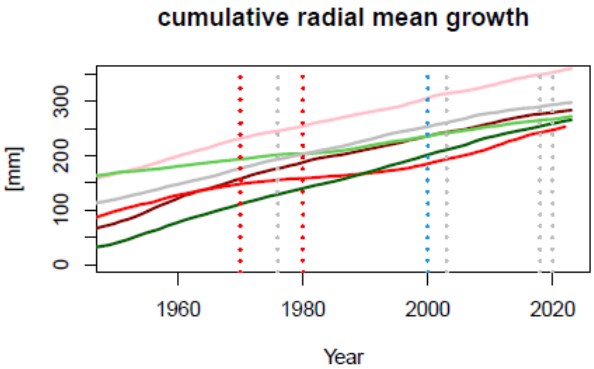
cumulative radial mean growth
[mm]
0
100
200
300
1960
1980
2000
2020
Year

B3: Mean TRW

	1970–1999	**200–2023**
TRW BFB	3.021000	2.814750
TRW BFS	2.638733	2.089667
TRW BTB	1.396667	1.578125
TRW BTS	1.185233	3.042375
TRW SCPAB	3.376667	2.570542
TRW SCPAS	4.392162	3.531667
TRW SCPBB	2.566933	1.942833
TRW SCPBS	2.447467	2.407375

Appendix C: RWI correlations with climate variability

C1: RWI correlations with mean temperature

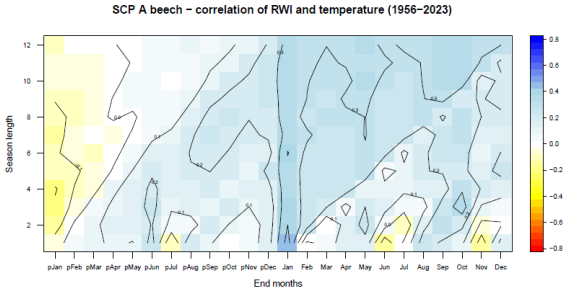

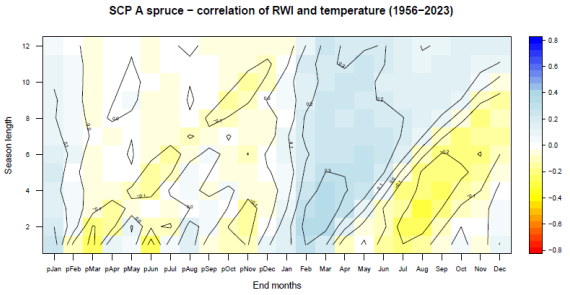

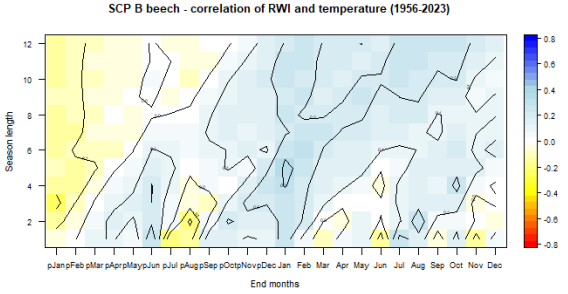

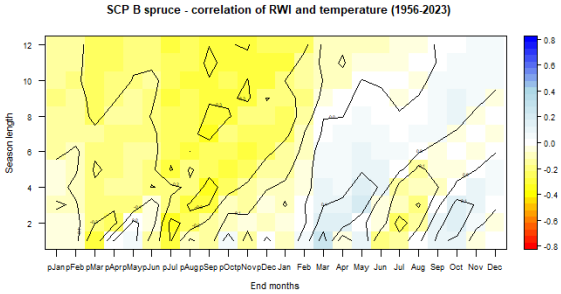

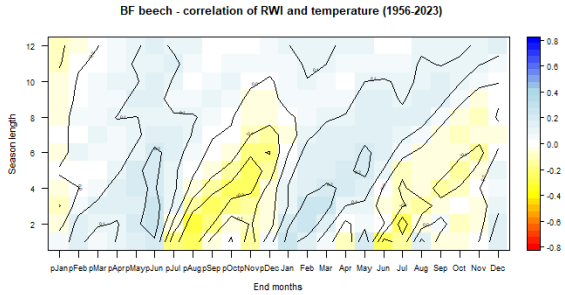

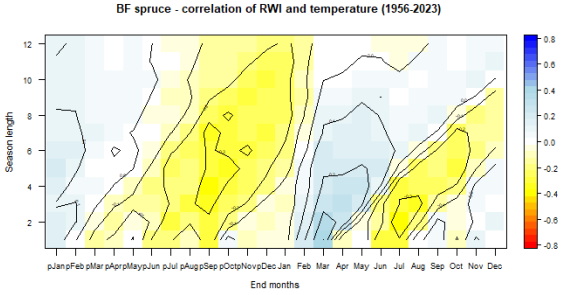

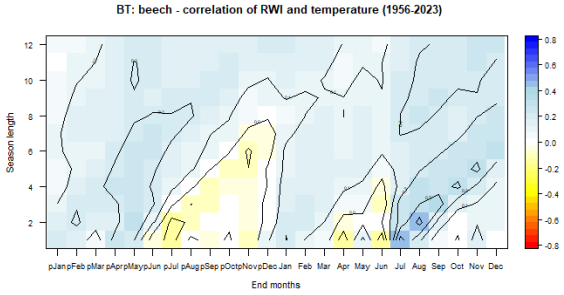

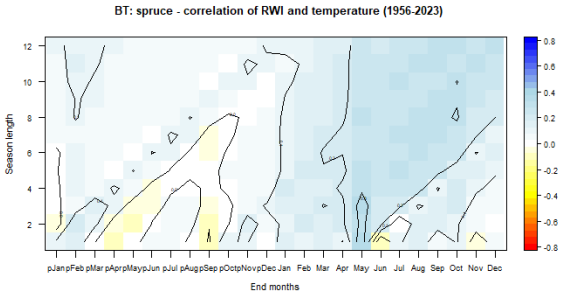

C2: RWI correlations with precipitation

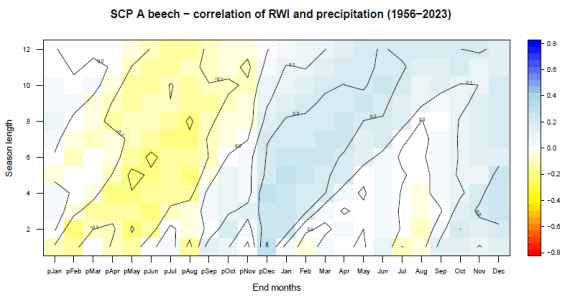

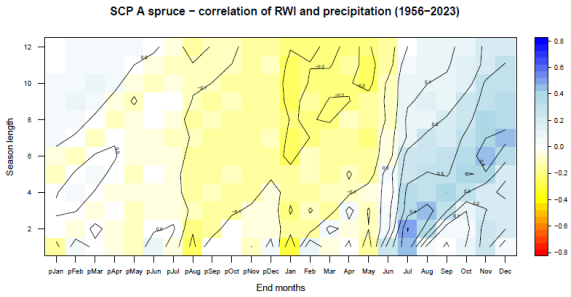

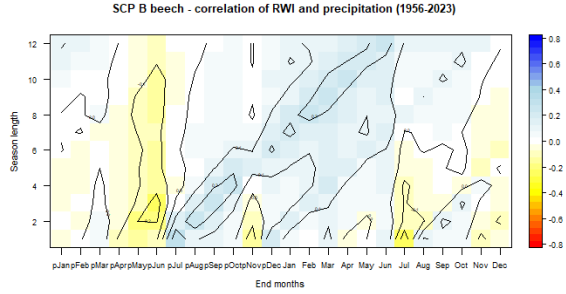

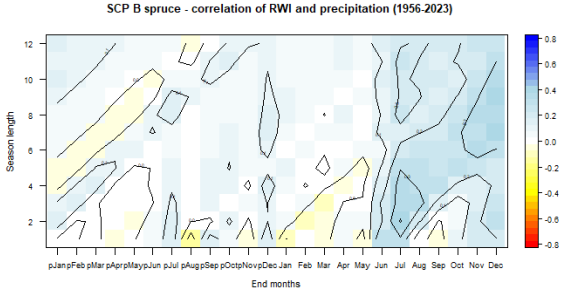

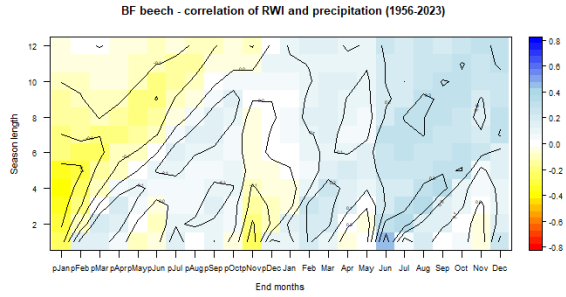

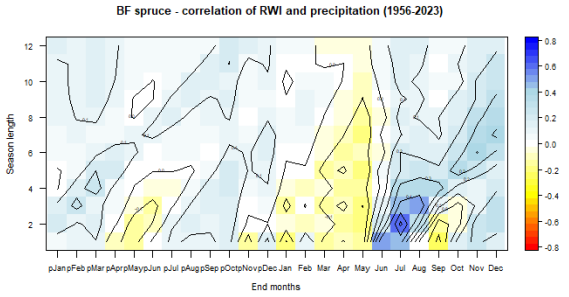

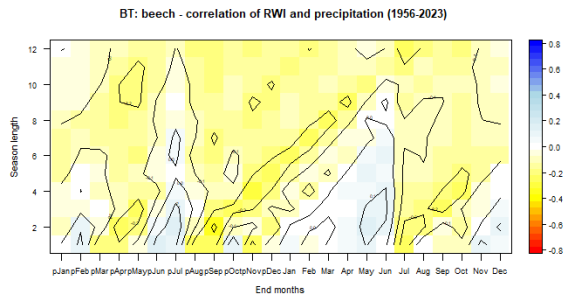

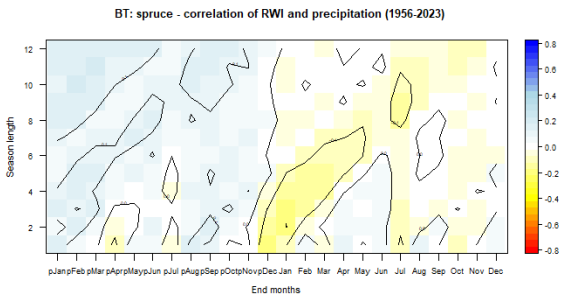

C3: RWI correlations with SPEI

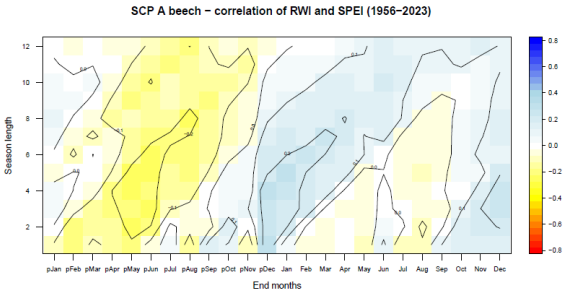

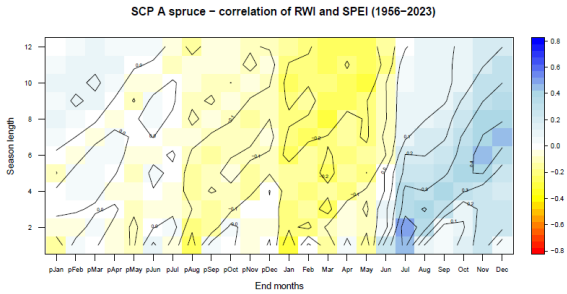

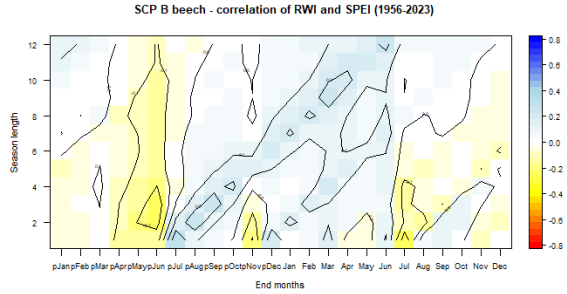

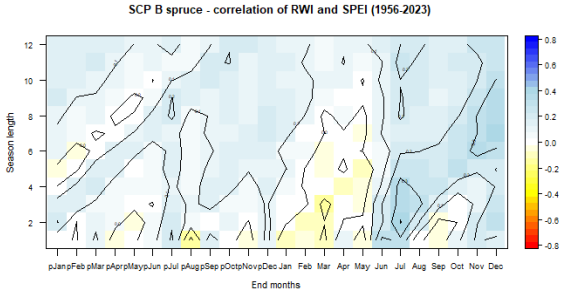

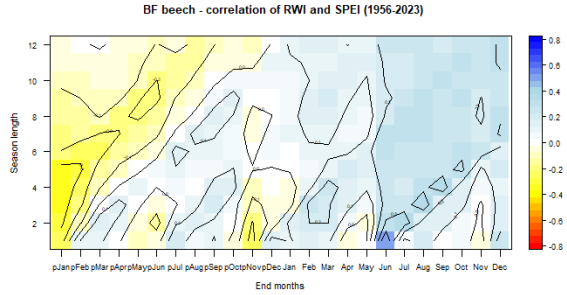

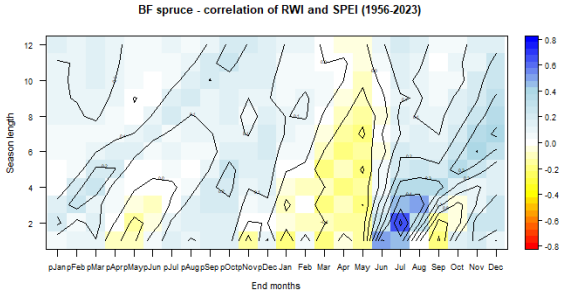

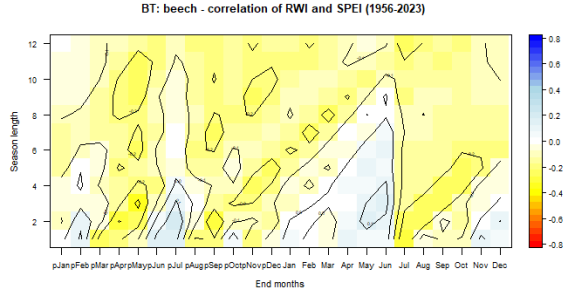

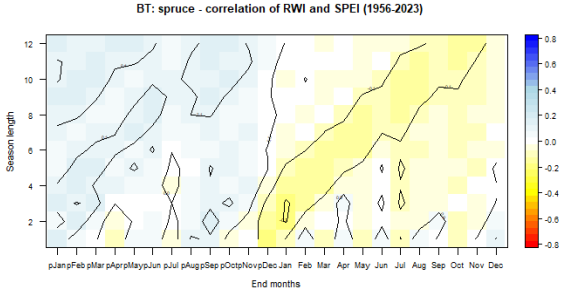

Appendix D: RWI and air pollution – single linear regression

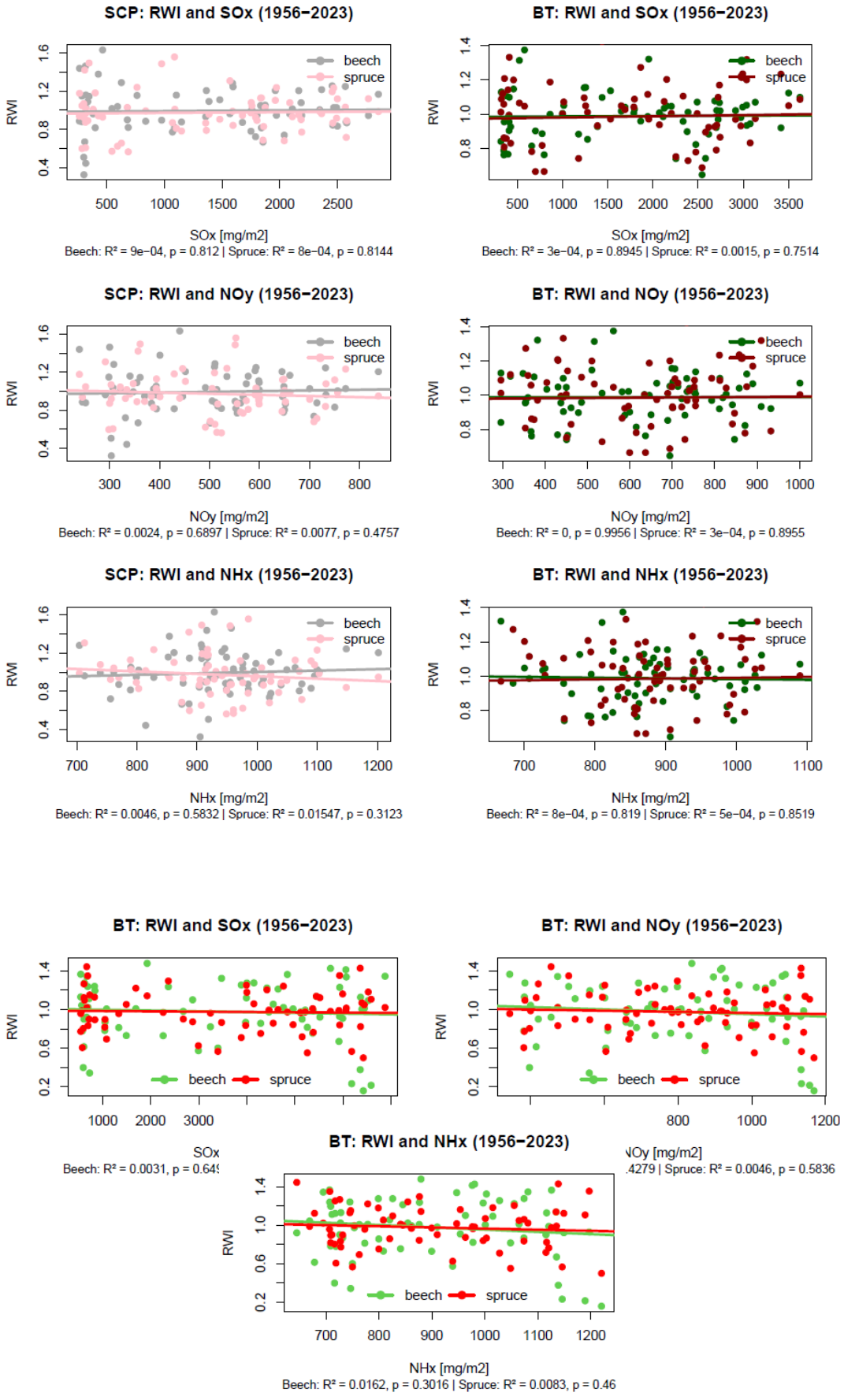

Appendix E: $\delta^{13}C$ raw data

E1: $\delta^{13}C$ raw data of trees

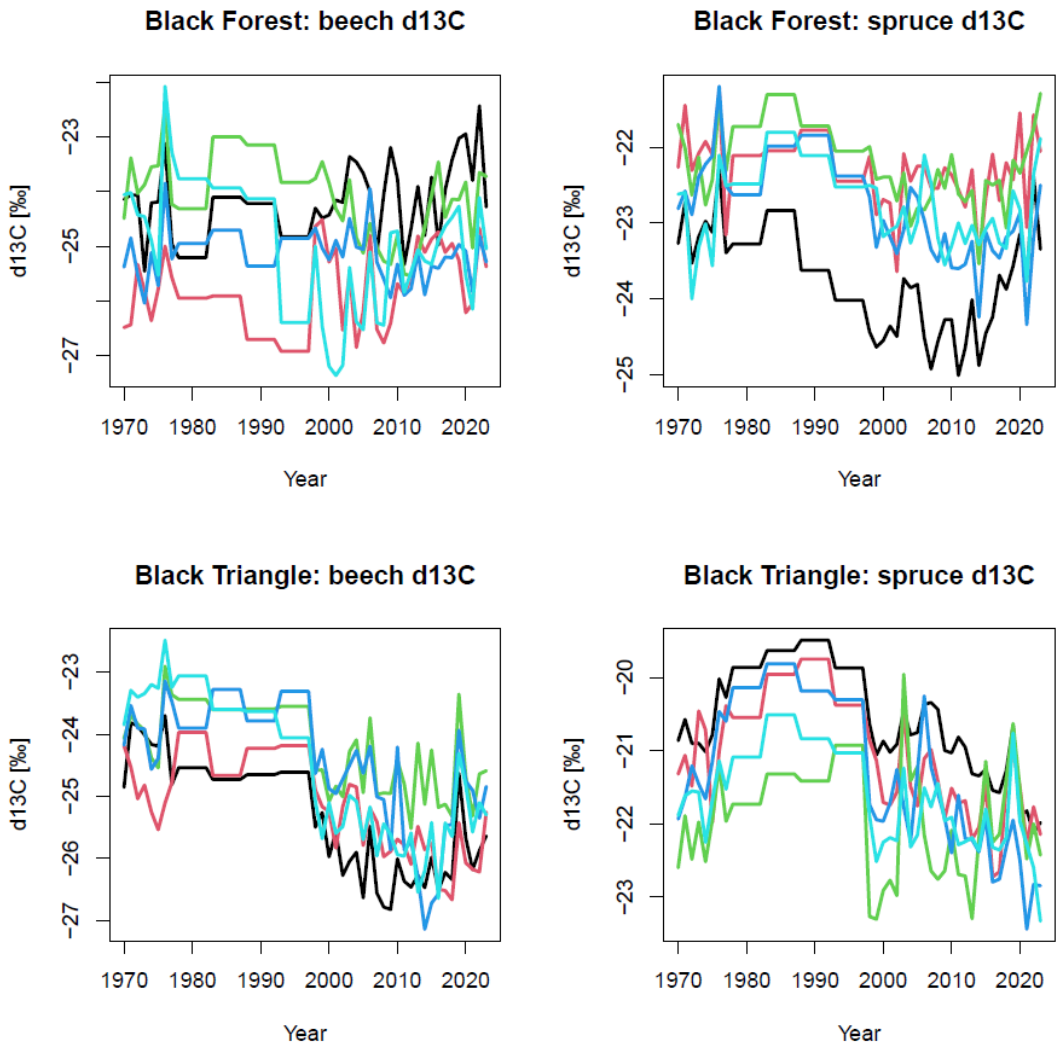

E2: $\delta^{13}C$ mean values

	1970–1999	**2000–2023**	**overall mean**
BFB	-24.75094	-24.97773	-24.852
BFS	-22.42351	-23.05733	-22.705
BTB	-24.01261	-25.46160	-24.657
BTS	-20.77297	-21.80271	-21.231

E3: $\delta^{13}C$ mean chronologies

with marked drought events (grey) and air pollution peak (red) and return to baseline (blue)

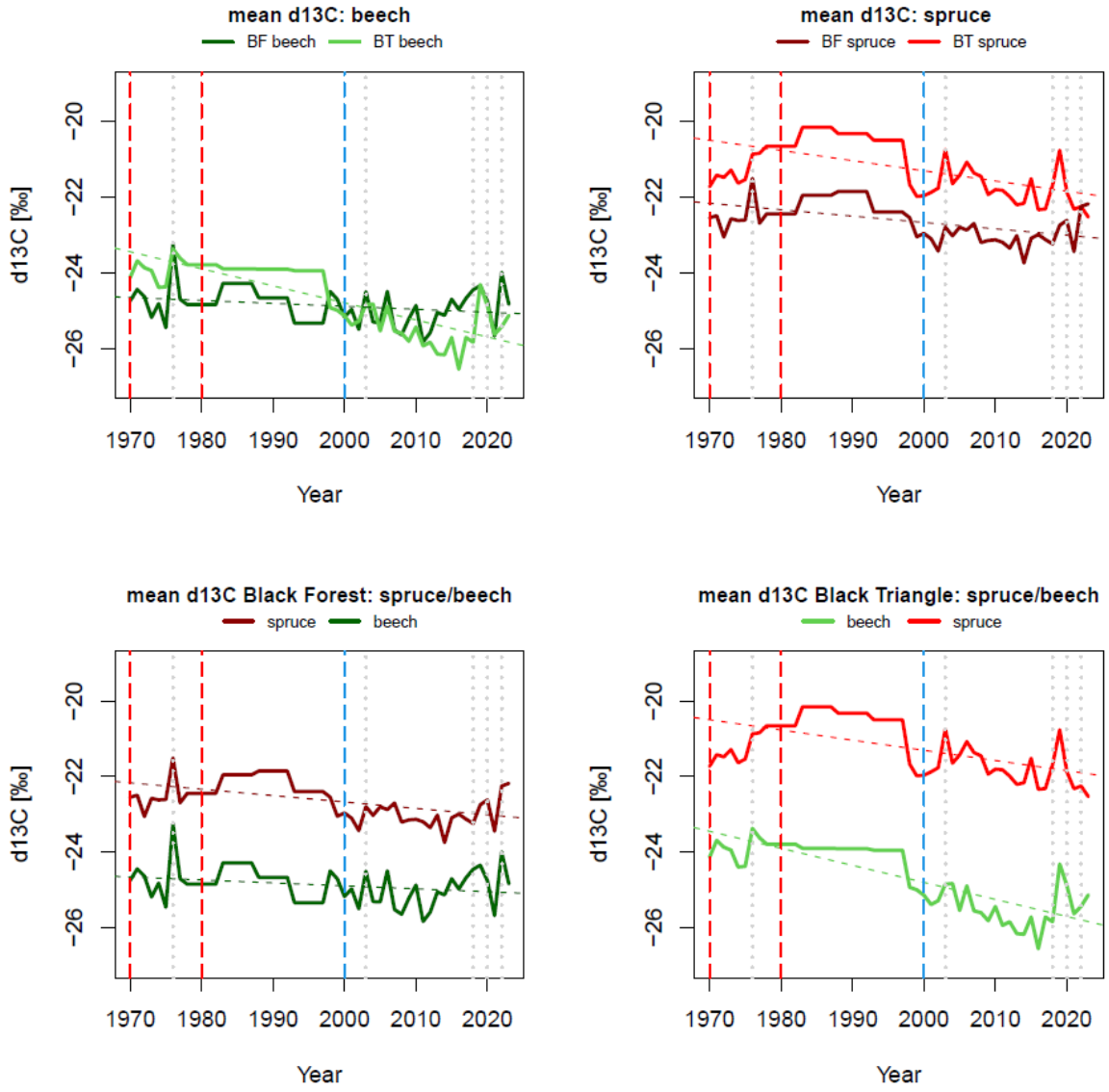

Appendix F: $\delta^{13}C$ correlations with climate variability

F1: $\delta^{13}C$ correlations with mean temperature

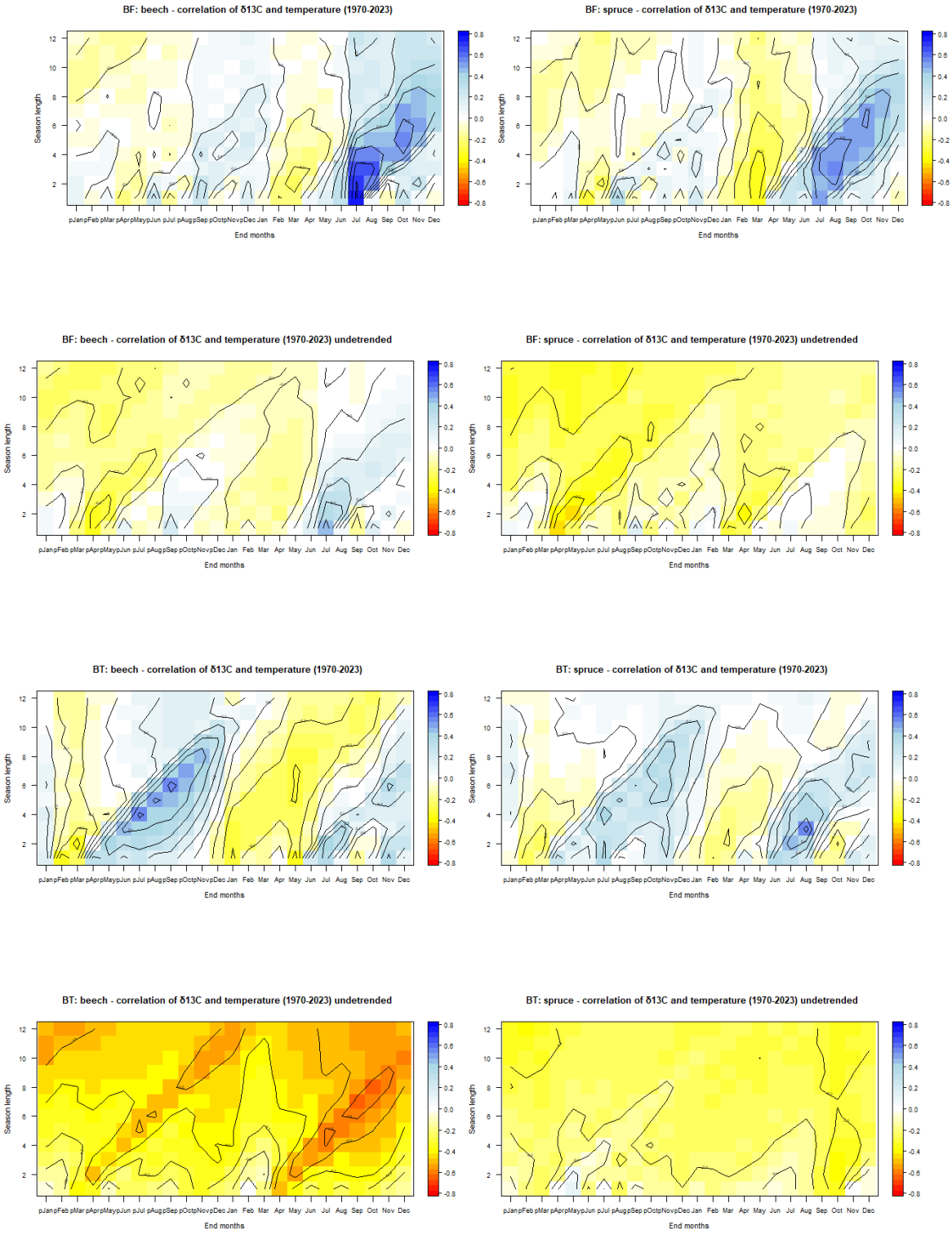

F2: $\delta^{13}C$ correlations with precipitation

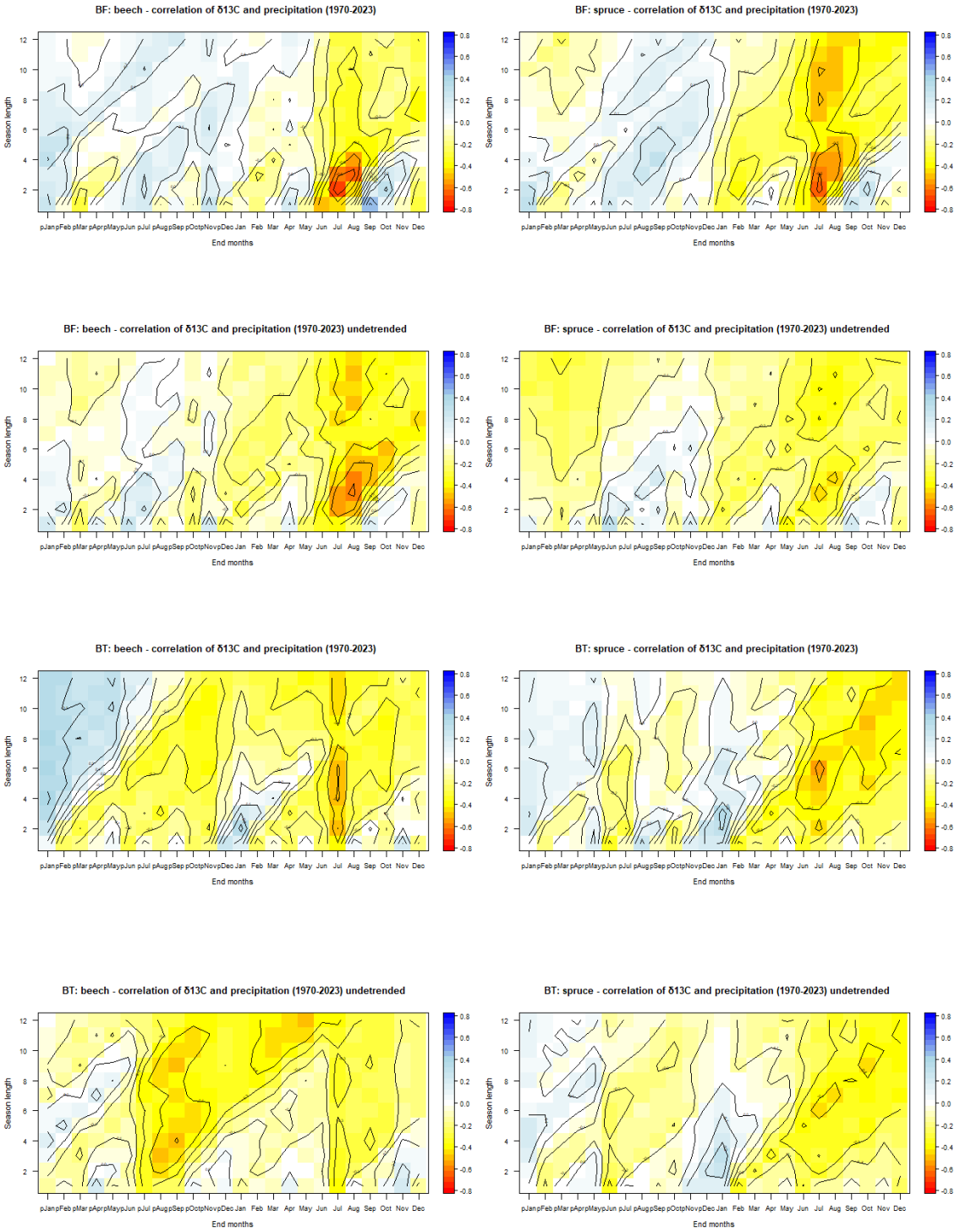

F3: $\delta^{13}C$ correlations with SPEI

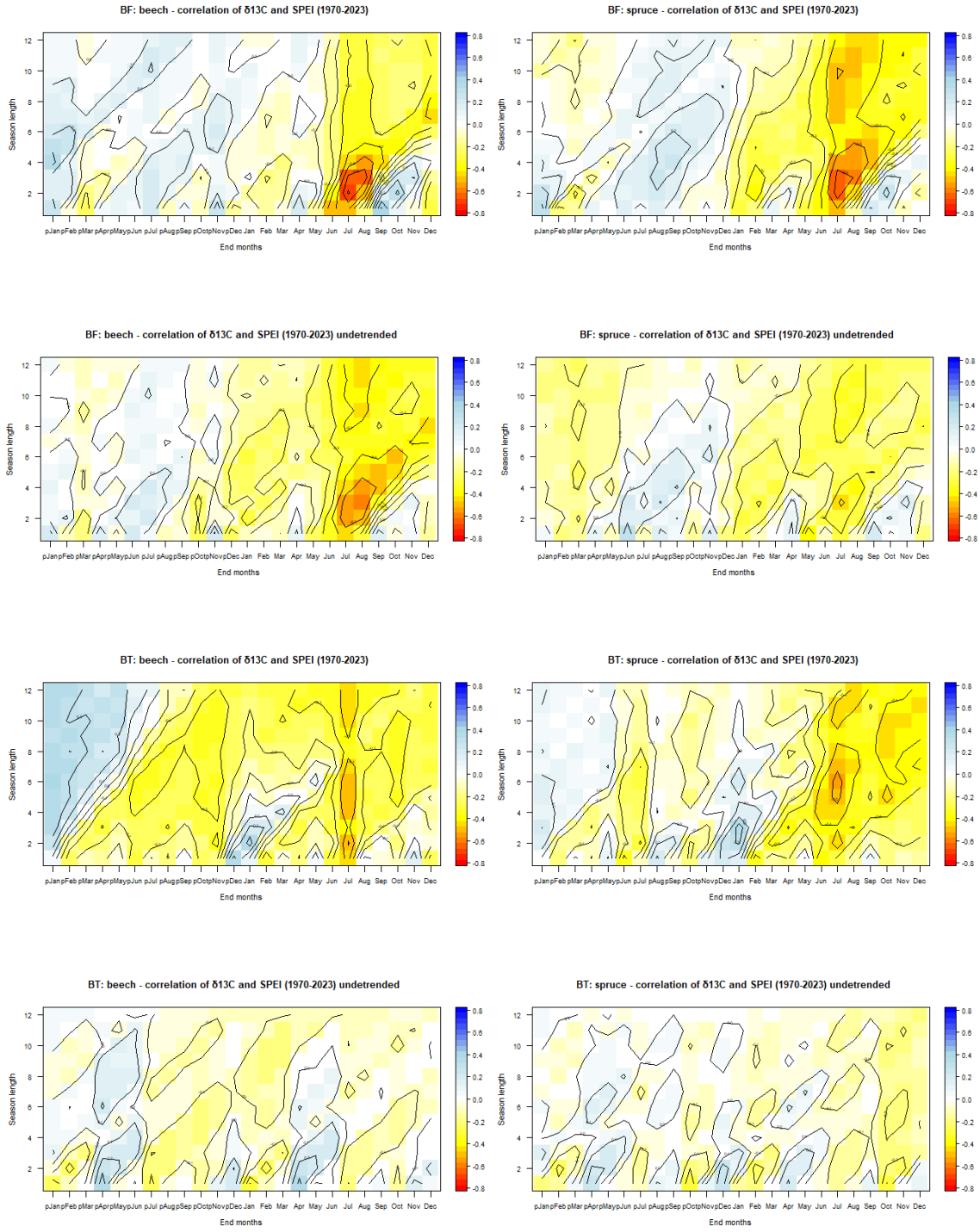

Appendix G: Multiple regression

undetrended_d13C~SOx+SPEI/ppt/tmean

Model	**SOx** (Estimate, p)	**SPEI/ppt/tmean** (Estimate, p)	
BFB (SOx+SPEI) May-July	+0.0002151, ***	-0.3097, ***	negative
BFS (SOx+SPEI) April-July	+0.0002856 ***	-0.1221, .	negative
BTB (SOx+SPEI) Feb-July	+0.0003278, ***	-0.1189, .	negative
BTS (SOx/SPEI) Feb-July	+0.0002060, ***	-0.1620, .	negative
BFB (SOx+ppt) May-Aug	+0.0001538, **	-0.002422, ***	negative
BFS (SOx+ppt) May-Aug	+0.0002581, ***	-0.001702, **	negative
BTB (SOx+ppt) Feb-July	+0.0003190, ***	-0.001052, .	negative
BTS (SOx+ppt) Feb-July	+0.0001944, ***	-0.001357, .	negative
BFB (SOx+tmean) April-July	+0.0004975, ***	+0.4403, ***	positive
BFS (SOx+tmean) May-Aug	+0.0004028, ***	0.2075, *	positive
BTB (SOx+tmean) June-July	+0.0003576, ***	+0.1037, n.s.	**positive**
BTS (SOx+tmean) June-July	+0.0002055, **	+0.01254, n.s.	**positive**

Correlation $\delta^{13}C$~tmean: R-values

	BFB (April-July)	**BFS** (May-Aug)	**BTB** (June-July)	**BTS** (June-July)	
d13C_30spline~tmean	+0.543	+0.507	+0.377	+0.473	positive
d13C_un-detrended~tmean	+0.172	+0.003	**-0.374**	**-0.080**	pos./ **neg.**

Appendix H: Air Pollution and TRW/ $\delta^{13}C$

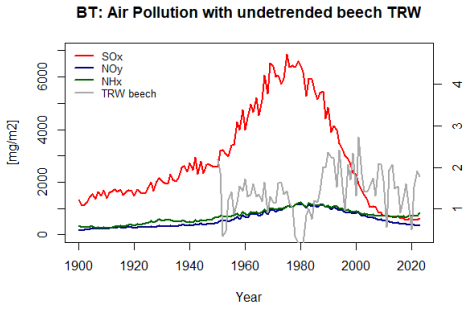

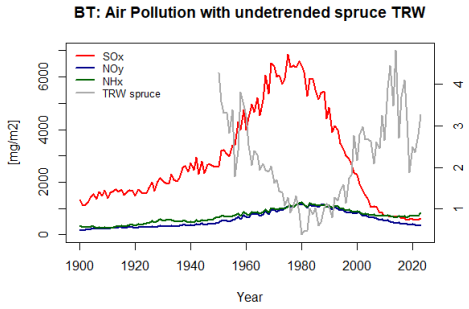

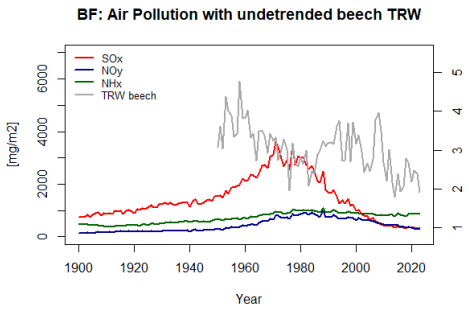

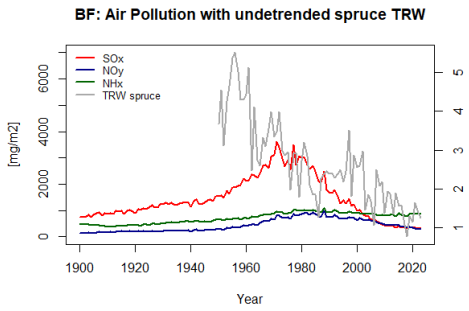

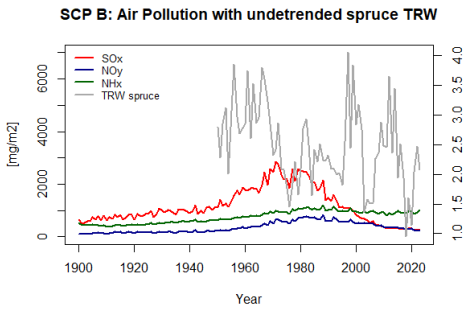

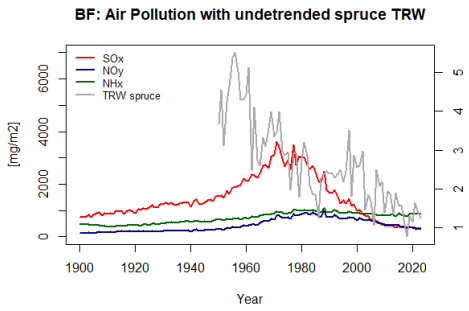

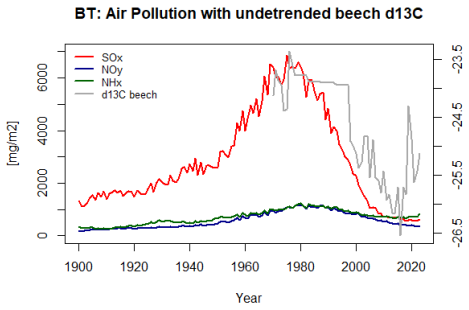

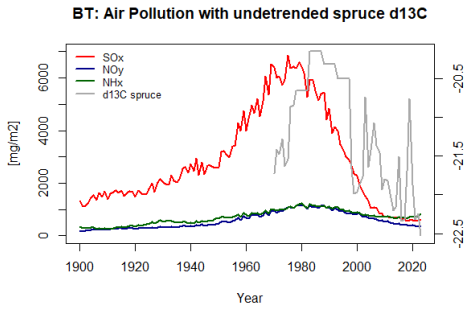

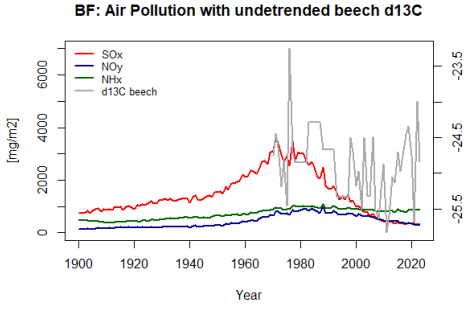

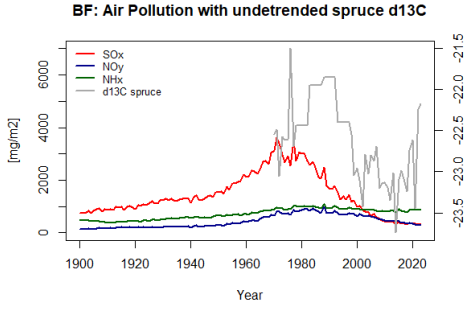

Personal Declaration

I hereby declare that the submitted thesis is the result of my own, independent work. All external sources are explicitly acknowledged in the thesis.

Winterthur, 28.01.2025

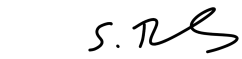

Seraina Brandes